The pair-production channel in atomic processes

Ali Belkacem[1] and Allan H. Sørensen[2]

[1]*Lawrence Berkeley National Laboratory, 1 Cyclotron Road, Berkeley, CA 94720, USA and*

[2]*Department of Physics and Astronomy, University of Aarhus, DK-8000 Aarhus C, Denmark*

(Dated: April 2, 2004)

Abstract

At sufficiently high energies, the cross sections for ionization and excitation upon photon impact and charge transfer upon ion impact decrease with increasing collision energies. However as the collision energy increases and pair creation comes into play, the cross section of "traditional" atomic processes such as photoionization and charge transfer reverses and starts to increase with increasing collision energies. Assisted by pair-creation, new channels for ionization, excitation and charge transfer are opened. This pair-production channel in atomic processes is very important and in many cases the contribution of this new channel to the total cross section of ionization, excitation, and charge transfer dominates other contributions that involve only the "positive-energy" electrons. In particular, an extensive body of theoretical and experimental work was done over the last two decades investigating charge changing mechanisms in relativistic heavy ion collisions that involve the pair production channel. We review some of these studies with a special emphasis on the work done by the authors.

I. INTRODUCTION

An atom, viewed in the simple Dirac picture, is a system that contains a finite number of electrons which occupy discrete positive-energy states and move on a background of an infinite number of electrons occupying all negative-energy states, the "Dirac sea". Since the early days of quantum mechanics atomic-collision studies have dealt mostly with the excitation, charge transfer, or ionization of the positive-energy electrons. Extensive studies of atomic processes in photon-atom, electron-atom, and ion-atom collisions have lead to a very good understanding of how such processes occur. By means of the theoretical and mathematical tools developed over the decades it is possible to predict cross sections quite accurately. At sufficiently high energies, the cross sections for ionization and excitation upon photon impact and charge transfer upon ion impact decrease with increasing collision energies. However, it was realized in the mid 1980s, that as the energy in the collision increases the negative-energy electrons will play a major role in atomic processes by opening new channels that involve pair creation. When pair production is taken into account, the cross section of atomic processes like photoionization and charge transfer reverses and starts to increase with increasing collision energies. Over the last two decades many studies have been published, both theoretical and experimental, of atomic processes assisted by the creation of an electron-positron pair during the collision. At high energies this vacuum-assisted channel in general outnumbers the channels involving only positive-energy electrons. The effort has largely been driven by the effect this increase in cross section has on the design and operation of high-energy accelerators.

In our contribution to the current Special Issue of Radiation Physics & Chemistry on pair production we review the pair-production channel in atomic processes and discuss how pair production affects well-known atomic processes such as charge transfer, ionization, excitation, and energy loss. The intent is not to provide an exhaustive review of all the work done in this field but rather to give a review that follows the line of the contributions of the authors to the field during the last few decades.

The contribution is divided into three major sections that include both theoretical and experimental work. Section II addresses atomic processes in photon-atom collisions. We review the various channels that lead to charge changing, excitation, and ionization when a high-energy photon impinges on an atomic or ionic target.

In Section III we extend our discussion to the case of ion-ion and ion-atom collisions. We make a special emphasis of the importance of bound-free pair production in ion-ion collisions at energies that are routinely encountered in relativistic heavy-ion colliders. In part of the section we use the equivalent photon method which is often as accurate as much more involved methods at very high energies. The method links the photon impact section to the heavy-ion impact section. However in some cases perturbative methods like the virtual photon method break down as is evident from experimental findings. Hence we discuss non-perturbative treatments of ion-ion and ion-atom collisions as well. We compare the non-perturbative results to experiments and to results of perturbative methods. The very important role that pair production plays in the energy loss of a relativistic heavy ion penetrating matter is also discussed.

The third and shortest part, Section IV, departs a little from the two previous parts as it deals with coherent and resonant effects in pair creation as such when the target is a single crystal. We review briefly the work done on coherent pair production in the perturbation limit as well as the effect on the pair production of the strong transverse field which exists in crystals.

Natural units are used throughout our contribution ($\hbar = m = c = 1$; except for cases involving the creation of heavier leptons, Subsecs. II.B.4 and III.B.4, m is the electron mass). The Compton wavelength $\lambdabar_C = \hbar/mc$ is hence the unit of length and cross sections come out in units of $\lambdabar_C^2 = 1.4912$ kilobarn (number for electron mass). In the section on photon impact, Sec. II, the atomic number of the target is denoted simply by Z. In the section on heavy-ion impact, Sec. III, the atomic number of at least one of the collision partners is always supplied with a subscript ($_p$ for the projectile, $_t$ for the target).

II. PHOTON IMPACT

We begin our journey into the world of vacuum-assisted atomic transitions by considering photoprocesses. Since photons essentially are nothing but electromagnetic field bunches, it is obvious that photon interactions are basic to the understanding of atomic collisions in general. The Weizsäcker-Williams method of virtual quanta provides a direct demonstration of this. Two vacuum-assisted processes will be considered in this section. In Subsec. II.B we discuss charge change of a bare ion mediated by photoconversion into a pair with the

negatively charged particle produced directly in a bound state centered on the ion. This process, which we shall term bound-free pair production, has also been given the alternative name of capture from pair production. In Subsec. II.C we discuss photoionization which is one of the most basic atomic collision processes and demonstrate how pair production plays a very crucial role at high energies. However, before turning to these two specific cases it is necessary to provide the reader with a suitable background knowledge of what we may call the standard case of pair creation, namely production of pairs of free electrons and positrons upon photon impact on an atom. This happens in the following Subsection II.A.

A. Production of free particles

The creation of free pairs upon photon impact on an atom is covered in many textbooks and reviews. Standard references are the classic books by Heitler (1954) and Jauch and Rohrlich (1980). Among the reviews that of Bethe and Ashkin (1953) may be mentioned as well as the introduction to the tabulation by Hubbell *et al.* (1980). For the sake of the discussion to follow we include a few central formulas and results.

Photoproduction of an electron-positron pair in the field of an atom involves the interaction of an electron with the radiation field as well as with the atom. The interaction with the radiation field is treated as a perturbation. The interaction with the atom will sometimes be treated exactly, but for the creation of unbound particles the standard treatment, which leads to the so-called Bethe-Heitler results, is a lowest order perturbation approximation for this interaction as well. In effect, pair creation is then a second-order (two-vertex) process. Correspondingly, the probability for a transition from an initial state O (negative-energy electron, incoming photon) to a final state F (electron excited to positive energy leaving a hole behind, recoiling atom) reads

$$P_{F|O} = 2\pi |\sum_n \frac{H_{F|n} H_{n|O}}{E_O - E_n}|^2 \rho_F \ . \tag{1}$$

Here ρ_F is the density of final states and the sum in the compound matrix element is over all intermediate states ($_n$ runs through a complete set of states in principle, in praxis only a few contribute). In Eq. (1) one of the matrix elements H corresponds to the absorption of the primary photon while the other corresponds to the scattering in the atomic field. Describing

the electron in the various states by plane waves, which are of the form

$$\psi = u e^{i\mathbf{p}\cdot\mathbf{r}} \tag{2}$$

where u is a space- and time-independent four-component spinor and $\mathbf{p}$ the electron momentum (Heitler, 1954), the matrix element for the interaction with the radiation field takes the form

$$H_{p_a 0|p_b 1} = e\sqrt{\frac{2\pi}{\omega}}\langle u_a|\alpha_\lambda|u_b\rangle \times \delta(\mathbf{p}_a - \mathbf{k} - \mathbf{p}_b) \ . \tag{3}$$

The index on the matrix element indicates a transition from a state composed of a photon (of momentum $\mathbf{k}$, energy $\omega = k$, and specified polarization) and an electron of momentum $\mathbf{p}_b$ to another with no photons but solely an electron of momentum $\mathbf{p}_a$. The δ-function assures momentum balance for the considered vertex and the quantity α_λ is the projection of the Dirac α-matrices on the direction of the photon polarization. By application of the plane-wave description (2) the matrix element for scattering in the atomic potential V takes the form

$$H_{p_c|p_d} = \int V(r) e^{i\mathbf{q}\cdot\mathbf{r}} d^3r \ \langle u_c|u_d\rangle \ , \tag{4}$$

where $\mathbf{q} = \mathbf{p}_d - \mathbf{p}_c$ is the recoil momentum taken by the atom. The lack of a photon index on the matrix element implies that the number of photons (0 or 1) is unchanged.

By collecting the above information, including the explicit expression for the density of final states, converting from probability to cross section, and summing over intermediate states, the cross section is obtained. To the extent that only unpolarized photons are of interest an average over initial states of polarization is further performed. Similarly, an average over spin directions in the initial state and a sum over spin directions in the final state are usually performed. Further integrations over emission directions and relative energy of one of the emitted particles are performed if spectra differential in these variables are not sought for. In this way, the following total cross section for pair production on an atomic nucleus of atomic number Z is obtained

$$\sigma_{BH} = Z^2\alpha^3\frac{28}{9}L \ , \tag{5}$$

where $\alpha = e^2$ is the fine-structure constant. For the production of numerical values we note that $4\pi r_e^2 = 4\pi\alpha^2$ equals 0.998 barn ($r_e \equiv e^2/mc^2 = \alpha$ being the classical electron radius).

In the limit of high photon energy the logarithmic factor L assumes the value

$$L_{\omega \gg 1} = \left\{ \begin{array}{ll} \ln(183 Z^{-1/3}) - 1/42 \; ; & \text{screened nucleus} \\ \ln(2\omega) - 109/42 \; ; & \text{bare nucleus} \end{array} \right\} , \tag{6}$$

where the upper expression applies for a nucleus whose field is screened out at large distances due to the presence of atomic electrons (Thomas-Fermi model). At extremely high energies additional suppression occurs in condensed media, see footnote 2 below.

Figure 1 displays the cross section for pair production in a screened nuclear field for three different targets (Z-values of 13, 26, and 82) as tabulated by Hubbell *et al.* (1980). The cross section (5) with L given by (6) is also shown. Screening is important at high energies. From threshold the cross section increases smoothly over a few orders of magnitude in photon energy before it saturates. For the two lighter targets the result for the bare nucleus listed in (6) applies approximately over a substantial part of the increase and the final saturated values agree closely with the value listed for the atom. For the heavy target deviations from both of the results listed in (6) show up. These deviations are due to nonperturbative effects which are discussed elsewhere, including in the references given in the beginning of this subsection, see for instance Hubbell *et al.* (1980). As Fig. 1 shows, nonperturbative corrections are in general moderate at high energies yielding reductions in total cross sections of no more than 10–20%. Close to threshold the Born approximation actually fails not only for the heavy elements, and production becomes somewhat more probable than this approximation predicts.

In addition to pair creation in the screened field of the atomic nucleus, incoherent production on individual atomic electrons may occur. This contribution to the cross section is also displayed in Fig. 1. As the figure shows, the incoherent contribution may be accounted for roughly by multiplying the cross section corresponding to coherent action of the entire atom by a factor $(1 + 1/Z)$.

When working with high-energy photons, electrons, and positrons the so-called radiation length is often encountered. It is a convenient measure which relates to both the emission of bremsstrahlung and pair creation: For an electron or a positron of sufficiently high energy, the major cause of slowing down is by far emission of bremsstrahlung.[1] Correspondingly, the

[1] The energy beyond which bremsstrahlung losses dominate over the ionization energy loss may be estimated by formulas of the form $E_0/(Z + a)$ where E_0 and a assume values of 610 MeV and 1.24 for solids and

radiation length ℓ_r is defined as the the penetration depth over which a high-energy electron on average loses all but a fraction $1/e$ of its initial energy. It is to be understood, that the energy is sufficiently high that the cross section is dominated by atomic screening whereby an energy-independent quantity results.[2] Easy-to-use formulas as well as a tabulation for the radiation length may be found in the report by the Particle Data Group (Hagiwara *et al.*, 2002). Examples of radiation lengths are 18.8 cm in pure graphite, 12.2 cm in diamond, 9.36 cm in silicon, 1.76 cm in iron, and 0.56 cm in lead. For very high-energy photons the total cross section for pair production is related to the radiation length approximately as

$$\sigma = \frac{7}{9}\frac{1}{N\ell_r} , \tag{7}$$

where N is the density of target atoms. Hence the radiation length also defines the typical length for the development of high-energy electromagnetic cascades.

The cross section differential in the energy of one of the produced particles as obtained in the Born approximation is illustrated in Fig. 2 for an iron target. Only the production on the screened target nuclei is included. Incoherent production on atomic electrons may be included approximately simply by assuming the cross section to be given in units of $4Z(Z+1)\alpha r_e^2$ rather than $4Z^2\alpha r_e^2$ as stated on the figure. The curves are calculated according to the formulas given by Bethe and Ashkin (1953). Whereas the two lowest curves (photon energies of 5 and 10) hold for any target material (in the Born approximation) the higher curves are target specific due to increasing influence of screening. However, the target dependence is relatively moderate as revealed by the horizontal line segments on the right side of Fig. 1. In the Born approximation the distribution is symmetric at all photon energies and in general rather flat. Close to threshold the distribution over kinetic energy actually becomes asymmetric due to attraction respectively repulsion by the nucleus.

An additional characteristic feature of pair creation which is shared by many high-energy radiation processes is the forward directed production: at high energies emission angles are of the order $1/\omega$. It is also of interest to note that at high energies recoil momenta are in

liquids, and 710 MeV and 0.92 for gasses (Hagiwara *et al.*, 2002).

[2] At extremely high energies (in the TeV region for solid targets) the radiation length actually begins to increase with energy due to partial suppression of the cross section (bremsstrahlung as well as pair production) as a result of the so-called Landau-Pomeranchuck (or Landau-Pomeranchuck-Migdal) effect (multiple Coulomb scattering over the formation length). The effect is discussed in another contribution to the current Special Issue (Klein, 2004).

general transverse to the incoming photon direction and smaller than or of the order of one unit (mc).

From the experimental perspective free electron-positron pair production with photon impact was extensively studied for the last several decades and good agreement for total and partial cross sections between theory and experiment was achieved. These studies spanned over two major areas that involve the part discussed above, corresponding to incoherent addition of contributions from different atoms, and the coherent production that takes place in ordered targets such as crystals. The coherent pair production in crystals will be discussed in Section IV. The high energy photons used in pair production experiments are generally produced via bremsstrahlung of a relativistic electron beam. Usually the choice of the radiator thickness results from a compromise between the need for photon intensity and the necessity to keep the probability of two-photon events at a low level. The electrons transmitted through the radiator are separated from the photons and directed into a tagging spectrometer by magnetic separation. The tagging spectrometer measures the energy of the electron after radiation thus "tags" the energy of the emitted photon. This tagging technique is also used in case of photons produced via Compton backscattering of laser photons on relativistic electrons. Dauvergne *et al.* (2003) used recently this technique at the European Synchrotron Radiation Facility (ESRF) to produce 0.7 - 1.5 GeV photons by backscattering laser photons on the 6 GeV electron beam in the storage ring. These photons were then used to study vacuum-assisted photoionization, see Subsection II.C, and also to measure the production of free electron-positron pairs for Au and Ag targets. Figure 3 shows the absolute electron-positron pair production probabilities measured for Au and Ag atoms as a function of target foil thickness. Linear fits of the data provide a cross section of 35.1 and 14.2 barns for Au and Ag, respectively. As can be seen in the figure, statistical fluctuations around mean probabilities are very small. These values are in very good agreement with the theoretical values (Hubbell *et al.*, 1980) of 36.6 and 14.7 barns, respectively, when the experimental photon energy range is folded in the calculations. This good agreement is a further indication that theory has achieved a good understanding of the free-free pair production process.

B. Production of bound-free pairs

In most studies of pair production with photon impact the atomic target is a neutral atom. If instead the target is a bare ion it will enable a new pair production channel in which the electron of the produced pair end up in a bound state of the ion. From a theoretical point of view this pair production channel, termed bound-free pair production, is in some ways simpler than free-free pair production: Once the final bound state of the electron is set, the energy taken by the positron is also set, reducing the number of variables. Furthermore, as the interaction with the atom is included already in the electronic states, or at least in the bound state, evaluation of a compound matrix element as in Eq. (1) is avoided. However, experiments on bound-free pair production with photon impact are very challenging and, to the knowledge of the authors, non-existent. Although it is possible to produce highly charged ions at several accelerators, it is necessary to perform an experiment by crossing an ion beam with a beam of high energy photons. There are no facilities at present with luminosities high enough to yield meaningful measurements. As will be discussed later in this chapter, virtual photons of two colliding heavy ion beams are used to study indirectly bound-free pair production for photon impact. In this section the theory of bound-free pair production for photon impact is reviewed. Most of the physics and the cross sections calculated here will be used later in the study of bound-free pair production in heavy ion collisions.

1. Perturbation calculation

The cross section for bound-free pair production for photon impact may be written as

$$\frac{d\sigma}{d\Omega} = \frac{\alpha p_+ E_+}{2\pi k} \frac{1}{2} \sum_{\lambda,i,b} |M|^2 \ . \tag{8}$$

Here p_+ and E_+ are the momentum and energy of the positively charged lepton while $\mathbf{k}$ again denotes the momentum of the incoming photon. The sums are sum over spin directions of the positive lepton ($\sum_i$), sum over magnetic quantum number for the bound lepton ($\sum_b$), and average over direction of photon polarization ($\frac{1}{2}\sum_\lambda$). The matrix element is given as

$$M = \int d^3r \ \psi_b^\dagger(\mathbf{r}) \alpha_\lambda e^{i\mathbf{k}\cdot\mathbf{r}} \psi_i(\mathbf{r}) \ , \tag{9}$$

where ψ_b denotes the Dirac spinor for the bound, negatively charged lepton and ψ_i is the initial Dirac spinor belonging to the negative-energy continuum with the bare ion present. Further details are given elsewhere (Agger and Sørensen, 1997; Heitler, 1954).

The cross channel for bound-free electron-positron pair creation is the photoelectric effect. At non-relativistic energies, calculations to lowest order of the photoeffect proceed by means of a plane-wave description of the outgoing electron (Heitler, 1954). However, at relativistic energies such description is insufficient for obtaining lowest-order results (Berestetskii *et al.*, 1989; Pratt *et al.*, 1973). Here, it is necessary to expand the wave function for the unbound electron to first order in αZ. Being the cross channel, the same holds true for bound-free pair production. The photo cross section, correct to lowest order at relativistic energies, was first derived by Sauter (1931). Using crossing symmetry Sauter's expression may be translated into a lowest-order cross section for bound-free pair production. Since it is often convenient to apply a simple plane-wave description let us compare the results of the two approaches (Sørensen, 2001):

By describing the electron in the final state by a plane wave, the cross section (8) may be expressed as (Belkacem and Sørensen, 1998)

$$\begin{aligned}\frac{d\sigma}{d\Omega} = \pi\alpha \; & \frac{p_+(E_+ + 1)}{k} \left[|\kappa| \left(g^2(q) + \left(\frac{p_+}{E_+ + 1} \right)^2 f^2(q) \right) \right. \\ & \left. - \; 2\kappa \frac{p_+}{E_+ + 1} \frac{\cos\theta(k - p_+ \cos\theta)}{q} g(q) f(q) \right] . \end{aligned} \tag{10}$$

The momentum transfer q is given in terms of the minimum value,

$$q_{min} = k - p_+ = k - \sqrt{(k - E_-)^2 - 1} \; , \tag{11}$$

and the emission angle θ of the positron relative to the direction of the incoming photon as

$$q^2 = q_{min}^2 + 2p_+ k(1 - \cos\theta) \; , \tag{12}$$

and $d\Omega = \sin\theta d\theta d\phi$ refers to the emission of the positron. The quantity κ relates to the total angular momentum quantum number j of the populated bound state as $\kappa = \mp(j + \frac{1}{2})$ where the upper sign applies for states where the orbital angular momentum quantum number l of the large component equals $j - \frac{1}{2}$ while the lower applies for $l = j + \frac{1}{2}$. The quantities $g(q)$ and $f(q)$ are given in terms of the radial part of the large and small component, $g(r)$

and $f(r)$, of the bound-state spinor

$$\psi_b(\mathbf{r}) = \begin{pmatrix} g_\kappa(r)\Omega_{jlm}(\mathbf{r}/r) \\ if_\kappa(r)\Omega_{j\bar{l}m}(\mathbf{r}/r) \end{pmatrix} \tag{13}$$

as

$$\begin{aligned} g(q) &= (2/\pi)^{1/2} \int_0^\infty dr\ r^2 g(r) j_l(qr) \ , \\ f(q) &= (2/\pi)^{1/2} \int_0^\infty dr\ r^2 f(r) j_{\bar{l}}(qr) \ , \end{aligned} \tag{14}$$

where j_l denotes a spherical Bessel function of order l and $\bar{l} \equiv l \pm 1 = j \pm \frac{1}{2}$ (again, upper and lower sign correspond to upper and lower sign in the relation $l = j \mp \frac{1}{2}$). In Eq. (13) the Ω's are the usual spin-angular bispinors (Agger and Sørensen, 1997; Greiner, 1990; Sørensen and Belkacem, 1994).

For the ground state of a hydrogenlike system of atomic number Z, the momentum waves assume the form (Sørensen and Belkacem, 1994)

$$\begin{aligned} g(q) &= N_0 \frac{1}{q} \frac{\Gamma(s+1)}{(1+q_Z^2)^{(s+1)/2}} \sin((s+1)\delta) \ , \\ f(q) &= N_0 \sqrt{\frac{1-s}{1+s}} \frac{1}{q} \ \times \\ &\quad \left[\frac{\Gamma(s+1)\cos((s+1)\delta)}{(1+q_Z^2)^{(s+1)/2}} - \frac{\Gamma(s)\sin(s\delta)}{q_Z(1+q_Z^2)^{s/2}} \right] \ , \end{aligned} \tag{15}$$

with $q_Z \equiv q/\alpha Z$, $\delta \equiv \arctan(q_Z)$, $s \equiv \sqrt{1-(\alpha Z)^2}$, and N_0 defined as

$$N_0 = 2^{s+1/2} \left(\frac{1+s}{\alpha Z \pi \Gamma(2s+1)} \right)^{1/2} \ . \tag{16}$$

In the limit $\alpha Z \ll 1$ the expressions (15) reduce to

$$g(q) = \sqrt{\frac{8}{\alpha Z \pi}} \frac{2}{q} \left(\frac{\alpha Z}{q} \right)^3 \ , \quad f(q) = -\frac{q}{2} g(q) \ . \tag{17}$$

Integration of (10) over angles then yields the result

$$\sigma = \sigma_0 \times \frac{p_+}{k^3} \left(E_+^2 - \frac{E_+}{3} + \frac{4}{3} \right) \ . \tag{18}$$

The quantity

$$\sigma_0 = \frac{4\pi\alpha(\alpha Z)^5}{k} \tag{19}$$

represents the high-energy limit of the cross section and contains the entire Z-dependence at all energies.

Formulas for the photoeffect may be transcribed into formulas for bound-free pair production — and vice versa — by simple substitutions. These involve replacement in matrix elements of the final-state electron momentum and energy by the negative of those of the positron. In addition it should be remembered, that the bound electron state appears as the initial state in the photoeffect but as the final state in the pair creation process. Transcription of Sauter's result for the photoeffect gives a cross section for pair creation, with the electron produced directly in the $1s$-state, of[3]

$$\sigma = \sigma_0 \times \frac{p_+^3}{k^4}\left(-\frac{4}{3} + \frac{E_+(E_+ + 2)}{E_+ - 1} \times \left[1 - \frac{1}{2E_+p_+}\ln\frac{E_+ + p_+}{E_+ - p_+}\right]\right) . \tag{20}$$

In the extreme high-energy limit also the expression (20) reduces to σ_0 and again there is no other dependence on Z than that contained in σ_0.

Figures 4 and 5 show a comparison of the plane-wave result (18) and the transcribed Sauter formula (20). Fig. 4 displays the two predictions for the cross section, both divided by the high-energy result σ_0, Eq. (19), as well as their ratio. At high energies both predictions approach the asymptotic formula, that is, they decrease roughly as $1/k$. And beyond twice the threshold energy they differ by less than 10% from each other. Differences are mainly confined to the first two units above threshold. Fig. 5 shows the predictions for the cross section directly without dividing out the asymptotic energy dependence. The cross section displays a peak at relatively low energy, and differences are mainly confined to the region near and below this maximum. In this narrow region, on the other hand, the ratio between the two predictions may become quite large.

The interested reader may find a discussion of the corresponding situation for the photoeffect elsewhere (Sørensen, 2001). Remarkably, it is found that the plane-wave and the Sauter results approach each other at asymptotically high as well as asymptotically low energies, while a maximum difference of 50% is encountered for $\omega \simeq 1$. Although differences

[3] By mistake the formula quoted by Agger and Sørensen (1997), Eq. (52) in their paper, is the formula for the photoeffect. To get the corresponding result for bound-free pair creation E_+ and p_+ appearing in that particular formula should be replaced by $-E_+$ and $-p_+$ whereby the current Eq. (20) results.

between total cross sections hence are moderate, the differences between the differential cross sections obtained with the plane-wave approach and by Sauter are substantial at high energies (Sørensen, 2001). However, as will be apparent from the discussion in the following subsection, the differential results of Sauter, in turn, quickly become insufficient with increasing Z due to nonperturbative action.

The minimum momentum transfer (11) varies only moderately with photon energy: it decreases monotonously from $1 + E_-$ at threshold to E_- at infinity. Since E_-, the bound-state energy of the electron, is between 0 and 1, and in most cases close to 1, q_{min} varies roughly between 2 and 1. With a minimum momentum transfer of order 1, the momentum transfer in bound-free pair creation is considerably above typical atomic momenta for any shell. In this region, the momentum-space density $q^2(g^2 + f^2)$ falls off fairly rapidly with increasing q. From the expression (12) it is then found that only emission angles where $4p_+k\sin^2\theta/2$ is smaller than, approximately, $K^2q_{min}^2$ contribute to the total cross section, the quantity K attaining a value in the vicinity of $\frac{1}{2}$–1. This reduces to the approximate restriction

$$\theta \lesssim K/k \tag{21}$$

beyond one or two units above threshold; hence characteristic emission angles show the usual $1/k$-scaling.

2. Nonperturbative treatment

In a nonperturbative calculation the plane-wave approach for the positron is abandoned and exact Coulomb waves are applied instead (as long as electron-positron pair creation on bare point-like nuclei is considered). This leads to some complications. A brief description follows below; details may be found elsewhere (Agger and Sørensen, 1997).

The total cross section for photon induced bound-free pair production may be obtained by summing the partial cross sections for ending up in particular scattering states, that is,

$$\sigma = \frac{1}{2}\sum_{m,\lambda,\lambda_+}\int d\Omega \frac{d\sigma(\vartheta,\phi)_{m\lambda\lambda_+}}{d\Omega}\ . \tag{22}$$

Alternatively, the sum may be taken over angular momentum eigenstates (partial waves) so that

$$\sigma = \frac{1}{2}\sum_{\lambda}\sum_{JLMm}\sigma_{JLM}\ . \tag{23}$$

In these equations λ and λ_+ represent the helicity of the incoming photon and outgoing positron, respectively, m is the magnetic quantum number of the bound electron and J, L and M are the angular momentum quantum numbers of the partial wave. Obviously, λ_+ is absent from (23) and J, L, and M from (22). As the Coulomb-Dirac wave functions may only be obtained as a partial wave expansion, the approach (23) is taken for the purpose of determinating the total cross section.

Since the process of bound-free pair production may be viewed as the excitation of an electron from the negative energy continuum to a bound state, the partial cross section σ_{JLM} is similar to the usual photoabsorption cross section given in standard references (Bethe and Salpeter, 1957; Merzbacher, 1971). It reads

$$\sigma_{JLM} = \frac{4\pi^2\alpha}{k}|M_{\lambda JLM}|^2 \ , \tag{24}$$

where the matrix element is given as

$$M_{\lambda JLM} = \int d^3\mathbf{r}\psi_b^\dagger(\mathbf{r})\boldsymbol{\alpha}\cdot\mathbf{e}_{\boldsymbol{\lambda}}e^{i\mathbf{k}\cdot\mathbf{r}}\psi_{JLM}(\mathbf{r}) \ . \tag{25}$$

Here ψ_{JLM} is the appropriate negative continuum wave function and ψ_b is the wave function of the bound electron. The difference in front factor in (24) as compared to (8) is related to a corresponding difference in the continuum waves, see below. The actual computation of matrix elements for the Coulomb wave functions is discussed at length by Agger and Sørensen (1997).

Figure 6 shows the K-shell cross section scaled with Z^5 as a function of photon energy for five elements together with the Born result (20). It is immediately clear that nonperturbative effects are strong: The absolute values for unit nuclear charge are close to the Born result (20), but as Z increases, values become lower corresponding to a slower Z-dependence of the cross section than the perturbative Z^5-scaling. For the highest charge presented in the figure, the reduction is by more than a factor of 5. As discussed above, such dramatic nonperturbative effects are not found in the creation of pairs of unbound particles. It is furthermore observed that the curves in Fig. 6, like the perturbative results presented in Fig. 5, all show a peak at low photon energies followed by a decrease which approaches an asymptotic $1/k$-dependence at high energies, cf. (19). The shapes for different Z are rather similar, but the peaking appears at lower energies for higher charges.

It may be noted that near threshold, bound-free pair production dominates over free-free pair production. For the case of Z=92, this holds true for nearly all of the first energy unit

beyond threshold. Right after curves cross, the bound-free cross section goes through its maximum while the cross section for production of free pairs continues to increase steeply.

If the cross sections of Fig. 6 are plotted in units of the Sauter cross section (19), each curve will be seen to tend to a constant at high energies (Agger and Sørensen, 1997). Hence, following Pratt (1960a) and Milstein and Strakhovenko (1993), the high-energy cross section may be written as

$$\sigma_K = \sigma_0 f(Z) \ , \qquad k \to \infty \ . \tag{26}$$

The function $f(Z)$ is a decreasing function of Z. Aste *et al.* (1994) have suggested a "purely heuristic" formula for this function,

$$f(Z) = \left(\frac{1}{2} + \frac{\alpha Z}{4}\right)^{2\pi\alpha Z} \ . \tag{27}$$

Even though the results for $f(Z)$ deduced from the analysis of the data presented in Fig. 6 are in good agreement with those of Aste *et al.* (1994), the formula (27) turns out to be slightly on the low side (by 5–10%). Better agreement is found with the numerical high-energy results of Pratt (1960a) obtained in studies of the photoelectric effect. Another useful approximation formula is the modified Hall formula (Pratt, 1960a)

$$\sigma = \sigma_0 (\alpha Z)^{2\xi} e^{-2\alpha Z \cos^{-1} \alpha Z} (1 - 4\pi\alpha Z/15) \ , \tag{28}$$

where $\xi = s_1 - 1 = \sqrt{1-(\alpha Z)^2} - 1 \ (\simeq -\alpha^2 Z^2/2)$.[4] The various results for $f(Z)$ are compared in Table I. Further comments are given by Agger and Sørensen (1997) who also note, that for energies beyond roughly 20 electron masses, there is good agreement between the results presented in Fig. 6 and those obtained by multiplying Sauter's result (20) by the numerically obtained $f(Z)$.

To first order in αZ the cross section for production in s-states beyond the ground state obeys a scaling law of the form (Pratt, 1960b)

$$\sigma_{ns} = \frac{1}{n^3} \sigma_K \ , \tag{29}$$

where n is the shell number. Furthermore, Gavrila's second order Born approximation for the $2s$-state gave identically $\frac{1}{8}$ of his second-order K-shell cross section (Gavrila, 1961).

[4] The original formula published by Hall, Rev. Mod. Phys. **8**, 358 (1936), is not a good approximation — despite so stated by various authors including Heitler (1954) in the discussion of the photoelectric effect.

Calculations by Pratt showed that in the high energy limit, the n^{-3}-scaling is very close to the exact result not only at low charge numbers but in general at all values of Z. The $2p$-states, on the other hand, have quite insignificant cross sections at low target charges while at high target charges the $2p$ cross sections will be of the same order of magnitude as those for the $2s$-state (though still smaller). In the Born approximation, that is, to lowest order in αZ, cross sections for p-states are expected to increase in proportion to Z^7 as compared to Z^5 for s-states (Gavrila, 1961). The result is that the cross section for bound-free pair production with capture to the L shell is approximately 12.5% of the K-shell cross section for low target charges, where the Born approximation is valid, and about 20% for high target charges. This prediction, which was originally based on Pratt's high-energy calculations, remains valid at practically all energies away from threshold (Agger and Sørensen, 1997).

Figure 7 displays the ratios of cross sections to the K-shell cross section for the three L-states as well as for the entire L-shell for three heavy targets. At energies beyond 5 units, all ratios are essentially constant. The $2s$-curves all saturate at a level close to the value 1/8. The $2p_{1/2}$-curves on the other hand show significant Z-dependence, even faster than the $Z^7/Z^5 = Z^2$ prediction of the Born approximation, whereas the $2p_{3/2}$-ratios only depend weakly on Z. Due to the Z-dependence of the $2p_{1/2}$-results, also the ratio for the entire L shell shows some Z-dependence with asymptotic ratios ranging from 18% to 21% for the three selected heavy targets (again to be compared with 12.5% in the low-Z limit).

The high-energy limit for the L-shell cross sections is most easily obtained by applying the high-energy values for the shell ratios and (26) for the K-shell cross section with $f(Z)$ taking values according to Table I. Agger and Sørensen (1997) provide a tabulation of shell ratios in the high-energy limit.

Total cross sections for bound-free pair production by high-energy photons where the electron ends up in the M or any higher shell are given by Milstein and Strakhovenko (1993). According to these authors, the contribution from M and higher shells amounts to approximately 60% of the L-shell contribution for all charge numbers.

3. Differential cross section

In order to obtain differential cross sections, the continuum state is represented by a scattering wave. In analogy to Eq. (8) the differential cross section then reads

$$\frac{d\sigma_{m\lambda\lambda_+}}{d\Omega} = \frac{\alpha p_+ E_+}{2\pi k} |M_{m\lambda\lambda_+}|^2 \,. \tag{30}$$

The matrix element is given as

$$M_{m\lambda\lambda_+} = \int d^3\mathbf{r}\psi_b^\dagger(\mathbf{r})\boldsymbol{\alpha}\cdot\mathbf{e}_{\boldsymbol{\lambda}} e^{i\mathbf{k}\cdot\mathbf{r}}\Psi^-_{\mathbf{p}_+}$$

$$= 4\pi\sqrt{\frac{\pi}{2E_+p_+}} \sum_{JLM} i^L e^{-i\delta_\kappa} \langle L\frac{1}{2}(M+\frac{1}{2}\lambda_+)\frac{1}{2}\lambda_+ | L\frac{1}{2}JM\rangle \, Y^*_{L,M+\frac{1}{2}\lambda_+}(-\hat{\mathbf{p}}_+) M_{\lambda JLM} \,. \tag{31}$$

where $M_{\lambda JLM}$ are partial wave matrix elements (25) (Agger and Sørensen, 1997).

Figure 8 displays the differential cross section for pair creation with the produced electron bound in the K-shell and the positron emitted with a total energy of 1.5 for five different target elements. At low target charges the differential cross section vanishes in the forward direction. This is in agreement with the prediction of the Born approximation.[5] At high charges, on the other hand, the angular distributions show a maximum in the forward direction. The transition from the low-Z to the high-Z behavior takes place already at moderate charge numbers; for Z=8, the value for forward emission is clearly different from zero and at Z=26 the global maximum is at zero angle. It may be noted that at low Z, but not moderate and high Z, the angular distribution is quite similar to that of the K-shell photoelectric effect, which for any charge number has a local minimum in the forward direction (Alling and Johnson, 1965). On the other hand, for single-quantum annihilation

[5] It may be noted that, for production of free pairs, the Born approximation gives a maximum in the forward direction (Heitler, 1954). For the related processes of the photoelectric effect and bremsstrahlung, a similar situation is encountered with the Born approximation yielding a zero in the forward direction for the former process but a maximum for the latter. This asymmetry of the Born results for the bound-free and free-free processes has caused some concern over the years. For instance, Fano, McVoy, and Albers [Phys. Rev. **116**, 1147 (1959)] tried to apply a detailed balance argument to show that the photoelectric effect must have the same angular distribution as bremsstrahlung if the final-state electron momentum is equivalent to that of the ground state, hence, they argued, the first Born approximation must be invalid. However, this argument does not hold: the second order Born approximation (Gavrila, 1961) also vanishes in the forward direction (note that Gavrila erroneously states the contrary earlier [Phys. Rev. **113**, 514 (1959)]), and the exact calculations discussed here also give results in good agreement with the Born approximation.

a maximum is encountered in the forward direction at high Z (Johnson, 1967) as we find it for the bound-free pair production.

Figure 9 displays the angular distributions at higher energies for a heavy target element as well as for unit nuclear charge. With the abscissa chosen as the product of positron energy and emission angle, the curves are all confined within a few units corresponding to a scaling of characteristic angles with the inverse of the positron energy E_+. When this result is combined with the asymptotic $1/E_+$-dependence of the total cross section it is obvious, that the differential cross sections scale roughly with E_+. Accordingly, as ordinate in Fig. 9 is used the differential cross section divided by energy as well as by Z^5. Plotted in this way, the shapes of the curves for a given element are similar at all energies and the variation in absolute values is moderate.

The differential cross section for production of electrons in the L-shell are displayed and discussed elsewhere (Agger and Sørensen, 1997). It may be noted that exactly like the total cross section also the differential cross section for production in the $2s$ state is close to one-eighth of the K-shell result for all values of Z.

For a study of polarization effects in photo-induced bound-free electron-positron pair creation the reader is referred to the publication by Agger and Sørensen (1997).

4. Heavy-lepton pair production

As compared to the electron-positron case, cross sections for production of particle-antiparticle pairs of heavy leptons on point nuclei are reduced by the square of the ratio of the mass of the heavy lepton to that of the electron. This holds true for both the production where the negative lepton is bound to the target nucleus as well as for production of unbound leptons. Finite nuclear size causes further depletion. The spatial extent of the creation process is the Compton wavelength for the created leptons. Using this as the unit of measure, the nuclear size is much smaller than unity for electrons (that is, the nucleus appears essentially pointlike), of the order of unity for muons, and several tens of units for taus. As a result, reduction due to finite nuclear size is basically fatal for bound-free tau production, at least as long as the nucleus is required to remain intact.

A study of bound-free heavy lepton pair production has been presented by Belkacem and Sørensen (1998). The study is restricted to cases where the capturing nucleus remains intact

during the lepton production. Furthermore, the positive lepton is represented by a plane wave, cf. Subsection II.B.1. This is an obvious approximation in case of tau production where the depth of the nuclear potential is only a few per cent of the tau mass. The approximation is also expected to be reasonable for muon production, at least not too close to threshold. In any case, for muon and tau production, corrections due to nonperturbative as well as Sauter-type effects are much smaller than those due to finite nuclear size.[6]

Consider first muon production. In order to compute cross sections the Dirac equation is solved numerically to obtain $\psi_b(\mathbf{r})$ for bound muon states in the field of an extended nucleus whose charge is distributed homogeneously within a radius of $1.18\text{fm}\times A^{1/3}$ where A is the mass number. The momentum waves $g(q)$ and $f(q)$ to be applied in Eq. (10) are obtained subsequently by numerical transformation according to (14). An example of the momentum-space density $q^2(g^2+f^2)$ for a negative muon bound in the K- or the L-shell of a bare uranium ion is shown by Belkacem and Sørensen (1998). For all states the density peaks at rather low momenta and then, beyond roughly 0.5 units, falls off rapidly by several orders of magnitude over one momentum unit. This rapid fall-off is an effect of the finite nuclear size. The level of the momentum content is essentially the same if the Fermi distribution of the nuclear charge is chosen, and below 2 momentum units the momentum-space densities obtained in a nonrelativistic calculation differ at most by a factor of 2–3 from the relativistic results displayed in the example.

Figure 10 shows total cross sections for muon pair production on a bare uranium ion with the negative muon bound in the K- or the L-shell. The structure is quite similar to that found for pointlike nuclei, cf. Figs. 5–6, 7, with a peak a few units above threshold followed by a fall-off essentially inversely proportional to the impact energy. Well above the peak, which appears somewhat later than for the pointlike case, the cross section may be

[6] For the production of heavy leptons finite nuclear size gives a strong suppression exactly in the region near threshold, where major differences are encountered for the Coulomb potential between the plane-wave approach and Sauter's approach: For production of μ-pairs on a uranium nucleus with the negatively charged lepton bound in the ground state, the maximum cross section as computed in the plane-wave approach appears at an energy of 7.8, see Fig. 10 below. This is much higher than the position of the plane-wave maximum for the Coulomb case and the Sauter maximum which appear at 3.8 and 4.7, see Fig. 5. The plane-wave approximation is expected to be sufficiently accurate, and no expansion of the wave function for the positively charged lepton is presumably needed, when the potential varies only moderately over the Compton wavelength of the particle in question (that is, when the Coulomb divergence is avoided).

estimated within a factor of two, or so, as

$$\sigma \sim K^2 \times 2\pi^2 \alpha g^2(q_{min})/k \ , \tag{32}$$

where K is a constant of order 1.[7]

Belkacem and Sørensen (1998) reported that the asymptotic value of the perturbative cross section for production in the uranium ground state is $0.0090\sigma_0$. This reduction by two orders of magnitude relative to the perturbative point-like case is due to the finite nuclear size. Nonperturbative effects for pointlike nuclei (electron-positron production) were previously found to cause a reduction by a factor of 5 for uranium, Table I. As discussed above the nonperturbative correction for muon pair production is expected to be much smaller since the strong Coulomb center is depleted on the scale of the Compton wavelength due to finite nuclear size.

Figure 10 further illustrates that in high-Z targets muon pair production with L-shell capture, when adding contributions from all substates, becomes at least as probable as production with K-shell capture. This is in contrast to the electron case where the capture to the $2s$-state is close to $1/2^3$ for all Z while the total L-shell cross section is roughly 0.20 times the K-shell cross section for high Z, Fig. 7. Inclusion of even higher states is expected to contribute significantly to the total cross section for bound-free muon pair production.

Belkacem and Sørensen (1998) computed the momentum content of bound muon states for a wide range of different target ions with the purpose to estimate the dependence of the total cross section on Z. For the point-like case perturbation theory predicts a scaling of the cross section with Z^5 for the ground state, see Eqs. (19–20). With the extended nucleus, a much slower scaling was found for heavy elements. Some discrepancies with earlier findings were reported.

Tau production was also discussed by Belkacem and Sørensen (1998). With the depth of the potential attaining at maximum 2% of the tau mass, the bound-state problem is basically nonrelativistic. Hence a nonrelativistic calculation was applied. Fourier transformation of the wave function for the tauonic ground state obtained by numerical solution of the Schrödinger equation for a homogeneously charged uranium nucleus yielded a mo-

[7] The expression on the right-hand-side of (32) holds exactly for the Sauter cross section. By application of the analytical result for the Coulomb $1s$ wave in the limit of high energies and low Z the constant is seen in this limit to assume the value $K = 1/4$.

mentum density reduced by approximately 15 orders of magnitude at one momentum unit as compared to the value at maximum. This implied a reduction of the cross section (as measured in units of the square of the Compton wavelength, that is, in units of 1.233×10^{-28} cm^2) of similar magnitude. As an example, by substitution of the nonrelativistic momentum wave for the large spinor component and neglect of terms beyond the first in square brackets of (10) a maximum cross section for tauonic pair production on a xenon nucleus with population of the $1s$ ground state of 4.3×10^{-44} cm^2 or 4.3×10^{-8} picobarn was obtained, a result which could not change by more than a factor of 2 in a relativistic calculation. This finding was of course fatal as far as measurements are concerned. Note, however, that incoherent production may well ease the situation, see below.

The lowest states are confined inside the nucleus where the potential for a homogeneous charge distribution is harmonic. It is interesting to note that although the harmonic oscillator energies approximate the actual binding energies for τ^- very closely, the relative difference amounts to 1 part in 10000 for K-shell of uranium, the tails of the momentum waves fall off much less dramatically than those pertaining to the pure oscillator. It may also be noted that application of the Fermi distribution causes a reduction of the momentum density in the relevant region by roughly an order of magnitude relative to the level obtained for the homogeneous charge distribution.

The further away from the potential minimum the bound state energy comes the less is the suppression of the momentum tails relative to the pointlike case. This implies that, for the heavy tau, pair production with K-shell capture on a high-Z nucleus is less probable than production with L-shell capture on the same nucleus, easily by an order of magnitude, and, also less probable than production with K-shell capture on a light nucleus, again easily by an order of magnitude. However, total bound-free pair production cross sections for the tau still seem to be well below 10^{-41} cm^2 for any nucleus.

As detailed above, the cross section for direct bound-free tau pair production is extremely small putting it out of reach of any experimental measurement. Alternative production mechanisms may hence be considered. One possibility is photoproduction of free pairs in a solid target with subsequent moderation and/or capture of the negative lepton possibly terminated by a cascade to the ground state. The very low cross sections for bound-free tau pair production discussed above (cross sections are low on the scale of the square of the Compton wavelength for the tau) reflect the difficulty of the bound-state wave function

to accommodate a momentum of order unity, $q \sim m_\tau c$. If this excess momentum instead is transferred to a third partner, the suppression of the cross section may come out less severe than, for example, the 15 orders of magnitude quoted above — even though the process will be of higher order. Hence alternative production mechanisms could involve an additional scattering event (rescattering for example) or production on individual nuclear constituents. In the latter case of incoherent production the excess momentum is taken by a single nucleon, which leaves the nucleus, and the negative tau is bound in a state around the new nuclear fragment. Such processes await further consideration. See the original publication (Belkacem and Sørensen, 1998) for further comments.

C. Ionization

In the previous subsection II.B it was seen that pair production can result in the change of the charge state of the target via direct capture to a bound state of the produced electron. In the following it is investigated how pair production can alter the state of an atomic target by direct ionization of a bound state electron.

Photoionization of an atom or an ion is one of the most basic charge changing mechanisms in atomic collisions. Ionization may proceed through the photoelectric effect or Compton scattering. For discussion of these processes as well as display of useful formulas the reader is referred to standard books (Berestetskii *et al.*, 1989; Heitler, 1954; Jauch and Rohrlich, 1980) as well as review articles (Pratt *et al.*, 1973). A useful tabulation is given by Hubbell *et al.* (1980). A tabulation of theoretical cross sections for the photoelectric effect in hydrogenlike systems has been published recently (Ichihara and Eichler, 2000).

At MeV photon energies and beyond the cross sections associated with both the photoeffect and Compton scattering drop off. The cross sections decrease with increasing photon energy ω essentially as $1/\omega$ whereby they become quite small in the highly relativistic energy regime. However, a new ionization channel opens up at MeV energies (Ionescu *et al.*, 1999): When the photon energy exceeds twice the rest mass of the electron plus the binding energy of the active atomic electron,

$$\omega > \omega_{tr} \equiv 2 + E_B \ , \tag{33}$$

the negative energy continuum will play an additional important role; photoionization of, say the K-shell, can now proceed through a new channel in which the photon energy is

shared between the K-electron and one of the negative-energy electrons. The final result is the creation of the K-vacancy along with an electron-positron pair. At highly relativistic energies the cross section of this new photoionization process becomes larger than the cross section of photoionization through Compton scattering or the photoelectric effect (Ionescu *et al.*, 1999). The channel has been named *vacuum-assisted photoionization.*

In vacuum-assisted photoionization an inner-shell electron may be freed by electron-electron (positron-electron) interaction or by photon-electron interaction. An example of the first situation is pair creation in the field of the atomic nucleus followed by knock-out of the inner-shell electron by one of the outgoing particles of the produced electron-positron pair. An example of the second situation is pair creation directly on the inner-shell electron giving it a recoil sufficiently large that it leaves the scene. The nucleus is not needed to propel this action. These two examples are discussed below in some detail together with the annihilation channel. Additional channels exist but contribute less to the cross section (Ionescu *et al.*, 1999).

1. Pair creation with $e^{\pm}$-e^{-} encounter

Succeeding a pair-creation event in the field of an atomic nucleus of charge Ze, the outgoing electron or positron is assumed to collide with an inner-shell electron and transfers an energy to it which is larger than its binding energy. Extensive calculations are required to determine the corresponding cross section according to the standard rules of quantum electrodynamics. Such calculations were not attempted in the original publication (Ionescu *et al.*, 1999). Instead a simple semiclassical model was applied which allowed for estimates of cross sections:

In the simple model, the electron and the positron are created with equal probability anywhere inside a sphere of radius equal the Compton wavelength of the electron and centered at the nucleus. No correlation between the points where the electron and the positron first appear is assumed and also any interaction between the two is neglected. Hence the probabilities for knocking out a bound electron is computed independently and added. From the point of first appearance each member of the pair is assumed to leave the scene on a straight path and the change in kinetic energy which classical mechanics would dictate due to motion in the background potential of the nucleus is ignored. For each of them, the

probability for knocking out a bound electron is determined by the local electron density along the path (as defined by the quantum state of the target atom) and the cross section for transferring an energy larger than the binding energy E_B. Since relatively large energy transfers are of interest, the cross section for collisions between free particles, that is, the Rutherford cross section, is applied (the finer details accounted for in the Møller and the Bhabha cross sections are neglected). The annihilation channel open to the positron when it encounters a target electron is discussed separately in Subsec. II.C.3.

In this model the cross section for vacuum-assisted photoionization is related to the cross section σ_{PP} for pair production in the field of the nucleus by the simple relation

$$\sigma_1 = \sigma_{PP} \times P \ , \qquad P = P_+ + P_- \ . \tag{34}$$

For the pair-production cross section the Bethe-Heitler result, pertaining to the Born approximation, is applied, Subsec. II.A. The quantities $P_\pm$ signify the knock-out probabilities for the electron and the positron. After averaging over points of creation, emission directions, and emission energies for the created particles Ionescu *et al.* (1999) obtain the following estimate for the total knock-out probability for energies not too close to threshold, that is, for energies typically beyond $2\omega_{tr}$,

$$P \simeq 2 \times \frac{(\alpha^2 Z)^2}{1-s} = 2 \times \frac{(\alpha^2 Z)^2}{1-[1-(\alpha Z)^2]^{1/2}} \ . \tag{35}$$

For $\alpha Z \ll 1$, the probability is $4\alpha^2$ and it changes only slightly for heavier elements ($0.90 \times 4\alpha^2$ for $Z = 82$). In other words the estimate for P is essentially Z-independent and well approximated as

$$P \simeq 2 \times 10^{-4} \ , \qquad \omega \gtrsim 2\omega_{tr} \ . \tag{36}$$

For energies below, roughly, twice the threshold energy some variation with photon energy is predicted. At such energies asymmetries in the pair production (neglected in the simple model) may furthermore be of some effect. Both estimates (35) and (36) are per electron in the K-shell.

With an essentially Z- and energy-independent probability, the estimate (34) for the cross section for pair creation with K-shell ionization, when the latter appears through electron-electron or positron-electron interaction, depends on atomic number and photon energy essentially as the Bethe-Heitler cross section for pair creation. Hence a Z^2-scaling is expected as well as a saturation of the cross section at high photon energies.

Estimates of the ionization of electrons bound in shells other than the K shell were also given by Ionescu *et al.* (1999). For an electron bound in a state of main and orbital angular quantum numbers n and l, the estimate corresponding to (36) is

$$P_{nl} \simeq \frac{2 \times 10^{-4}}{n(2l+1)} , \tag{37}$$

again for energies not too close to threshold. As before the estimate is per electron in the particular state. With (37) the total probability for any completely filled shell is

$$P_{shell} \simeq 4 \times 10^{-4} , \qquad \omega \gtrsim 2\omega_{tr} . \tag{38}$$

For the case of lead or gold the total probability for ionizing the atom following a pair creation event would hence end up near 1.8×10^{-3} in this simple model.

2. Pair creation in the field of a bound electron

Ionescu *et al.* (1999) also applied a relatively simple model for the calculation of the vacuum-assisted ionization due to pair creation directly on the active bound atomic electron. The model is based on knowledge of the recoil-momentum distribution for pair creation in the field of a free electron. Binding is imitated through a simple restriction on the recoil momentum. The hard part is to obtain the cross section differential in the recoil momentum.

With the cross section differential in recoil momentum at hand for pair creation on a free electron, $d\sigma_e/dq$, the contribution to the vacuum-assisted ionization due to pair creation directly on the active bound atomic electron is approximated as

$$\sigma_2 = \int_{q_{cut}}^{q_M} dq \frac{d\sigma_e}{dq} . \tag{39}$$

Here the minimum momentum transfer is chosen as

$$q_{cut} = \sqrt{(1+E_B)^2 - 1} , \tag{40}$$

where E_B is the binding energy of the atomic electron. The cut at the value (40) mimics the requirement of energy transfers being sufficiently large for ionization to occur. The maximum momentum transfer on the other hand is determined by kinematics. It reads

$$q_M = \frac{k(k-1) + (k+1)\sqrt{k(k-4)}}{2k+1} . \tag{41}$$

Note that kinematics requires a photon energy in excess of 4 units for the process to proceed. It is a good approximation to apply the so-called Borsellino expression for the differential cross section $d\sigma_e/dq$ in the expression (39) for σ_2 (Ionescu *et al.*, 1999).

3. Pair creation with subsequent annihilation

Positron annihilation is an additional source of vacancy production. Following the initial conversion of the incoming photon into an electron-positron pair, the positron may well subsequently annihilate on an inner-shell electron. The final product is an atom with an inner-shell vacancy, and an electron and two photons leaving the scene. This channel was analyzed by Ionescu *et al.* (1999) in yet a simple model corresponding to that discussed above in Subsec. II.C.1.

Assume the initial photoconversion to happen in the field of the atomic nucleus. All that is needed in order to estimate the relative strength of the annihilation channel is then an estimate of the probability P_{ann} that the positron, once created, will annihilate with an inner-shell electron. The ratio of P_{ann} to the knock-out probability of Eqs. (35–36) and (37) will provide the estimate of the relative strength of the annihilation channel.

By the assumption of annihilation being a localized event requiring the annihilation partners to be at the same spot in space, the annihilation probability assumes a form similar to the knock-out probability. The density factor is the same as before whereas the basic cross section no longer is the Rutherford cross section but rather the cross section for (two-photon) annihilation of a non-relativistic positron on a free electron at rest which reads (Heitler, 1954)

$$\sigma_{ann}^{rest} = \pi\alpha^2/v_+ \ . \tag{42}$$

Here v_+ is the speed of the positron. By the assumption that the same expression holds for annihilation on an electron in bound motion only with replacement of the positron velocity by the relative positron-electron velocity an upper limit of the contribution due to annihilation on a K-electron is obtained by replacing v_+ in Eq. (42) by $\langle p^{-1}\rangle_{1s}$.

Comparison of the cross-section factors shows that, in general, the cross section σ_3 for vacuum assisted K-shell vacancy production via annihilation is relatively small compared

to σ_1, their ratio being limited approximately as

$$\frac{\sigma_3}{\sigma_1} < \frac{2}{3\pi}\alpha Z \ . \tag{43}$$

For a lead target, the right-hand side amounts to, roughly, 1/8. In conclusion, the magnitude of σ_3 seems nowhere substantial compared to σ_1.

4. Results

Figure 11 shows the cross section for creation of a K-shell vacancy in lead (Z=82) for different photoionization processes. Tabulated values (Hubbell *et al.*, 1980) are used to plot the curves for the photoelectric effect and Compton scattering. The cross section σ_1 is obtained by application of Eq. (34) with tabulated values (Hubbell *et al.*, 1980) for the nuclear pair production cross section and a probability corresponding to (35) but accounting also for the variation close to threshold. For the cross section σ_2 associated with pair creation in the field of a bound electron Eqs. (39–41) are used. Due to its smallness the contribution from the annihilation channel is not displayed. Note that the cross sections are given per electron; to account for both K-shell electrons it is necessary to multiply by a factor of 2. From Fig. 11 it is seen that the cross section for the creation of a K-vacancy in Pb at photon impact energies below 1 MeV is dominated by the photoelectric effect. However with increasing photon energy the photoelectric cross section first decreases as a high negative power of the photon energy and then (above roughly 10 MeV) as the inverse of the photon energy, the high-energy asymptote being given by (19) in the perturbation limit (for two electrons in the K-shell). The Compton cross section exhibits a slightly slower fall off. In contrast, the contribution from vacuum-assisted photoionization increases with increasing photon energy, starting from a threshold of approximately 1 MeV for σ_1 and 2 MeV for σ_2, so as to outnumber the other processes at high energies. At 1 GeV, 90% of the cross section for creating a K-vacancy is due to contributions from vacuum-assisted photoionization. The contributions from σ_1 and σ_2 saturate at 7.5 mb and 2.5 mb, respectively.

Among the channels for vacuum-assisted photoionization pair production in the nuclear field followed by electron-electron or electron-positron interaction (σ_1) provides the largest contribution to the cross section for the creation of a K-shell vacancy in Pb according to the simple models, cf. Fig. 11. The situation is different for targets of low and medium atomic

number. Here the largest contribution to the cross section comes from pair production in the field of a bound electron (σ_2). The dependence on the atomic number of the target is illustrated in Fig. 12. Pair production on a bound electron dominates for low-Z targets but decreases steadily with increasing Z as a consequence of the increased binding energy which requires higher and higher momentum transfer to free the electron. The contribution from pair production in the nuclear field followed by electron-electron or positron-electron interaction increases almost as the square of the nuclear charge and consequently dominates for high-Z atoms. Unlike the individual contributions, the sum of the cross sections of the two mechanisms, neglecting any possible interference, changes by at most 30% over the whole range of atomic targets and exhibits a broad minimum around Z=20.

For higher shells the contributions to photoionization from the photoelectric effect, Compton scattering, and pair production are very different. The photoelectric effect brings almost no contribution to the creation of a vacancy in the higher-shells while the probability for Compton scattering is proportional to the number of electrons in that shell. The contribution from vacuum-assisted photoionization is somewhat more complicated to assess because of the very different behavior of the mechanisms that contribute to the total cross section. As can be seen from Eq. (38), the probability to create a vacancy in any filled shell through the first mechanism (σ_1) approximately does not dependent on the shell according to the simple model. For the second mechanism (σ_2) the probability to create a vacancy in a filled shell increases somewhat faster than in proportion to the number of electrons in the shell: The contribution to the cross section for each electron is comparable to σ_2 for a K-electron although somewhat larger due to smaller binding energy (smaller q_{cut} in Eq. (39)). The bottom line is that also for shells beyond the K-shell vacuum-assisted photoionization is the most probable source of ionization for photon impact at high energies.

5. *Experiment*

Experimental studies of vacuum-assisted photoionization necessitate not only measuring the pair production rate but also probing the state in which the target is left. Because of this difficulty it is only in the last couple of years that experimental measurements have been reported in the literature (Dauvergne *et al.*, 2003). The recent experimental work was carried out at the European Synchrotron Radiation Facility (ESRF). The high-energy

photons (0.7 - 1.5 GeV) are produced at the GRAAL beam line by Compton backscattering of laser photons off the 6 GeV electrons of the ring. A sketch of the layout is shown in Fig. 13. The expanded insert in Fig. 13 shows some details of the target and detection area. A thin scintillator B1 of large area set upstream from the target is used as a veto of any event that involves a charged particle impinging directly on the target. The high-energy electron and positron created in the Au and Ag foils fly downstream along the same direction as the initial photon. Electron-positron pairs created in the target are detected by a thin scintillator B2. An amplitude analysis of the response of a thicker scintillator detector B3 allows the selection of events in which two relativistic charged particles (e^+ and e^-) are created simultaneously in the target.

A signature of vacuum-assisted photoionization is given by a simultaneous detection of a K- or L-vacancy with the production of an electron-positron pair. The pair is detected with scintillator B3 and the inner-shell vacancy is detected through its characteristic K_α or K_β lines when the vacancy is filled. A large area x-ray germanium detector is used for that purpose. Figure 14 shows a typical x-ray spectrum for a Ag target. The corresponding pulse height spectrum of the pair detector B3 is shown in Fig. 14b. It exhibits well separated peaks for one- and two-particle contributions. The one-electron peak is correlated mostly to the background seen by the Ge detector and is likely due to Compton scattering in all the surrounding material. The two-particle peak is strongly correlated with the K_α and K_β lines. The interest here is to extract the contribution of vacuum-assisted photoionization that is the process in which both inner-shell vacancy and pair creation take place on the same atom.

Figure 15 shows the variation of the absolute probability for inner-shell vacancy production in coincidence with pair production for Au (K- and L-shell) and Ag (K-shell), as a function of target thickness. The process that involves two different atoms varies as the square of the target thickness; it dominates for the thick targets. A clear departure from the quadratic dependence is seen for the thin targets. The finite linear term of the fit gives a measure of vacuum-assisted photoionization. Table II summarizes the cross sections extracted from the fits. The theory values of vacuum-assisted photoionization include contributions from σ_1 and σ_2 discussed in the theory section. The experimental value appears to be slightly smaller than theory for Au K-shell. This may be an indication that the contribution of σ_1 that involves pair creation on the nucleus is smaller than predicted by the simple

calculation presented in the theory section. However the error bars of this measurement are large and further experimental studies are needed to draw any definitive conclusion on the relative contributions of the various mechanisms that lead to the ionization of the target via pair production.

6. Remarks

The most important prediction of the calculations on vacuum-assisted photoionization — confirmed by the experiment — is that vacuum-assisted photoionization will dominate the other known photoionization processes at high energies. An interesting parallel can be made with capture from pair production which dominates charge transfer in relativistic heavy ion collisions. Both results highlight the crucial role that the negative energy continuum plays in the relativistic regime in atomic collision processes.

There are many physics insights to be gained from the somewhat simple models presented here. However, there are also some serious limitations of the calculations. Several approximations and simple models were built into the theory to make the calculation of cross sections somewhat tractable. One of the limitations is the use a semiclassical picture for calculating σ_1 which neglects any interference between the creation of the pair and the subsequent electron-electron or electron-positron interaction. This is obviously a gross approximation that is probably quite inaccurate for high-Z atoms since the size of the K-shell is comparable to the volume in which the pair is produced. Another potentially important effect not considered in the models as well as an additional limitation may be mentioned:

a. *The Chudakov effect* In calculating σ_1 the actions of the created electron and the created positron were considered independent. However, from the point of creation and on the way out through the atom in which the production occurred, the two leptons move at close distance from each other on the atomic scale. This implies that mutual screening may well be of importance leading to lower knock-out probability, and thereby to a lower cross section, than estimated in Subsec. II.C.1. The effect of mutual screening of an electron and a positron originating from the same pair-creation event has previously been studied for ionization in subsequent atoms, that is, in atoms other than that in whose field the pair is produced. It is sometimes labeled the Chudakov effect after one of those who first looked

at it (Chudakov, 1955; Perkins, 1955). Some references are listed at the end (Burkhardt, 1958; Mito and Ezawa, 1957; Wolter and Miesowicz, 1956; Yekutieli, 1957; Zielinski, 1985).

b. Localization In the simple model applied in Subsec. II.C.1, the electron and the positron are created with equal probability anywhere inside a sphere of radius equal to the Compton wavelength of the electron centered at the nucleus. This assumption may seem somewhat questionable in particular since screening plays an important role in moderating pair production at high energies, that is, in preventing an unlimited logarithmic growth of the cross section with increasing photon energy, Fig. 1. The fact that screening is important at high photon energies means that distances of order the Thomas-Fermi screening length $\simeq \alpha^{-1}Z^{-1/3}$ are of importance at such energies. Ionescu *et al.* (1999) suggested to improve of the distribution in direct space through inversion of the distribution in recoil momentum. It was not tried. Instead they just noted that if the pair creation cross section (for screened nuclei) as given by Ter-Mikaelian (1972), and corrected for misprints, is integrated only over recoil momenta larger than $\alpha Z \simeq 1/a_K$, where a_K is the K-shell radius, the result for impact on a lead target at energies of 100 and 1000 is $0.50\sigma_{BH}$ and $0.39\sigma_{BH}$, where σ_{BH} is the total Bethe-Heitler cross section corresponding to unrestricted integration for the same collision system. So even at such high energies and for such a heavy target the estimate for the density factor as outlined in Subsec. II.C.1 is expected to be good within a factor of, roughly, 2.

III. HEAVY ION IMPACT

In this section we consider heavy-ion induced equivalents of some of the photo-induced processes discussed in Sec. II. Cross sections may be obtained theoretically by various means, some methods being quite involved and others purely numerical. However, having the photo cross sections at hand, first estimates of the cross sections for the ion-induced processes may be obtained through application of a simple scheme. The scheme is the Weizsäcker-Williams method of virtual quanta, also known as the virtual photon method. Standard references are Williams (1935) and Jackson (1975); see also Berestetskii *et al.* (1989) and Ter-Mikaelian (1972). Below, the Weizsäcker-Williams scheme (WW) will be applied to take first bearings of cross sections for the processes to be considered before

more elaborate methods are invoked. The method is of course approximate, but it has the advantage of providing quick estimates and, furthermore, at very high energies it often turns out to be as reliable as much more involved methods. See also the reviews by Berturlani and Baur (1988) and Baur *et al.* (2002).

Consider a relativistic bare ion of atomic number Z_p impinging on a target which, depending on the process under consideration, could be another bare ion, an atom, or otherwise. The projectile is assumed to move on a rectilinear path at a constant velocity v throughout the collision and the electromagnetic field which it generates at the position of the target or "struck" system upon passage is ascribed to an equivalent bunch of photons provided the distance of closest approach is beyond a certain minimum, b_{min}. The equivalent photon bunch interacts with the target through previously determined photo cross sections for the corresponding photo process. The quantity b_{min} is specific to the considered process and has to be determined such that the approximations, on which the scheme relies, remain valid. This includes that the action should be perturbative and that the impact parameter b be in excess of the struck system. The latter requirement comes from the assumption of a uniform photon flux over the extent of the struck system corresponding to the electromagnetic field strength of the projectile at a distance b from its rectilinear path. At the same time b_{min} should be chosen such that there is hope for estimating the cross section for impacts closer than b_{min} by other, and preferably simple, means. In the Weizsäcker-Williams approach, the cross section for the ion-induced process hence in general takes the form

$$\sigma_{ion} = \sigma_{close} + \sigma_{dist} \ , \tag{44}$$

where the distant-collision contribution to the cross section corresponding to collisions with impact parameters beyond b_{min} is given in terms of the intensity of the virtual photon bunch, $dI/d\omega$, corresponding to all such collisions and the cross section for photon impact, $\sigma_\gamma(\omega)$, as

$$\sigma_{dist} = \int d\omega \sigma_\gamma(\omega) \omega^{-1} dI/d\omega \tag{45}$$

($\omega^{-1} dI/d\omega$ is the number of photons per frequency bin).

As discussed in various sources the conditions for the applicability of the virtual photon method to pair creation processes in general lead to a requirement of b_{min} being of the order of the Compton wavelength of the created lepton; see e.g. Berestetskii *et al.* (1989). Under certain circumstances additional constraints exist. Fine-tuning of the cut-off parameter

(which has no physical significance) may bring the distant-collision contribution alone to agree with cross sections obtained by other means. Hence, application of the virtual photon scheme to ion-induced pair production most often amounts to the sole determination of the distant-collision contribution (45). As to the apparent neglect of the close-collision contribution it may be noted that with $b_{min} \sim 1$ closer collisions yield momentum transfers in excess of one unit. In this region the cross sections for the photo-induced processes fall off rapidly with increasing momentum transfer leading to an effective maximum momentum transfer of order 1; see Jackson (1975) for a discussion for the closely related case of bremsstrahlung.

The photon spectrum to enter Eq. (45) is obtained by integrating the spectrum $dI(b,\omega)/d\omega$ pertaining to a given impact parameter b over impact parameters in excess of b_{min}, the b-specific spectrum being determined by the Fourier component $\mathbf{E}(\mathbf{b},\omega)$ of the electromagnetic field of the projectile (Jackson, 1975). The result is

$$\frac{dI}{d\omega} = \frac{2\alpha Z_p^2}{\pi v^2}\left[\xi K_0(\xi)K_1(\xi) - \frac{v^2\xi^2}{2}(K_1^2(\xi) - K_0^2(\xi))\right], \qquad \xi = \frac{\omega b_{min}}{\gamma v}, \tag{46}$$

where K_0 and K_1 denote modified Bessel functions of the second kind and the quantity γ is the usual Lorentz-factor $\gamma = 1/\sqrt{1-v^2}$. It is noted that K_0 and K_1 fall off exponentially for arguments larger than 1. By application of the asymptotic expansions of the modified Bessel functions, Eq. (46) reduces to

$$\frac{dI}{d\omega} = \frac{2\alpha Z_p^2}{\pi v^2}\left[\ln\frac{1.123}{\xi} - \frac{v^2}{2}\right] \tag{47}$$

in the limit of small arguments $\xi \ll 1$.

A. Production of free pairs

Formulas for the cross section for creation of free pairs upon charged particle impact as obtained by the Weizsäcker-Williams method may be found in Heitler's book (Heitler, 1954). See also Williams (1935).

The pair creation cross section may be obtained numerically from Eq. (45) by application of a numerically given photo cross section σ_γ and the photon intensity (46). In addition an exact choice for b_{min}, which is known to be of order unity, is now required. The value of the minimum impact parameter may be obtained by fine tuning to results obtained elsewhere. An example of such procedure is given by Ter-Mikaelian (1972) for

bremsstrahlung and photo-induced production of free pairs. At this point it will rather be argued that 0.5 is a good value. For one thing, the effective maximum momentum transfer which Jackson (1975) obtains for bremsstrahlung is 2 which, in turn, corresponds to $b_{min} \simeq 1/2$. A value about 0.5 may also be deduced from the work on bremsstrahlung by Williams (1935): His (34) agrees with Heitler's (33) p. 252 by the choices $A = 4$ and $g = 2\exp(-1/3)$. Furthermore, comparison of Williams' (8) with Jackson (1975) shows that $g = 1.123\exp(-1/2)/b_{min}$. A combination of the two expressions for the quantity g leads to the result $b_{min} = 1.123\exp(-1/2)/[2\exp(-1/3)] = 0.48$.

As a test case consider bare sulphur ions incident on a gold target at an energy of 200 GeV per nucleon corresponding to a γ-value of 215 for which an experimental study has been reported (Vane *et al.*, 1994). A value of 138 barn results when we estimate the pair-production cross section by (45) with the intensity (46), $b_{min} = 1/2$, and the nonperturbative photo cross section tabulated by Hubbell *et al.* (1980). In comparison, Heitler's perturbation formula (20) p. 265 yields 141 barn with the recommended choice $\beta = 1/4$. Vane *et al.* (1994) cite the result of an "exact Monte Carlo evaluation of the two-photon terms in lowest-order QED (MCQED)" (Bottcher and Strayer, 1989), it amounts to 140 barn. The first-order perturbation calculation of Ionescu and Eichler (1993) yields 130 barn. Obviously, all these numbers are close to each other. However, the good agreement must be considered accidental to some extent since the relative scatter in the results is less than, e.g., the relative difference between the perturbative and the nonperturbative photo cross sections for the heavy element, see Fig. 1. The numbers are summarized in Table III.

According to Fig. 1 an estimate of the perturbative pair-production cross section for photon impact on bare nuclei may be obtained by taking the maximum of the numerical value for screened nuclei (Hubbell *et al.*, 1980) and the cross section corresponding to the lower line in Eq. (6). A simple estimate for the pair-production cross section for ion impact on bare target nuclei may hence be obtained from the numerical WW calculation by applying this maximum for the photo cross section σ_γ to enter (45). For 200 GeV/n bare sulphur ions incident on bare gold ions a cross section of 156 barn results. Heitler's expression (19) p. 264 for the unscreened case gives a number which is higher than that obtained from his Eq. (20) for the screened case and quoted above by only a fraction of a per cent. Based on lowest order perturbation theory Racah (1937) produced a closed formula for the cross section for pair creation on a bare Coulomb center, see below. The number obtained with the numerical

WW-scheme agrees well with the 158 barn which may be obtained from Racah's formula quoted as Eq. (54) below. Also these numbers are summarized in Table III.

In the experiment (Vane *et al.*, 1994) only the cross section for production of pairs in which the positron had an energy less than 17 MeV was measured. The result was 85 ($\pm$22) barn. The corresponding numbers obtained in the various theoretical approaches are included in Table III.

As another example consider bare lead ions impinging on a lead target with $\gamma = 168$. For that case the numerical WW scheme described above yields a cross section for pair production of 3.34 kilobarn (atomic target; Heitler's perturbative formula (20) gives 3.29 kilobarn) which may be compared to the number of 3.50 kilobarn cited by Datz *et al.* (1996). Racah's analytical perturbation formula for a bare Coulomb target gives 3.75 kilobarn which again agrees well with the 3.73 kilobarn that is obtained in the numerical WW-calculation for an unscreened target nucleus (procedure described above; Heitler's (19) gives 3.30 kilobarn). The conclusions are as for the sulphur case.

For the relativistic heavy ion collider (RHIC) at Brookhaven the most extreme collision system is head-on collisions of bare gold ions of 100 GeV/u each. The corresponding γ-value is 23050. For this collision system the formula of Racah gives 35.9 kilobarn. In comparison, the numerical WW-scheme gives a value which is lower by only 3%, namely 34.8 kilobarn, with the perturbative photo cross section. It may be noted, that for the γ-value quoted the result for a bare gold ion incident on an atomic gold target is 24.2 kilobarn (with the exact photo cross section), that is, due to the higher energy, the effect of screening is now considerably larger than in the examples discussed above.

While the numerical WW approach is quite successful as demonstrated in all the examples above it is important to realize that the results are sensitive to the exact choice of the cut-off b_{min}. The sensitivity decreases with increasing energy whereby the exact choice is of less importance at high energies (like those of RHIC and LHC), while at moderate energies like those of the CERN experiments performed in the 1990s, see for example Table III, the predictions for the total cross section decrease to about two thirds of the values cited above if b_{min} is increased from 1/2 to 1.

The reader may find lists of references to a wide variety of papers dealing with production of free pairs for charged particle impact elsewhere (Eby, 1989; Wright, 1973).

1. Racah's calculation

As some of the examples above have indicated, Racah's 1937 formula is still competitive with many more recent calculations. On the other hand it is often not applied but just neglected in recent work which in part may be due to the fact that Racah wrote his paper in Italian. The work deserves a few comments.

As formulated by Racah, the problem is to determine the probability that a massive particle of charge Ze, in the presence of a nucleus of charge $Z_t e$, makes a transition from a state of one momentum to another while an electron is excited from a state of momentum $-p_0$ and energy $-w_0$ to one of momentum p and energy w, that is, while a positron of momentum momentum p_0 and energy w_0 and an electron of momentum p and energy w are created.[8]

The steps in Racah's calculation are quite similar to those in the standard calculation of bremsstrahlung and pair production upon photon impact, cf. Heilter (1954). Fermi's golden rule is applied with the transition matrix element determined in the lowest order Born approximation, that is, the second-order approximation. The perturbations are the interaction of the electron with the projectile which is assumed pointlike and with the target nucleus which is treated merely as the source of a static Coulomb potential. The first step is to sum over intermediate states. Next the usual spin sums are taken, that is, sum over final states of the electron and the positron as well as average over initial states of the projectile. Integrations over the directions of the electron and the positron follow. The calculations are purely algebraic and not difficult but, as stated by the author, rather lengthy. A cross section is produced which is differential in the total energy of the created pair ϵ, the energy of the created electron, and the momentum loss of the projectile η.

At this point Racah splits his calculation into two parts according to the energy of the created pair being larger (region I) or smaller (region II) than a certain fixed energy $\overline{\epsilon}$ which fulfills the requirements

$$1 \ll \overline{\epsilon} \ll \gamma \ . \tag{48}$$

Different approximations are applied in the high- and low-energy regimes. In region I masses

[8] In this and the following subsection the naming of momenta and energies of the created particles follows that given in the original paper by Racah. To translate to the nomenclature used elsewhere in this paper the following substitutions should be made: $(w_0, p_0) \to (E_+, p_+)$ and $(w, p) \to (E_-, p_-)$.

of the individual particles are neglected compared to their energies and $|\eta^2 - w^2|$ is neglected compared to w; the latter approximation corresponds to an assumption of momentum transfers being not much larger than 1. Following these approximations the simplified expression for the differential cross section is integrated over η. Before the final integrations over ϵ and w are performed for the high-energy region two additional approximations are invoked: the projectile energy is taken everywhere to equal its initial value $E_0 = \gamma M$ and terms of relative order $(\epsilon/E_0)^2$ are neglected. With this Racah's expression for the cross section for region I reads

$$\sigma_I = \frac{Z^2 Z_t^2 \alpha^4}{\pi} \int_{\bar{\epsilon}}^{E_0} \frac{d\epsilon}{\epsilon} \int_0^1 \overline{Z_I} d\left(\frac{w}{\epsilon}\right) \tag{49}$$

where

$$\begin{aligned}\overline{Z_I} = \frac{2}{3}\left[3 - 4\tau + 4(1-\tau)\tau z\right] \times \left[\left(2l_0 + \ln\tau - \frac{1}{2}\ln\frac{1+\tau z}{\tau z}\right)\ln\frac{1+\tau z}{\tau z} - R\left(\frac{1}{\tau z}\right)\right] \\ -\frac{8(1-\tau)}{3}(2l_0 + \ln\tau - 1) + \frac{2}{3}(1-\tau z)\ln\frac{1+\tau z}{\tau z} + \frac{2}{3} \\ +\frac{8\tau}{3(1+\tau z)}\left(2l_0 + \ln\tau - \ln\frac{1+\tau z}{\tau z} - 2\right) .\end{aligned} \tag{50}$$

Here the parameters z and τ are defined as

$$z = (\epsilon/\gamma)^2 , \qquad \tau = w w_0/\epsilon^2 \tag{51}$$

and the function R is given by the expression

$$R(x) = \int_0^x \frac{\ln(1+y)}{y} dy . \tag{52}$$

(Heitler (1954) uses the symbol $F(x)$ in place of $R(x)$ and gives the expansion for small arguments as well as a transformation formula linking the values of the function evaluated at x and at $1/x$; see p. 252.) The bar over the quantity Z_I is a reminder of the last two approximations performed. By changing the order of integration, that is, by first performing the integration over the total pair energy and subsequently over the distribution of the energy among the created particles Racah obtains the result

$$\begin{aligned}\sigma_I = \frac{Z^2 Z_t^2 \alpha^4}{\pi}\left[\frac{28}{27}(l_0^3 - 3l_0 l^2 + 2l^3) - \frac{178}{27}l_0^2\right. \\ +\frac{436}{27}l_0 l - \frac{86}{9}l^2 - \frac{406}{27}l_0 + \frac{1622}{81}l \\ \left.+\frac{7\pi^2}{9}(l_0 - l) - \frac{6643}{243} + \frac{10}{27}\pi^2 + 7S\right] .\end{aligned} \tag{53}$$

Here $l_0 \equiv \ln(2\gamma)$ and $l \equiv \ln(2\overline{\epsilon})$ while the quantity S is defined by the prescription $S = \sum_{n=1}^{\infty} n^{-3}$ and amounts to 1.202... (S may be expressed in terms of Riemann's ζ-function as $S = \zeta(3)$.)

In the determination of the contribution from the low-energy region II Racah no longer neglects the electron mass in comparison with the energies of the electron and the positron. On the other hand, the mass of the projectile is still neglected in comparison with its energy, and its loss of momentum and energy is ignored. The calculation is lengthy and relatively complicated, and since the low-energy region turns out to contribute only a minor part of cross section solely the combined result for regions I and II will be revealed here: Racah's result for the total cross section, which applies for bare collision partners, reads

$$\sigma = \frac{Z^2 Z_t^2 \alpha^4}{\pi} \left[\frac{28}{27} l_0^3 - \frac{178}{27} l_0^2 + \frac{370 + 7\pi^2}{27} l_0 - \frac{116}{9} - \frac{13}{54}\pi^2 + \frac{7}{9} S \right] . \tag{54}$$

Note that this total cross section, Eq. (54), is independent of the dividing energy $\overline{\epsilon}$ as it should be. The cross section is dominated by the production of pairs of relatively high energy: With the choice $\overline{\epsilon} = \sqrt{\gamma}$, which obviously fulfills the requirements (48), the high-energy contribution σ_I of Eq. (53) amounts to more than 70% of the total cross section σ of Eq. (54) over the interval $10^2 \leq \gamma \leq 10^4$. Figure 16 illustrates the cross sections (53)–(54) obtained by Racah together with a considerably simpler expression quoted by Heitler (1954).

2. Energy loss

When a heavy ion penetrates matter it looses energy through the interaction with target constituents. Over a wide energy range, whose upper end extends far into the relativistic regime, loss of energy appears mainly as a result of excitation and ionization of target electrons. For a nonperturbative theory of the stopping of relativistic heavy ions due to such interactions the reader is referred to the publication by Lindhard and Sørensen (1996).

As the projectile energy is raised to very high values, radiative processes become increasingly important energy-loss channels. In particular the creation of electron-positron pairs and the emission of bremsstrahlung prove important. At sufficiently high energies these processes will account for the major part of the energy loss of a heavy ion. We warn the reader that dramatically different estimates of the pair-production contribution to the stopping

have been published over the years and that the importance of the bremsstrahlung channel has been overestimated in various papers (Sørensen, 2003).

To obtain a formula for the energy-loss rate due to pair production the differential cross section from Racah's calculation may be used. Alternatively, one could think of applying the Weizsäcker-Williams method of virtual photons. However, while the results for the cross sections in the WW-scheme do come out quite close to those produced by Racah's formula (54) as shown above, the virtual photon method produces energy-loss rates which are lower than those obtained on the basis on Racah's cross sections by roughly a factor of 2. This difference is due to exponential suppression of high-energy pairs in the WW-scheme. In comparison Eq. (50) predicts a power-law dependence $\overline{Z_I} \propto 1/z$ for fixed τ.

Since high-energy pairs contribute relatively more to the average energy loss than to the cross section (first versus zeroth moment of the probability distribution), the dominance of the high-energy region I already in the cross section implies that it is safe solely to consider pairs of energy beyond $\overline{\epsilon}$ in the evaluation of the energy-loss rate. Hence an estimate of the energy loss due to pair production may be based on Racah's differential production cross section for region I, Eq. (49). To obtain the energy-loss rate Racah's expression is multiplied by the pair energy ϵ and integrated over the two variables, first ϵ and then w/ϵ. Expansion is performed in the parameter $\delta \equiv \overline{\epsilon}/\gamma$.

It is convenient to express the energy-loss rate due to pair production as[9]

$$-\frac{dE}{dx}^{PP} = \pi Z^2 Z_t^2 \alpha^2 r_e^2 N \gamma m c^2 \, \Lambda \, , \tag{55}$$

where N is the atomic density of the target. To lowest order in δ, the dimensionless quantity Λ then reads

$$\Lambda_0 = \frac{19}{9}(l_0 - 3\ln 2 - \frac{11}{6}) = \frac{19}{9}(\ln\frac{\gamma}{4} - \frac{11}{6}) \, . \tag{56}$$

In an expansion of the form $\Lambda = \Lambda_0 + \Lambda_1 + ...$ the first correction to (56) assumes the value

$$\begin{aligned} \Lambda_1 = \; & \delta \left[\frac{4178}{81\pi^2} - \frac{21}{27} - \frac{248}{27\pi^2} l_0 \right. \\ & \left. + \frac{1}{\pi^2}(\frac{28}{9} l_0 - \frac{446}{27}) \ln\delta^2 + \frac{14}{9\pi^2}(\ln\delta^2)^2 \right] \, . \end{aligned} \tag{57}$$

With the previous choice for $\overline{\epsilon}$ the quantity δ equals $1/\sqrt{\gamma}$.

[9] At this point r_e^2 and mc^2 are kept explicitly to emphasize that the quantity Λ is dimensionless.

Screening of the target nucleus by atomic electrons is important at high energies. In this region higher-order corrections similar to (57) are small and there is no need to worry about screening corrections to such terms. For the lowest-order term screening may be accounted for approximately by applying, at all energies, the following expression in place of (56):

$$\frac{19}{9}\ln\frac{183Z_t^{-1/3}}{1+4e^{11/6}183Z_t^{-1/3}/\gamma} \equiv \Lambda_0^{screen} . \tag{58}$$

Furthermore, pair production on atomic electrons may be accounted for very roughly by multiplying the rates obtained so far by the factor $(1+1/Z_t)$.

Results obtained according to the scheme above compare well with various results obtained more than thirty years ago for muon stopping. In particular, the analytical result for bare target nuclei compares quite well with similar results obtained numerically by Mando and Ronchi (1952), while the simple and approximate procedure for inclusion of screening produces losses which are close to those considered most accurate and reliable in a critical review of the early literature (Wright, 1973). The results also compare well to losses computed by van Ginneken (1986) for muons and protons. Critical remarks on some more recent publications aimed at heavy ion impact have been given elsewhere (Sørensen, 2003).

A recent list of references to theoretical articles dealing with the pair-production contribution to muon stopping may be found in the introduction to the comprehensive tabulation of muon stopping power and range reported by Groom *et al.* (2001). A useful list may also be found in a recent report by the ATLAS collaboration (Amaral *et al.*, 2001) on a precise measurement of the energy losses of 180 GeV muons in iron.

A comparison has been made with the tabulations of Groom *et al.* (2001). In the range 100 GeV to 100 TeV ($\gamma = 10^3 - 10^6$) the simple result obtained by applying (55) with Λ replaced by Λ_0^{screen} of (58) and with the inclusion of the extra factor $(1+1/Z_t)$ agrees with the tabulated data for all elements from hydrogen to uranium within 10%. If the correction (57) is included the 10% agreement extends down to 10 GeV ($\gamma \simeq 100$) where pair production only brings a small correction to the electronic stopping (3% in uranium). This relatively close agreement for all elements and all energies is remarkable since the procedure described amounts to plugging in numbers in a simple analytical formula while the data of Groom *et al.* (2001) are obtained by numerical integration of quite involved expressions, see their Section 4.2 and Appendix B. Furthermore, it is remarkable that the agreement holds down to the very lightest element, hydrogen, where the electron contribution in the present approach

(multiplication by $(1 + 1/Z_t)$) brings exactly half of the total. It may finally be noted that the deviations of the results obtained as described above from those of Groom *et al.* (2001) are quite systematic: in the region around 1 TeV the two sets of results are in general quite close to each other (the point of closest agreement decreases somewhat as the target-atomic number is increased) while the present results undershoot the tabulated data by 8–9% at the highest tabulated energy (100 TeV). A simple empirical correction formula could easily be invented.

Pair production can account for the systematic deviation reported by Datz *et al.* (1996) between experimental energy-loss data and theoretical values for the electronic stopping of bare lead ions in a lead target at $\gamma = 168$ (Sørensen, 2003). Table IV displays the deviations as well as the predictions for the energy loss due to pair production. When converted to the so-called stopping number by dividing out the factor $\frac{4\pi Z^2 e^4}{mv^2} N Z_t$ which appears as a front factor in the ionization energy loss rate, pair production scales linearly with Z_t (in the perturbation limit; up to screening corrections). Clearly, pair production is of just the right magnitude to explain the deviations observed. For the heavier target materials the theory values are very close to the experimental numbers, for the lighter materials the experiment overshoots the rather small theory values (but remember, the correction to the total energy loss is only 1–2 % for the two lightest targets).

In principle also bound-free pair creation, with the electron ending up in a bound state around the incident bare lead ion, contributes to the energy loss. In the laboratory system, the energy of the pair is roughly 2γ, or 172 MeV in the considered CERN experiment (Datz *et al.*, 1996). For lead on lead at $\gamma = 168$ the cross section amounts to roughly 50 barn according to the formula cited in the caption to Table V (when adding 20% to allow for production in shells other than the K-shell). The product of these two numbers leads to an energy loss due to bound-free pair production of 25 keVcm^2/mg. This is only 4% of the experimentally observed deviation of 650 keVcm^2/mg (the latter corresponding to the correction 0.73 to the stopping number entering Table IV). In essence, bound-free pair production is without importance for the projectile energy loss.

Bremsstrahlung emission also contributes to the stopping of heavy ions at high energy. A brief discussion of this matter is given in a previous publication (Sørensen, 2003). An overview of the contribution of the various processes to the stopping of lead ions in a lead target, including a rough estimate of the loss to bremsstrahlung, is provided by Fig. 17. We

note that there are significant differences in the statistics of the processes with the average energy loss due to bremsstrahlung having substantial support from rare high-loss events.

3. Multiple pairs

Production of multiple pairs becomes significant for close collisions of heavy ions at high energies. The situation has been analyzed elsewhere (Rhoades-Brown and Weneser, 1991). However even at RHIC and LHC energies where the γ-factor in an equivalent fixed-target experiment reaches as high as 2×10^4 and 3×10^7, respectively, multiple production is only significant at distances of order the Compton wavelength even for the heaviest collision partners: For Au on Au at the maximum RHIC energy, an average of 1.4 pairs is expected per interaction at an impact parameter of 1 unit. For Pb on Pb at the maximum LHC energy, an average of 5.2 pairs is expected at an impact parameter of 1 unit dropping to 1.0 pairs already at 2.2 units.[10] Values for the weighted cross section $\sum_N N\sigma_{Npair}$ as well as for the N-pair cross sections σ_{Npair} for the two examples may be found in the cited publication (Rhoades-Brown and Weneser, 1991).

B. Production of bound-free pairs

Bound-free pair production in heavy ion collisions is a process in which the electron of the pair is created directly in a bound state of one of the colliding ions. The process can take place between two bare ions, resulting in a charge change of one of the ions. This charge changing mechanism is a major contributor to beam loss at relativistic heavy ion colliders (Fatyga *et al.*, 1990). Bound-free pair production was also used at CERN to produce the first antihydrogen atoms (Baur *et al.*, 1996). The photo cross sections reported in Subsec. II.B may be applied in a Weizsäcker-Williams construction to estimate the contribution to bound-free pair production in heavy-ion collisions. Such procedure was followed in previous publications for electron-positron pair production (Agger and Sørensen, 1997) as well as for

[10] It may be of interest to the reader to know that at an impact parameter of 1 unit the average number of pairs produced per interaction in the two cases of moderate energy discussed above are both below 1: for sulphur on gold at $\gamma = 215$ the value is as low as 0.01, while for lead on lead at $\gamma = 168$ a value of 0.33 obtains.

the production of pairs of heavy leptons (Belkacem and Sørensen, 1998). Corresponding accounts will be given in the first and the last of the four subsections to follow. The second subsection highlights the experimental evidence for production of bound-free electron-positron pairs, while the third subsection is devoted to a discussion of nonperturbative effects in bound-free pair production for charged particle impact.

1. Production of electron-positron pairs

As discussed in the introduction to Sec. III the WW-method demands that the impact parameter b be in excess of the extension of the struck system. As for the case of inner-shell ionization, this implies that b_{min} cannot be smaller than the radius of the considered shell (Williams, 1935). The contribution from close collisions has to be estimated by other means. However, at high energies, the total cross section is dominated by the distant-collision contribution.

Agger and Sørensen (1997) considered charged particle impact on bare heavy ions with Z-values of 79, 82, and 92. For production of K-shell electrons the minimum impact parameter was chosen as b_{min}=2 since this length essentially reflects the radius of the K-shells for the three selected target ions. The value is twice that chosen by most other authors who select the Compton wavelength for b_{min} irrespectively of the actual width of the electronical orbit. In Fig. 18 the resulting distant collision contribution to the pair production cross section is displayed as a function of the γ-value of the projectile. In Table V the results are compared to another set of values also obtained with the virtual photon method (Aste *et al.*, 1994) as well as to results of other calculations (Baltz *et al.*, 1994; Becker *et al.*, 1987). The latter are perturbative in the projectile field but based on exact Coulomb waves for the target states. Cross sections obtained by Agger and Sørensen (1997) with b_{min}=1 are included as well. It is noted that with the latter choice, the numbers of Aste *et al.* (1994) are essentially reproduced and that, by chance, the results obtained by the choice b_{min}=1 essentially equal the sum of the results for b_{min}=2 and an estimate of the contribution for closer collisions. Furthermore, the Born cross section for the distant collisions, obtained by taking the difference between the last two columns in Table V, is close to the value for b_{min}=2 at all three energies.[11]

[11] In a recent publication (Meier *et al.*, 2001) a comparison is given between results obtained from various sources for Au on Au at the highest energy presented in Table V. Among the results are numbers taken

It may be noted, that in view of the shell ratios displayed in Fig. 7 ion-induced bound-free pair production is increased by roughly 20% beyond the values displayed in Fig. 18 and Table V when production of L-electrons is included. Inclusion of all shells beyond the L-shell may well contribute an additional 10%.

2. Experiment

[12]The first bound-free pair production measurements were reported in the mid 1990s by Belkacem and coworkers (Belkacem *et al.*, 1998, 1993, 1994). These measurements were performed with 10.8 GeV/n Au^{79+} ($\gamma = 12.6$) at the Brookhaven National Laboratory's Alternating Gradient Synchrotron and with 1 GeV U^{92+} and La^{57+} at the Lawrence Berkeley National Laboratory's Bevalac. The experimental set up used at both facilities is similar. The signature of bound-free pair production is given by the detection of a positron emitted at the target in coincidence with charge change of the bare ion projectile to a hydrogen-like ion. The positrons emitted at the target are magnetically guided and separated from the many electrons scattered from the target by the projectile. This is done with a magnetic spectrometer shown in Fig. 19 (Belkacem *et al.*, 1997). The positron is detected and its kinetic energy, which extends to beyond 10 MeV for the highest impact energy, is measured by a plastic scintillator-photomultiplier detector. The positron annihilates in the plastic scintillator, producing a pair of 511 keV photons. One of the photons is detected by a NaI-photomultiplier detector located behind the plastic detector.

The measured cross section for $\gamma = 12.6$ Au ions is shown in Table VI and compared to perturbative results by Becker *et al.* (1987). A reasonably good agreement is achieved by

from the article by Agger and Sørensen (1997) and scaled with Z^5; this leads to the quoted values of 77 barn ($b_{min} = 2$) respectively 85 barn ($b_{min} = 1$). However, the correct scaling is with $Z^5 f(Z) f(Z)$ where $f(Z)$ is defined by Eq. (26). This gives 87 barn with $b_{min} = 2$ respectively 96 barn with $b_{min} = 1$. Assuming the latter choice of b_{min} again to compensate for the close-collision contribution the estimate of the total cross section is 96 barn. This is close to the value which the authors obtained with their own scheme; 94.6 barn.

[12] In this singular subsection Z_t is used for the atomic number of the collision partner that does not pick up the electron from the created electron-positron pair while Z_p is associated with the charge-changing partner. The notation follows that in the literature on experimental studies of bound-free pair production in heavy ion collisions and has its roots in the fact that in the experiments the physical target is the supplier of the perturbing fields while the bare incoming projectile nucleus is the one that catches the electron.

the perturbative approach for all targets. As seen in the previous subsection the Weizsäcker-Williams method is expected to yield good numbers at high energies but the uncertainty in the scheme is substantial at these low energies since close collisions bring a large fraction of the cross section.

Figure 20 shows the reduced cross sections (measured cross section divided by Z_t^2, where Z_t is the target atomic number). A least-squares fit to the data gives a dependence of $Z_t^{1.93}$ which is in good agreement with Z_t^2 expected both by perturbation theory and the Weizsäcker-Williams approach.

Figure 21 shows the positron energy spectra for bound-free pair production for a 0.96 GeV/n U^{92+} beam on Au. The "forward" label in the figure refers to the integrated yield of positrons emitted in the forward direction up to an angle of 75°. The "backward" label refers to positrons emitted in the backward direction. The positrons emitted in the transverse plane (between 75° and 105°) are missed by the detection system. The data are taken simultaneously and therefore are normalized to the same number of incident uranium ions. As seen in the figure, even at these low collision energies, the positron is more likely to be emitted in the forward direction than in the backward direction. Both these results and the results taken at $\gamma = 12.6$ are consistent with $1/\gamma$ opening angle for the positron emission. The spectra in Fig. 21 show a lack of low energy positrons. This is due to the repulsion of the positrons by the Au target nuclei at rest in the laboratory frame. The "forward" positron energy spectrum displays a broad maximum around 800 keV while the "backward" spectrum displays a maximum around 400 keV. Figures 22 and 23 show the spectrum of positrons emitted in the forward direction for La^{57+} on Au and U^{92+} on Cu. The spectra exhibit the same general features as in Fig. 21 which shows that at these energies the projectile and target atomic number have little or no effect on the shape of the positron spectrum. Figure 24 shows the energy spectrum for free-free pair production (1.3 GeV/n La^{57+} on Au). Here again the spectrum displays the same general features as in bound-free pair production.

Figure 25 gives the angular distribution of the positron yield with respect to the beam direction integrated over positron energy. The distribution exhibits a maximum of the yield between 30° and 45°, which agrees roughly with a maximum at $1/\gamma$ angle. The total cross section (after integration over energy and angle) for bound-free pair production for U^{92+} on Au is 2.19 ± 0.25 barn. The perturbative result yields a value of only 1.01 barn. The measured total cross section for free-free pair production is 3.3 ± 0.65, a value that is only

slightly larger than the bound-free value. The ratio of free-free to bound-free pair production increases very rapidly and reaches several orders of magnitude at RHIC and LHC energies.

An important feature of bound-free pair production and free-free pair production is the dependence of their cross section on the atomic number of the target and projectile. Fig. 26 shows the reduced cross section of free-free and bound-free pair production as a function Z_t for 1.3 GeV/n La^{57+}. A Z_t^2 dependence is represented by the horizontal lines. Free-free pair production appears to follow a Z_t^2 dependence while bound-free pair production has a slightly stronger dependence (closer to Z_t^3) as evidenced by the positive slope. A comparison of the cross section measured at 0.96 GeV/n for La^{57+} and U^{92+} on Au yield a dependence of the bound-free pair production on the projectile atomic number of $Z_p^{6.54\pm0.65}$. In contrast, free-free pair production exhibits a dependence between Z_p^2 and Z_p^3. The difference between the calculated and measured total cross sections and Z-dependence is a strong indication of nonperturbative effects.

3. Nonperturbative calculation

In the early 1990s calculations by Rumrich *et al.* (1991) showed strong nonperturbative effects for production of bound-free electron-positron pairs in heavy-ion collisions. The predictions of enhancements over perturbation theory by orders of magnitude in certain cases (generally close collisions at moderate energy) were based on numerical calculations. However, as these numerical methods had obvious limitations a new approach was called for in order to decide on the actual magnitude of nonperturbative effects.

The coupled-channel calculation by Rumrich *et al.* (1991) which initially prompted much interest was questioned for being based on a too small basis set which could well cause an overestimation of the bound-free PP channel. Other calculations were based on so-called grid methods in configuration space. A common problem of these grid methods is the fact that the electron density in configuration space dissolves during the collision from the initially well-localized bound state (a time-reversed calculation is performed) because continuum components of the wave function arise due to the ionization and transfer reaction and "spread" over large and ever expanding volumes in configuration space. At the boundaries, however, the values of the wave function have to be set to zero. Therefore, the propagation in time has to be stopped as soon as nonnegligible components of the wave function are

beginning to "hit the wall".

In the mid 1990s a method that essentially removes the boundary-condition problems was presented (Momberger *et al.*, 1995, 1996). The trick is to solve the time-dependent Dirac equation in momentum space. In momentum space continuum states are strongly localized exactly like bound states. The same is true for the time-evolved electron wave function. The Dirac equation is solved on a grid within a finite volume. If the volume in momentum space is sufficiently large, the values of the wave function can, in a very good approximation, be set to zero at the boundaries of the grid. Furthermore, the method yields information not only on bound-free pair production but at the same time also on inner-shell ionization, excitation, and electron transfer: everything is computed in one shot, and to extract information on a specific atomic process is only a question of performing a suitable projection of the terminal electron density.

In the calculation a point-like projectile of charge $Z_p e$ is assumed to travel on a rectilinear path at constant speed v along the z-axis and at impact parameter b along the x-axis relative to a stationary hydrogen-like system of nuclear charge $Z_t e$. The one-electron Dirac equation for the electron interacting with the two nuclei then takes the following form in momentum space (within the Lorentz-gauge)

$$\begin{aligned} i\frac{\partial}{\partial t}\psi(\mathbf{k},t) &= [\boldsymbol{\alpha}\cdot\mathbf{k}+\beta]\,\psi(\mathbf{k},t) \\ &+ \frac{1}{2\pi^2}\int d^3k' \left[-\frac{Z_t e^2}{q^2}\right]\psi(\mathbf{k}',t) \\ &+ \frac{1}{2\pi^2}\int d^3k' \left[\frac{-Z_p e^2(1-v\alpha_z)\; e^{i(q_x b+q_z vt)}}{(q_x^2+q_y^2+q_z^2/\gamma^2)}\right]\psi(\mathbf{k}',t)\ , \end{aligned} \tag{59}$$

where $\mathbf{q} = \mathbf{k}' - \mathbf{k}$ denotes the momentum transfer ($\boldsymbol{\alpha}$ and β are the Dirac matrices). As initial state for the calculation the hydrogenic $1s$-state is chosen. After propagation through the collision, projection of the time-evolved electron state on other bound states of the target system gives atomic excitation probabilities while projection on bound states of the projectile gives probabilities for charge transfer. Projection of the final state onto the continuum states of positive and negative energy (that is, continuum Coulomb-Dirac states centered on the target nucleus) yields the probabilities for ionization and bound-free pair production, respectively (after suitable correction for the transfer channel). Details on the calculational procedure may be found elsewhere (Momberger *et al.*, 1996).

Momberger *et al.* (1995, 1996) give examples of results obtained with the numerical momentum-space method. One case considered is the collision of a bare gold ion with a kinetic energy of 0.24 GeV per nucleon with a stationary hydrogenlike uranium ion in the ground state. The energy is selected such that the projectile velocity matches closely the velocity of the target electron in the bound state. Accordingly, a large probability for charge transfer is obtained in the calculation. The wave function of the electron, which in the initial state is localized around the origin, is after propagation through the collision mainly localized around a momentum corresponding to the projectile velocity where it also peaks. A Fourier transform of the wave function to configuration space shows explicitly how a peak develops around the projectile during the collision and travels with it out from the target area.

Another example of more interest for bound-free pair production is bare gold ions of kinetic energy of 0.93 GeV per nucleon again incident on a stationary hydrogenlike uranium ion in the ground state. In this case the energy is selected to match experimental conditions, discussed in the previous subsection. The evolution with time of a collision with vanishing impact parameter is shown in Fig. 27. The propagation in time has been performed from $t = -30$ to $t = 20$. At $t = -5$ (first picture) the distribution is still very close to that pertaining to the initial $1s$-state except for a slight shift in the direction of the incoming projectile which reflects acceleration of the electron towards the projectile. Drastic changes appear around and shortly after $t = 0$. Thereafter the distribution starts to relax towards its final shape. Continuum waves of higher momenta are visible.

Figure 28 shows the probabilities that result by projection of the wave function from Fig. 27 onto various sets of target states. Besides the probability for the electron to remain in the $1s$-state, the figure displays the probabilities for K-shell ionization (projection onto Coulomb-Dirac continuum states of positive energy), excitation (projection onto bound states other than the ground state), and bound-free pair production (projection onto Coulomb-Dirac continuum states of negative energy). As seen, the initial $1s$-state gets strongly depleted around $t = 0$ after which its population converges rapidly to a final value of about 29.5%. The final value for excitation to higher bound states amounts to 9.8% and it is found that the final excitation probabilities for the higher shells essentially exhibit a $1/n^3$ behavior. The final value for K-shell transfer, which is not displayed in the figure, amounts to 2.5%. The projection onto the positive continuum produces a probability (square of pro-

jection) that reaches a maximum value of about 61% at time $t = 10$ after which it decreases to about 54.3%.

For the bound-free pair production Fig. 28 shows how the square of the projection onto the negative continuum reaches very high values of the order of several percent around $t = 0$ after which it drops by orders of magnitude, a behavior also reported previously from coupled channel calculations. At large positive times the square of the projection onto the negative-energy states converges to a final value of 3.9×10^{-4} which is about 4.4 times larger than the perturbation theory value of 0.89×10^{-4}. The correction of the result due to the overlap with the projectile $1s$-state (charge transfer) leads to a further reduction of the value by about 10%. Such correction is not considered significant and, therefore, it has not been included in the figure. The energy distribution obtained by the projections on the positive and negative continuum are shown in Fig. 29. For comparison, the figure also displays the predictions by perturbation theory for ionization and bound-free PP spectra. The figure clearly shows that the nonperturbative enhancement of bound-free pair production comes mainly from positrons with a kinetic energy less than 1. All in all, an enhancement due to nonperturbative action is found with the momentum-space method (Momberger *et al.*, 1996) but it is by no means as big as reported in earlier publications.

The impact-parameter dependence of the probabilities for the initial $1s$-state, excitation, and ionization is shown in Fig. 30. The impact parameter ranges from 0 to 4 units. Ionization is at maximum at zero impact parameter and drops continuously with increasing impact parameter, while excitation has its maximum around 0.5 units (193 fm). The excitation probabilities for the $2s_{1/2}$ and the $3s_{1/2}$-states have maxima around 0.5, while the probabilities of the $2p$ and $3p$-states extend over a large impact parameter range. Total excitation and ionization probabilities have been estimated from the data of Fig. 29 by assuming exponential depletion beyond $b = 4$.The result for the ionization cross section is 14.4 kilobarn which practically agrees with the value in perturbation theory of 14.7 kilobarn. For excitation, the total cross section amounts with the exponential extrapolation to 8.26 kilobarn. The $2s_{1/2}$ and $3s_{1/2}$ states contribute here 1.37 and 0.25 kilobarn, respectively.

Extraction of a cross section for bound-free pair production was complicated by the appearance of calculationally generated noise at the level of 10^{-4}. A crude estimate of the cross section was obtained by subtracting a constant, impact-parameter independent background. Using the results hence obtained out to $b = 2$ from which point an extrapolation

based on perturbation theory was applied led to a cross section of 2.33 barn. This value overshoots the perturbative cross section of 0.96 barn by only a factor of 2.4 and furthermore agrees well with the experimental cross section of 2.2 barn given above (the latter including capture to all bound states, which typically account for about 20% of the total cross section).

In general nonperturbative effects in bound-free pair production are expected primarily at moderate energies in close impacts. Furthermore, the virtual photon method, besides being perturbative in the projectile action, is more shaky at moderate than at high energies (as Table V shows, close and distant contributions are comparable in magnitude at 10 GeV/u). Hence at moderate energies nonperturbative numerical calculations are required to extract reliable cross sections theoretically. On the other hand, at high energies where distant collisions bring the dominant contribution the virtual photon method may be expected to produce reasonable values for the cross section when based on exact photo cross sections.

4. Heavy-lepton pair production

Before closing the section on bound-free pair production consider briefly the creation of pairs of heavy leptons. To keep the colliding nuclei intact requires that the impact parameter in the heavy ion collision be in excess of the sum of the nuclear radii. This sum exceeds the Compton wavelength of both the muon and the tau as well as the spatial extent of the deeply bound lepton states for the tau, and for heavy nuclei also for the muon. Hence the entire cross section for heavy-ion impact is in general well estimated by the virtual photon method with the choice $b_{min} = R_1 + R_2$.

Since the modified Bessel functions K_0 and K_1 appearing in the intensity (46) fall off exponentially for arguments larger than one, and since the photon energy has to be in excess of roughly 2 mass units, an effective threshold for bound-free pair production in heavy-ion collisions is implied at, roughly, $\gamma_{th} = (A_1^{1/3} + A_2^{1/3})\, r_m/164$, where r_m denotes the ratio of the lepton to the electron mass. Typically, this estimate amounts to something like 15 for muons and 250 for tau. From (46) it is further inferred that well above the effective threshold the cross section for heavy ion impact exceeds the (maximum) cross section for photon impact by a factor of order $(2/\pi)\alpha Z_p^2 \ln(\gamma/\gamma_{th})$, which number easily is beyond 100.

Figure 31 shows the cross sections for bound-free muon pair production in uranium-uranium collisions. The photo cross sections applied are those of Fig. 10. A comparison

with other calculations may be found elsewhere (Belkacem and Sørensen, 1998).

The production of bound-free pairs of τ leptons due to coherent scattering on the target nucleus is strongly suppressed, and thereby out of reach experimentally, since the corresponding photo cross sections are extremely small, see Subsec. II.B.4. The remarks on alternative production mechanisms posted there obviously also apply for charged particle impact.

IV. PAIR PRODUCTION IN CRYSTALS

When a charged particle penetrates a single crystal in a direction close to a major crystallographic axial or planar direction, it has a fair chance to scatter coherently on many target atoms along its way. *Channeling*, where the charged particle motion actually is governed by many correlated small-angle scattering events, is the ultimate example of this (Feldman *et al.*, 1982; Gemmel, 1974; Sørensen and Uggerhøj, 1987). The coherence in scattering experienced by a charged particle penetrating an aligned crystal is carried on to radiation processes and, consequently, radiation emission by an electron or positron penetrating a single crystal may greatly exceed bremsstrahlung emission in an amorphous medium composed of the same type of atoms with the same density. Similarly with the cross channel, pair creation. A number of reviews are available on these matters (Sørensen, 1996; Sørensen and Uggerhøj, 1987, 1989).

A. Coherent pair production; the perturbation limit

According to custom, the pair production which results when the interaction with the crystal may be treated as a perturbation is termed *coherent pair production*. As discussed in Subsec. II.A the pair-production probability in this limit is proportional to the square of a second-order matrix element which, in turn, is composed as a sum of terms, each proportional to the product of two first-order matrix elements, one for the interaction with the radiation field and one for the scattering in the atomic field; Eq. (1). Since the projectile states are plane waves, it is found immediately that the cross section is proportional to the square of the Fourier transform of the interaction potential, Eq. (4). For incidence on a total of N

atoms, the atomic potential V needs to be replaced by the total interaction potential[13]

$$V \longrightarrow \sum_n V(\mathbf{r} - \mathbf{r}_n) \; . \tag{60}$$

Here $\mathbf{r}_n$ denotes the position of the n'th atom. In applying the expression (60), changes appearing in the potential as a result of rearrangements of the outermost parts of the atomic electron cloud due to mutual atom-atom interactions are neglected. This is justified since, as far as pair production is concerned, the target electrons essentially only enter in the screening of the nuclear charge. Substituting the sum (60) for the interaction potential into Eq. (4), the following relation between the differential cross sections for photon production at energy ω on an isolated atom and on the group of N atoms is obtained,

$$\left.\frac{d\sigma}{d\omega\; d^3q}\right|_{N \text{ atoms}} = \left.\frac{d\sigma}{d\omega\; d^3q}\right|_{\text{single atom}} \times \left|\sum_n e^{i\mathbf{q}\cdot\mathbf{r}_n}\right|^2 . \tag{61}$$

For an amorphous medium, the last factor yields just N. On the other hand, for a perfect static single crystal in the limit $N \to \infty$ the interference factor reads

$$\left|\sum_n e^{i\mathbf{q}\cdot\mathbf{r}_n}\right|^2 = N\frac{(2\pi)^3}{N_0\Delta}\,|S(\mathbf{g})|^2 \sum_{\mathbf{g}} \delta(\mathbf{q} - \mathbf{g}) \; . \tag{62}$$

Here $\mathbf{g}$ denotes a reciprocal lattice vector, $S(\mathbf{g})$ the structure factor, and N_0 is the number of atoms contained in a unit cell which has the volume Δ. This result is well known from diffraction theory.

The interference structure suggested by Eqs. (61–62) is softened somewhat as a result of thermal vibrations. Furthermore, the interference (or *coherent*) spectrum is accompanied by an incoherent contribution (due to thermal diffuse scattering). Except for a slight reduction (by one minus a Debye-Waller factor), this part is identical to the Bethe-Heitler result discussed in Subsec. II.A.

Figure 32 displays coherent pair production as computed according to the above description for 100 GeV photons incident in directions close to the $\langle 110 \rangle$ axis of a germanium single crystal cooled to 100K. The peak-structured spectrum pertains to incidence parallel to the $\{100\}$ planes and shows a large enhancement over the Bethe-Heitler rate (dotted line) applying for amorphous germanium (of the same density as the crystal). The amorphous rate

[13] The symbol N is used locally in this single subsection for the total number of atoms. It should not be confused with the otherwise global use of N as the atomic density.

is encountered in the crystal upon incidence far from all major crystallographic directions. The peaks appear as a result of periodic passing of axes. For incidence far from all planes the peak structure washes out but the high level of enhancement is maintained as long as the polar angle of incidence to the axis is unchanged since the major source of enhancement over the amorphous rate is coherent scattering on atoms belonging to a given row of atoms. This is revealed by the dashed curve which shows the average of the production rate over the azimuthal angle of incidence. It may be noted that the enhancement is quite sensitive to the magnitude of the thermal vibrations in the crystal: The (one-dimensional) vibration amplitude applied in the calculation is 0.0526 Angstrom; if the Debye-model result of 0.045 Angstrom (for $T_D = 360$K) were applied instead the highest peaks in the spectrum would reach 3.5 cm^{-1}.

For very close alignment with the crystal axis, the perturbation rate shown in Fig. 32 drops off. This drop in rate is a result of a break-down of the perturbation approximation and not a physical effect. Actually, for incidence closer than ~ 0.5 mrad, non-perturbative calculations as for instance the constant-field approximation to be discussed below predict an enhancement comparable to the maximum encountered in the figure.

B. Nonperturbative pair production

The electric fields near atomic nuclei extend only over atomic distances, that is, over distances of the order of one Angstrom. However, when a charged particle is penetrating a single crystal in a direction close to a low-index crystallographic direction its motion is governed by many correlated collisions with lattice atoms. As a result, in the interaction with, say, a row of atoms the charged particle deflects as off a continuum string obtained by smearing the atomic charges uniformly along the direction of the row. The coherence in scattering hence manifests itself as motion in effective fields of atomic strength but extending over relatively long distances along the direction of motion. For close alignment strong steering effects are experienced leading to a break down of perturbation schemes.

Figure 33 shows an example of the radial (or transverse) variation of the electric field produced by strings in the continuum approximation. The maximum electric field strength can reach large values ($\sim 10^{11}$ V/cm) near the strings. The motion in the continuum model is of course relatively simple since the electric field is purely transverse. Furthermore, the

motion of nearly aligned high-energy electrons or positrons is essentially classical. The relativistic γ-factor for a 100 GeV electron is nearly 2×10^5 and quantum mechanical effects, such as wave-packet spreading, are greatly suppressed at this mass enhancement. The classical nature of the motion is utilized in various theoretical schemes for calculation of radiation and pair creation in the GeV region.

For sufficiently close alignment between the incident photon and the crystal axis (typically below ~ 0.5 mrad; the value depends on the material), pair creation can be described by assuming the produced charged particles to be subject to a constant and uniform field during the characteristic time of transition between initial and final states. The production rate is obtained by averaging over the fields encountered. Using this averaging, pair production rates for energetic photons incident along a major axial direction of a crystal can be easily calculated. The differential pair-creation rate in a uniform field is (Kimball and Cue, 1985):

$$\frac{dW}{dE_+} = \frac{\alpha}{\omega^2 \pi^{1/2}} \left[\int_x^\infty Ai(\xi) d\xi - \frac{2}{x} (\frac{1+y^2}{1-y^2}) Ai'(x) \right] , \tag{63}$$

where Ai and Ai' are the Airy function and its derivative[14],

$$y = (E_- - E_+)/\omega , \tag{64}$$

and

$$x = \alpha^{-2} (\frac{4}{\omega \mathcal{E}(1-y^2)})^{2/3} . \tag{65}$$

As usual the quantities E_- and E_+ are the energies of the created electron and positron while ω is the energy of the incident photon. The quantity $\mathcal{E}$ is the strength of the uniform electric field in atomic units (1 a.u. $= e/a_0^2 = e\alpha^{-2} = 5.14 \times 10^9$ V/cm).

The total pair-creation rate is obtained through an integration of the differential rate. The result is (Kimball and Cue, 1985)

$$W = \frac{\alpha}{\omega \pi 3\sqrt{3}} \int_0^1 \frac{9-y^2}{1-y^2} \times K_{2/3} \left(\frac{8\alpha^{-3}}{3\omega \mathcal{E}(1-y^2)} \right) dy , \tag{66}$$

where $K_{2/3}$ is a modified Bessel function. For moderate values of the product $\omega\mathcal{E}$ the large-argument expansion of the Bessel functions may be applied. This leads to exponential

[14] The definition of the Airy function used here is that given by Landau and Lifshitz (1975). The definition by Abramowitz and Stegun (1972) differs by a factor of $\pi^{-1/2}$. If the latter definition is applied $\pi^{-1/2}$ should be removed from the front factor in the expression (63). The ambiguity disappears entirely if the rate instead is expressed in terms of the Bessel functions $K_{1/3}$ and $K_{2/3}$.

suppression of the pair-creation rate

$$W \sim \alpha^4 \mathcal{E} \frac{3}{16} \left(\frac{3}{2}\right)^{1/2} \exp\left(-\frac{8\alpha^{-3}}{3\omega\mathcal{E}}\right) . \tag{67}$$

The formula (67) clearly shows that this coherent part of pair production is significant only when the product $\omega\mathcal{E}$ is comparable to or larger than $8\alpha^{-3}/3 \simeq 7 \times 10^6$. In crystals, the electric field can easily reach 10 to 100 atomic units, see Fig. 33. The coherent contribution hence becomes significant for values of ω of 10^5, that is, in the region of tens to hundreds of GeV.

Experimental measurements of pair production in alignment conditions were reported first in mid 1980s by Belkacem and coworkers (Belkacem *et al.*, 1984, 1986, 1987). The experimental set up is shown in Fig. 34. Electron beams of 70 and 150 GeV were produced from the primary proton beam in the North Area of the SPS-accelerator at CERN. A doublet of scintillators (B1 and T1) centered on the beam axis allowed the rejection of the events due to the beam halo. The tagged photon beam was produced from bremsstrahlung of the electron beam in a 0.5 mm thick lead foil. The electrons were separated from the bremsstrahlung photons and directed onto the tagging spectrometer (Tag) by means of the magnet M1. The energy ranges of the tagged photons produced from electron beams of 200, 150 and 70 GeV were 90–155, 55–130 and 22–55 GeV, respectively. The germanium crystals had thicknesses ranging from 0.185 to 1.4 mm and were liquid-nitrogen cooled to 100K. The total pair creation rate was measured with the thin scintillator B2 located just downstream from the thin crystal.

Figure 35 shows the energy dependence of the total pair production rate when the high energy photons are incident parallel to the $\langle 110 \rangle$ axial direction of Ge. The pair production rates are expressed in units of the Bethe-Heitler (BH) rate that corresponds to the incoherent pair production in the field of individual atoms. These rates were found to be independent of incident photon energy and in close agreement with predicted BH value. In contrast, the pair production rate for axial alignment is nearly equal to the BH value at 30-40 GeV and then increases sharply with photon energy. At 150 GeV the rate along the crystal axis is eight times higher than the BH rate. The calculated values are shown in Fig. 35. A good agreement between theory and experiment is obtained when both the coherent and the incoherent contributions are added.

Figure 36 shows the dependence of the pair production rate on the tilt angle θ between

the photon beam and the crystal axis. The enhancement of pair production over the BH value extends to several milliradians. The maximum rate occurs at an angle that appears to decrease roughly as ω^{-1} as the photon energy increases. For a theoretical treatment of the angular dependence the reader may consult the literature (Baier *et al.*, 1989).

The reader will find more information on pair production in crystals, including additional information on both nonperturbative theory and experiment, in the original papers as well as in the reviews cited at the beginning of Sec. IV. Pair creation in crystals and related matters are also discussed in the topical issue of Nuclear Instruments and Methods edited by Andersen *et al.* (1996). Results of a more recent experiment are reported by Kirsebom *et al.* (1998).

V. CONCLUDING REMARKS

Conclude the paper.

Acknowledgments

This work was supported by the Danish Natural Science Research Council, and by the Director, Office of Energy Research, Office of Basic Energy Sciences, Chemical Sciences Division, of the U.S. Department of Energy (DOE) under contract No. DE-AC-03-76SF00098. CHECK number!

References

Abramowitz, M., and I. Stegun (eds.), 1972, *Handbook of Mathematical Functions* (Dover, New York).

Agger, C. K., and A. H. Sørensen, 1997, Phys. Rev. A **55**, 402.

Alling, W. R., and W. R. Johnson, 1965, Phys. Rev. **139**, A1050.

Amaral, P., A. Amorini, K. Anderson, A. Artikov, R. Benetta, S. Berglund, C. Biscarat, O. Blanch, G. Blanchot, A. Bogush, C. Bolm, V. Boldea, *et al.*, 2001, Eur. Phys. J. C **20**, 487.

Andersen, H. H., R. E. Carrigan, and E. Uggerhøj (eds.), 1996, *Channeling and other crystal effects at relativistic energy*, topical issue, Nucl. Instr. and Meth. B **119** (issues 1–2).

Aste, A., K. Hencken, D. Trautmann, and G. Baur, 1994, Phys. Rev. A **50**, 3980.

Baier, V. N., V. M. Katkov, and V. M. Strakhovenko, 1989, Nucl. Sci. Appl. **3**, 245, see also Nucl. Instrum. Meth. B **16**, 5 (1986).

Baltz, A. J., M. J. Rhoades-Brown, and J. Weneser, 1994, Phys. Rev. A **50**, 4842.

Baur, G., G. Boero, A. Brauksiepe, A. Buzzo, W. Eyrich, R. Geyer, D. Grzonka, J. Hauffe, K. Kilian, M. LoVetere, M. Macri, M. Moosburger, *et al.*, 1996, Phys. Lett. B **368**, 251.

Baur, G., K. Henken, D. Trautmann, S. Sadovsky, and Y. Kharlov, 2002, Phys. Rep. **364**, 359.

Becker, U., N. Grün, and W. Scheid, 1987, J. Phys. B **20**, 2075.

Belkacem, A., G. Bologna, M. Chevallier, A. Clouvas, N. Cue, M. J. Gaillard, R. Genre, J. C. Kimball, R. Kirsch, B. Marsh, J. P. Peigneux, J. C. Poizat, *et al.*, 1984, Phys. Rev. Lett. **53**, 2371, erratum: Phys. Rev. Lett. **54**, 852 (1985).

Belkacem, A., G. Bologna, M. Chevallier, N. Cue, M. J. Gaillard, R. Genre, J. C. Kimball, R. Kirsch, B. Marsh, J. P. Peigneux, J. C. Poizat, J. Remillieux, *et al.*, 1986, Nucl. Instrum. and Meth. in Phys. Res. B **13**, 9.

Belkacem, A., G. Bologna, M. Chevallier, N. Cue, M. J. Gaillard, R. Genre, J. C. Kimball, R. Kirsch, B. Marsh, J. P. Peigneux, J. C. Poizat, J. Remillieux, *et al.*, 1987, Phys. Rev. Lett. **58**, 1196.

Belkacem, A., N. Claytor, T. Dinneen, B. Feinberg, , and H. Gould, 1998, Phys. Rev. A **58**, 1253.

Belkacem, A., H. Gould, B. Feinberg, R. Bossingham, and W. E. Meyerhof, 1993, Phys. Rev. Lett. **71**, 1514.

Belkacem, A., H. Gould, B. Feinberg, R. Bossingham, and W. E. Meyerhof, 1994, Phys. Rev. Lett. **73**, 2432.

Belkacem, A., H. Gould, B. Feinberg, R. Bossingham, and W. E. Meyerhof, 1997, Phys. Rev. A **56**, 2806.

Belkacem, A., and A. H. Sørensen, 1998, Phys. Rev. A **57**, 3646.

Berestetskii, V. B., E. M. Lifshitz, and L. P. Pitaevskii, 1989, *Quantum Electrodynamics* (Pergamon Press, New York).

Berturlani, C. A., and G. Baur, 1988, Phys. Rep. **163**, 299.

Bethe, H. A., and J. Ashkin, 1953, in *Experimental Nuclear Physics*, edited by E. Segrè (Wiley, New York), volume I, p. 166.

Bethe, H. A., and E. E. Salpeter, 1957, *Quantum Mechanics of One- and Two-Electron Atoms*

(Springer, Berlin).

Bottcher, C., and M. R. Strayer, 1989, Phys. Rev. D **39**, 1330.

Burkhardt, G. H., 1958, Il Nuovo Cim. **9**, 375.

Chudakov, A. E., 1955, Izv. Akad. Nauk. SSSR, Ser. Fiz. **19**, 651, english translation: B. Acad. Sci. USSR Phys. **19**, 589 (1955).

Datz, S., H. F. Krause, C. R. Vane, H. Knudsen, P. Grafström, and R. H. Schuch, 1996, Phys. Rev. Lett. **77**, 2925.

Dauvergne, D., A. Belkacem, F. Barrué, J. P. Bocquet, M. Chevallier, B. Feinberg, R. Kirsch, J. C. Poizat, C. Ray, and D. Rebreyend, 2003, Phys. Rev. Lett. **90**, 153002.

Eby, P. B., 1989, Phys. Rev. A **39**, 2374.

Fatyga, M., M. J. Rhoades-Brown, and M. J. Tannenbaum (eds.), 1990, *Brookhaven National Laboratory Report*, BNL-52247.

Feldman, L. C., J. W. Mayer, and S. T. Picraux, 1982, *Materials Analysis by Ion Channeling* (Academic Press, New York).

Gavrila, M., 1961, Phys. Rev. **124**, 1132.

Gemmel, D. S., 1974, Rev. Mod. Phys. **46**, 129.

van Ginneken, A., 1986, Nucl. Instr. and Meth. A **251**, 21.

Greiner, W., 1990, *Relativistic Quantum Mechanics – Wave Equations* (Springer, Berlin).

Groom, D., N. Mokhov, and S. Striganov, 2001, Atomic Data and Nuclear Data Tables **78**, 183.

Hagiwara, K., K. Hikasa, K. Nakamura, M. Tanabashi, M. Aguilar-Benitez, C. Amsler, R. M. Barnett, P. R. Burchat, C. D. Carone, C. Caso, G. Conforto, O. Dahl, *et al.* (Particle Data Group), 2002, Phys. Rev. D **66**, 010001, the material is available through the website: http://pdg.lbl.gov/.

Heitler, W., 1954, *The Quantum Theory of Radiation* (Oxford University Press, London), 3rd edition, available in reprint from Dover, New York, 1984.

Hubbell, J. H., H. A. Gimm, and I. Øverbø, 1980, J. Phys. Chem. Ref. Data **9**, 1023.

Ichihara, A., and J. Eichler, 2000, Atomic Data and Nuclear Data Tables **74**, 1.

Ionescu, D. C., and J. Eichler, 1993, Phys. Rev. A **48**, 1176.

Ionescu, D. C., A. H. Sørensen, and A. Belkacem, 1999, Phys. Rev. A **59**, 3527.

Jackson, J. D., 1975, *Classical Electrodynamics* (Wiley, New York).

Jauch, J. M., and F. Rohrlich, 1980, *The theory of photons and electrons* (Springer-Verlag, New York).

Johnson, W. R., 1967, Phys. Rev. **159**, 61.

Kimball, J., and N. Cue, 1985, Phys. Rep. **125**, 69.

Kimball, J. C., N. Cue, and A. Belkacem, 1986, Nucl. Instrum. and Meth. in Phys. Res. B **13**, 1.

Kirsebom, K., Y. V. Kononets, U. Mikkelsen, S. P. Møller, E. Uggerhøj, T. Worm, C. Biino, K. Elsener, S. Ballestrero, P. Sona, S. H. Connell, J. P. F. Sellschop, *et al.*, 1998, Nucl. Instr. and Meth. B **135**, 143.

Klein, S. R., 2004, eprint hep-ex/0402028.

Landau, L. D., and E. M. Lifshitz, 1975, *The Classical Theory of Fields* (Pergamon Press, Oxford).

Lindhard, J., and A. H. Sørensen, 1996, Phys. Rev. A **53**, 2443.

Mando, M., and L. Ronchi jr., 1952, Nuovo Cimento **9**, 105.

Meier, H., Z. Halabuka, K. Hencken, D. Trautmann, and G. Baur, 2001, Phys. Rev. A **63**, 032713.

Merzbacher, E., 1971, *Quantum Mechanics* (Wiley, New York).

Milstein, A. I., and V. M. Strakhovenko, 1993, Zh. Eksp. Teor. Fiz. **103**, 130.

Mito, I., and H. Ezawa, 1957, Progr. Theo. Phys. **18**, 437.

Momberger, K., A. Belkacem, and A. H. Sørensen, 1995, Europhys. Lett. **32**, 401.

Momberger, K., A. Belkacem, and A. H. Sørensen, 1996, Phys. Rev. A **53**, 1605.

Perkins, D. H., 1955, Phil. Mag. **46**, 1146.

Pratt, R. H., 1960a, Phys. Rev. **117**, 1017.

Pratt, R. H., 1960b, Phys. Rev. **119**, 1619.

Pratt, R. H., A. Ron, and H. K. Tseng, 1973, Rev. Mod. Phys. **45**, 273.

Racah, G., 1937, Nuovo Cimento **14**, 93.

Rhoades-Brown, M. J., and J. Weneser, 1991, Phys. Rev. A **44**, 330.

Rumrich, K., K. Momberger, G. Soff, W. Greiner, N. Grün, and W. Scheid, 1991, Phys. Rev. Lett. **66**, 2613.

Sauter, F., 1931, Ann. Phys. (Leipzig) **11**, 454.

Sørensen, A. H., 1996, Nucl. Instr. and Meth. B **119**, 1, the page order in the reprinted article is wrong, page 19 should be read before page 17.

Sørensen, A. H., 2001, Phys. Rev. A **64**, 012703.

Sørensen, A. H., 2003, in *Proc. 17th International Conference on Applications of Accelerators in Research and Industry*, edited by J. L. Duggan and I. L. Morgan (American Institute of Physics, Melville, New York), volume 680 of *AIP Conference Proceedings*, p. 102.

Sørensen, A. H., and A. Belkacem, 1994, Phys. Rev. A **49**, 81.

Sørensen, A. H., and E. Uggerhøj, 1987, Nature **325**, 311.

Sørensen, A. H., and E. Uggerhøj, 1989, Nucl. Sci. Appl. **3**, 147.

Ter-Mikaelian, M. L., 1972, *High-Energy Electromagnetic Processes in Condensed Media* (Wiley, New York).

Vane, C. R., S. Datz, P. F. Dittner, H. F. Krause, R. Schuch, H. Gao, and R. Hutton, 1994, Phys. Rev. A **50**, 2313.

Williams, E. J., 1935, Kgl. Dan. Vidsk. Selsk. Mat. Fys. Meddl. **XIII**(4).

Wolter, W., and M. Miesowicz, 1956, Il Nuovo Cim. **4**, 648.

Wright, A. G., 1973, J. Phys. A **6**, 79.

Yekutieli, G., 1957, Il Nuovo Cim. **5**, 1381.

Zielinski, I. P., 1985, Nucl. Instr. Meth. A **238**, 562.

Figures

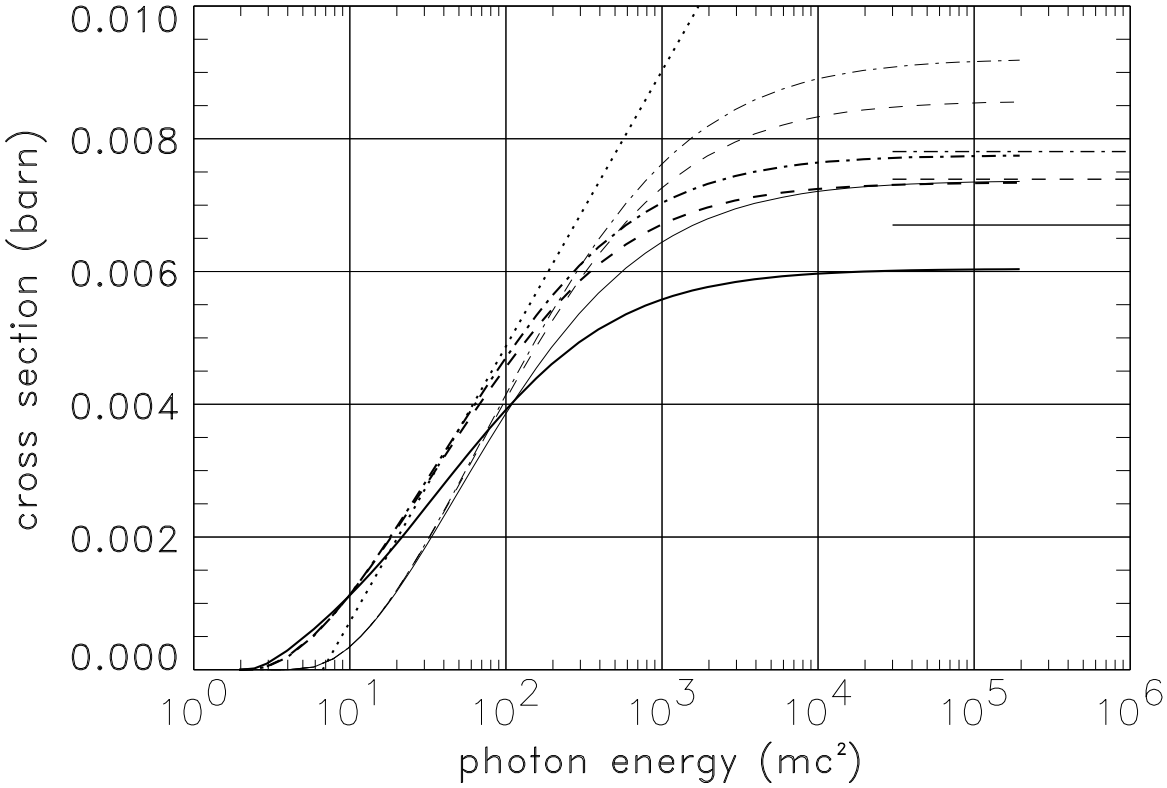

FIG. 1 Cross section for photoproduction of electron-positron pairs as a function of the photon energy. The values tabulated by Hubbell *et al.* (1980) for lead ($Z = 82$, solid lines), iron ($Z = 26$, dashed lines), and aluminum ($Z = 13$, chained lines) are displayed. The thick curves display the cross section, divided by Z^2, for production in the screened nuclear field. The thin curves display the cross section, divided by Z, for production on atomic electrons. The horizontal line segments to the right in the figure show the asymptotic Born values for the coherent contribution pertaining to the Thomas-Fermi atom (full screening), upper expression in Eq. (6). The dotted line corresponds to the unscreened value given in the lower expression in the same equation.

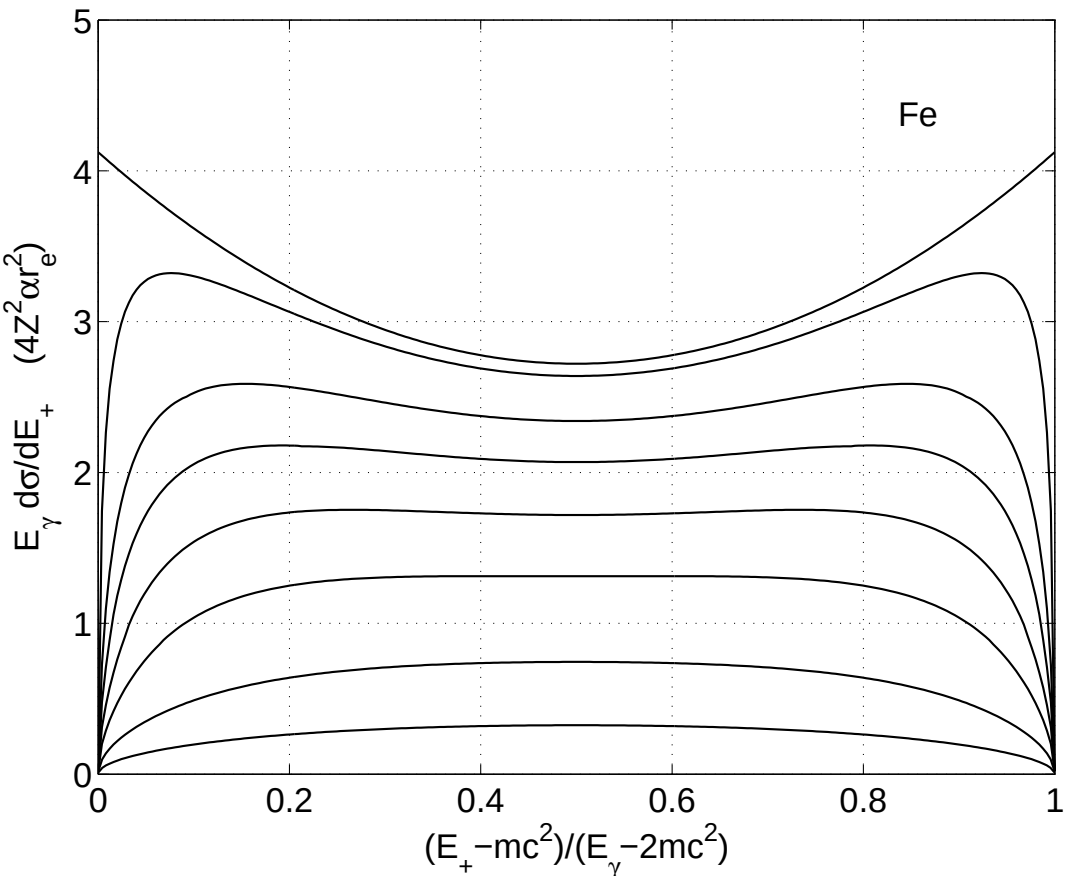

FIG. 2 Differential cross section for photoproduction of electron-positron pairs in an iron target as obtained in the Born approximation. The cross section multiplied by the photon energy is shown as a function of the kinetic energy of the positron, relative to the total energy available as kinetic energy, for photon energies of, starting from below, 5, 10, 25, 50, 100, 200, and 1000 mc^2, as well as for infinitely high photon energy. Based on standard formulas (Bethe and Ashkin, 1953).

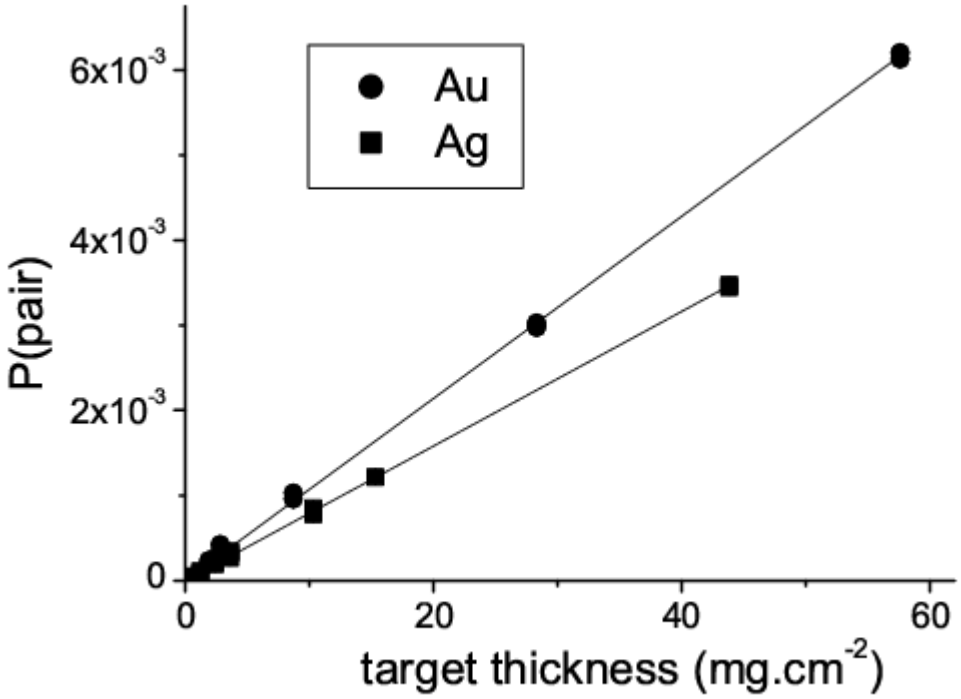

FIG. 3

FIG. 3 Pair Production Probability in silver and gold as a function of target thickness (Dauvergne *et al.*, 2003).

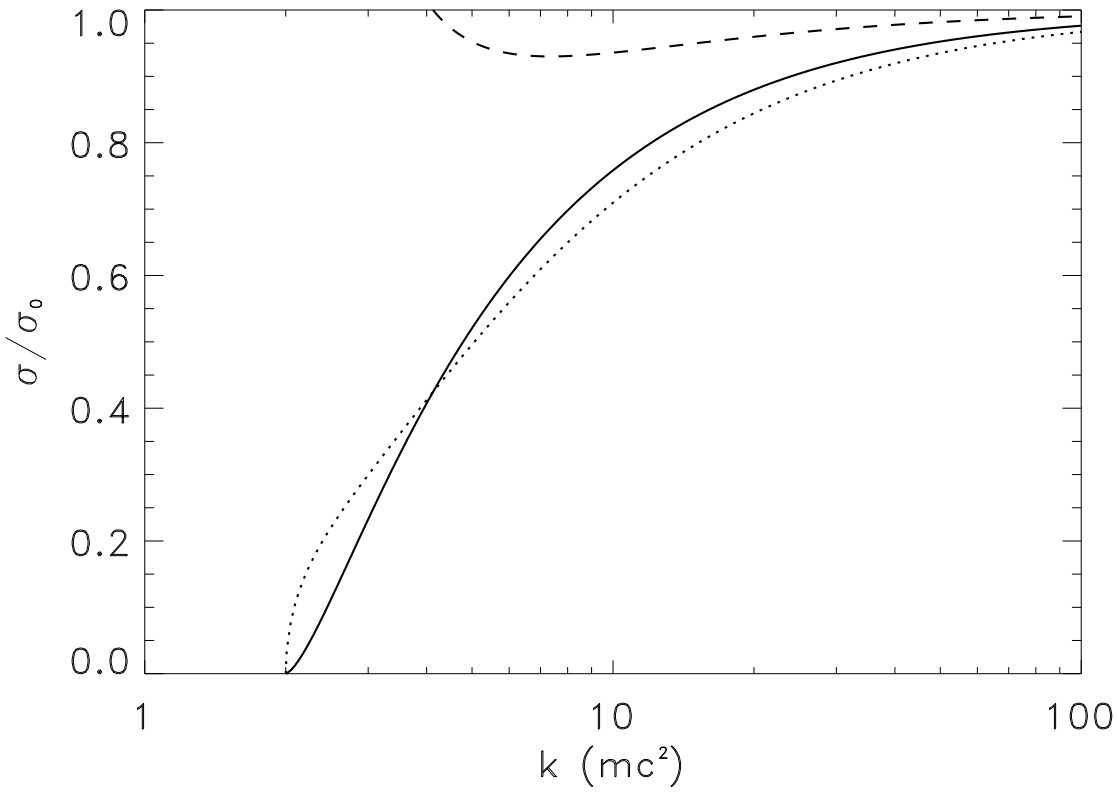

FIG. 4 Cross section for bound-free pair production as a function of photon energy. The photon is incident on a bare nucleus and the electron is produced in the ground state of the resulting hydrogenlike atom. The solid curve shows the perturbative Sauter expression (20) while the dotted line shows the plane-wave result (18). Both predictions are divided by the asymptotic cross section σ_0 of Eq. (19). The dashed curve displays the ratio of the plane-wave to the Sauter result.

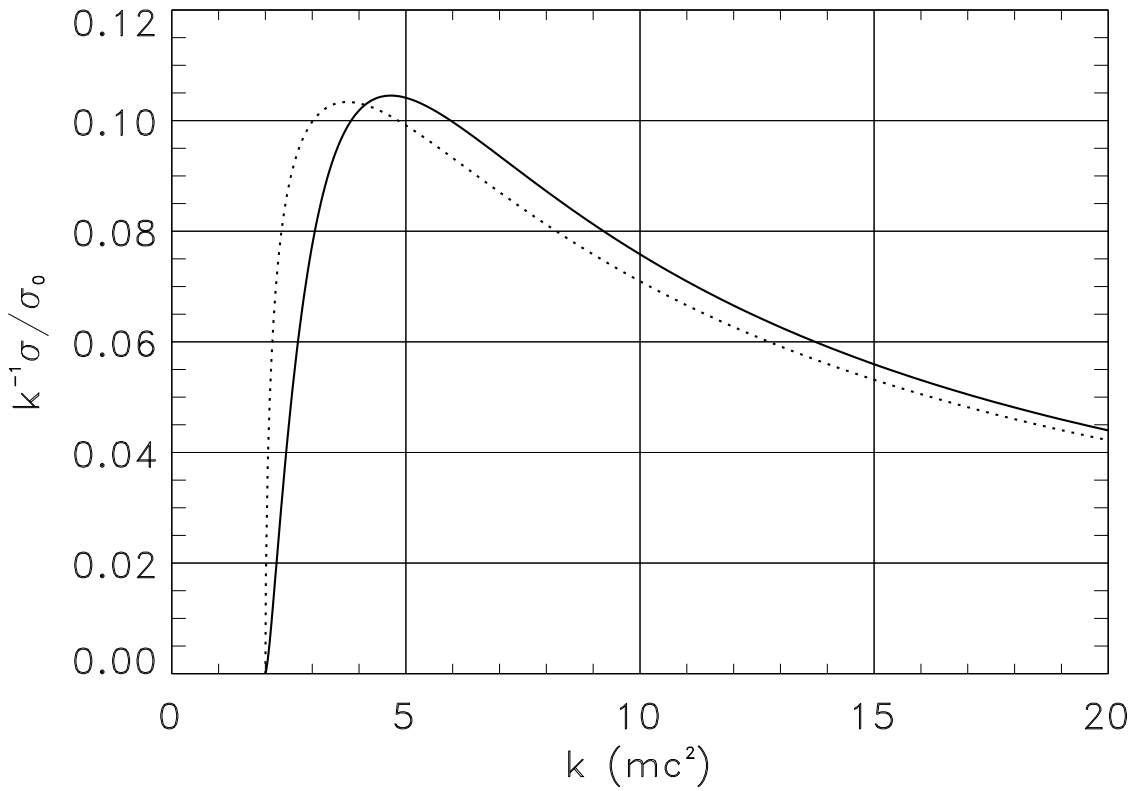

FIG. 5 Cross section for bound-free pair production as a function of photon energy. As in Fig. 4, the electron is produced in the ground state. The solid curve shows the Sauter expression (20) while the dotted line shows the plane-wave result (18). Cross sections are shown in units of $4\pi\alpha(\alpha Z)^5$.

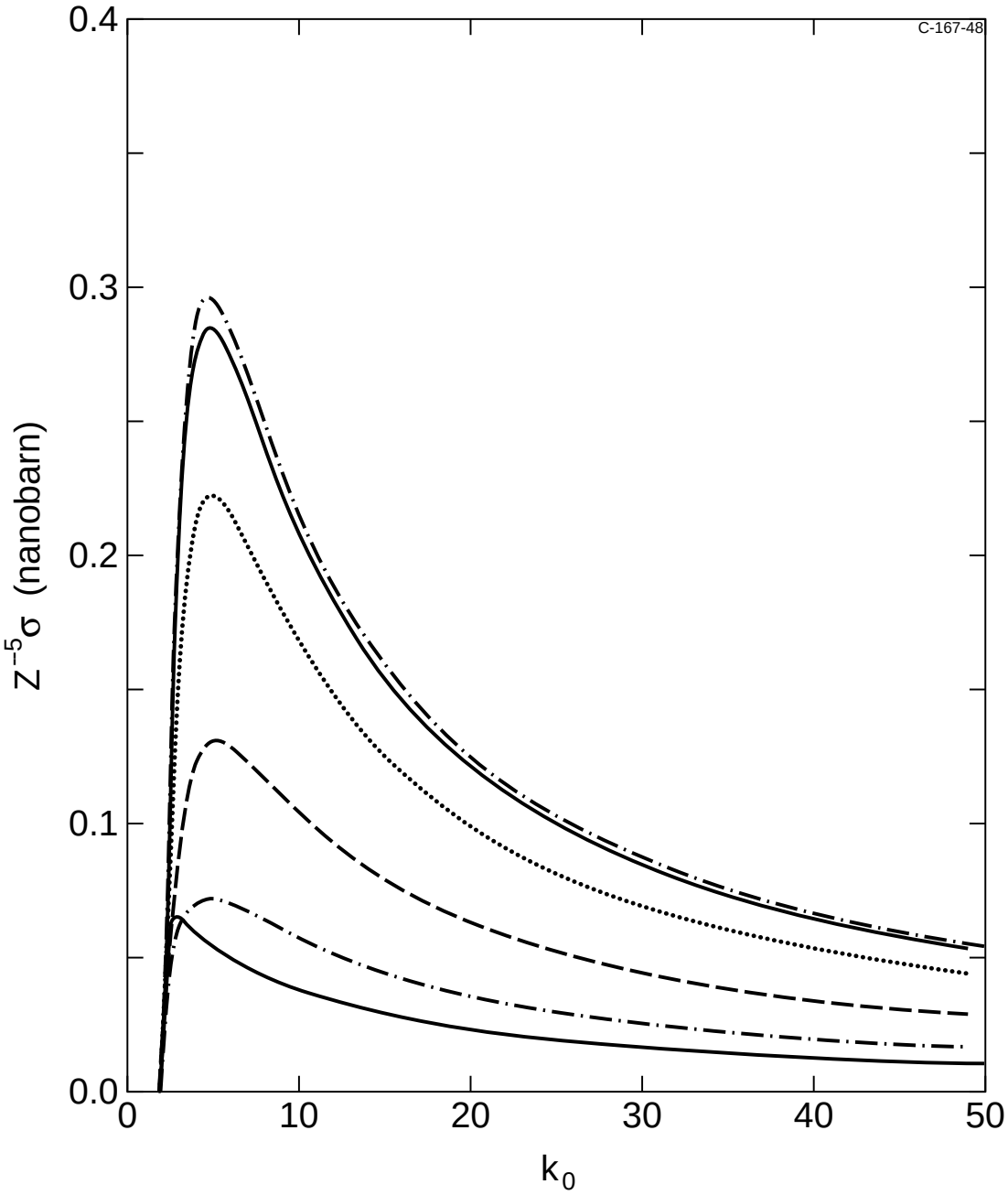

FIG. 6 Exact total cross section for pair production with the electron bound in the $1s$-state as a function of photon energy (Agger and Sørensen, 1997). The nuclear charge number Z assumes values of 1 (upper full-drawn curve), 8 (dotted), 26 (short dashes), 55 (dot–dashed), and 92 (lower full-drawn curve). Cross sections are scaled with Z^5, the unit on the ordinate is 10^{-33} cm^2, and the photon energy is given in units of mc^2, the electron rest energy. The uppermost curve (dot–dashed) corresponds to the Born result (20).

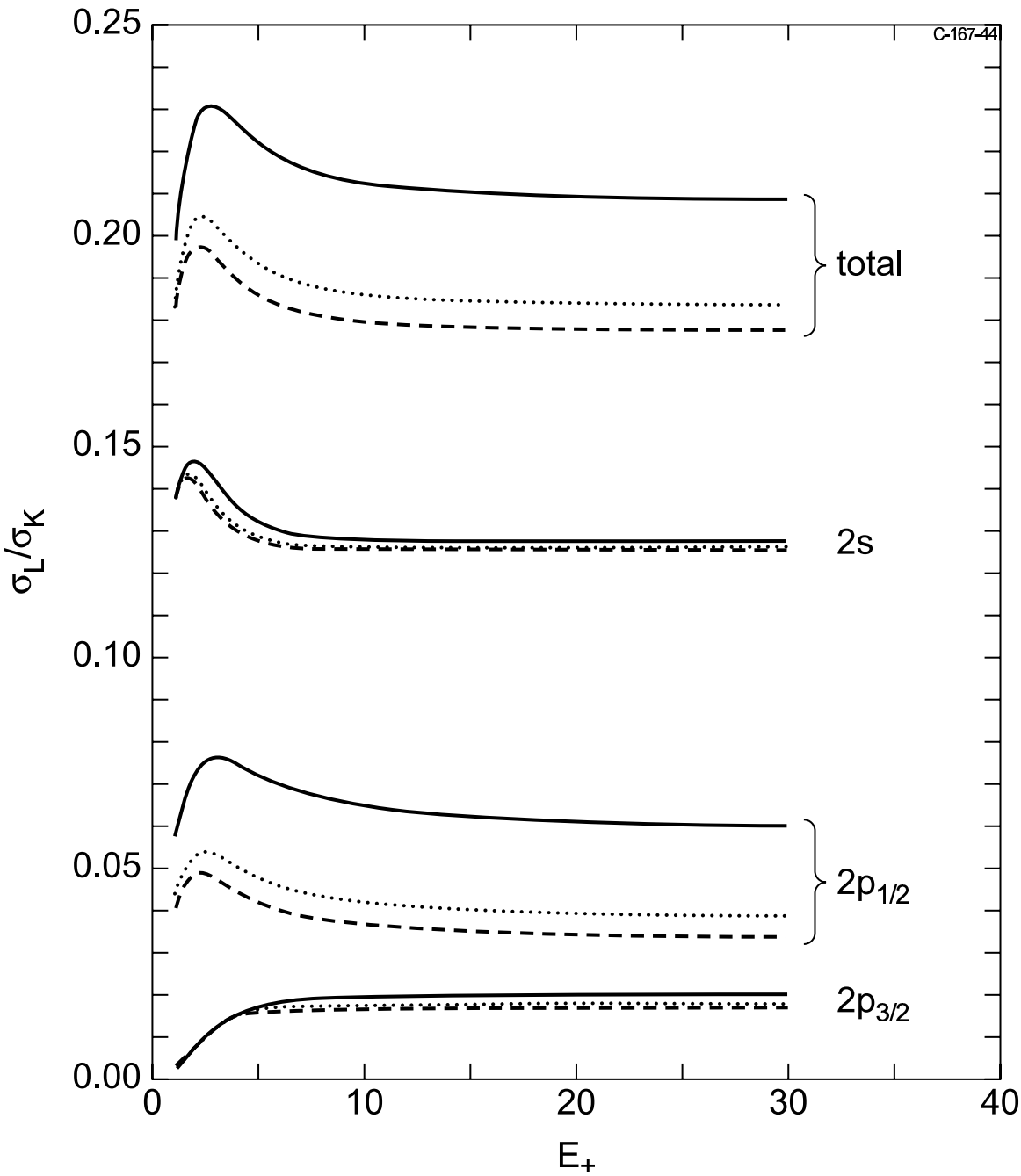

FIG. 7 Shell ratios for photo production of bound-free electron-positron pairs on bare nuclei (Agger and Sørensen, 1997). The ratios of exact cross sections for pair production with capture into the individual L subshells to the exact cross section for capture into the K shell are shown as functions of positron energy in units of mc^2 for three different elements; Z=92 (full curve), 82 (dotted) and 79 (dashed). The three close-lying curves at the bottom of the figure display results for the $2p_{3/2}$-state, then follow the three curves for the $2p_{1/2}$-state, the close packed group of curves for the $2s$-state and, at the top of the figure, the sum of the partial ratios.

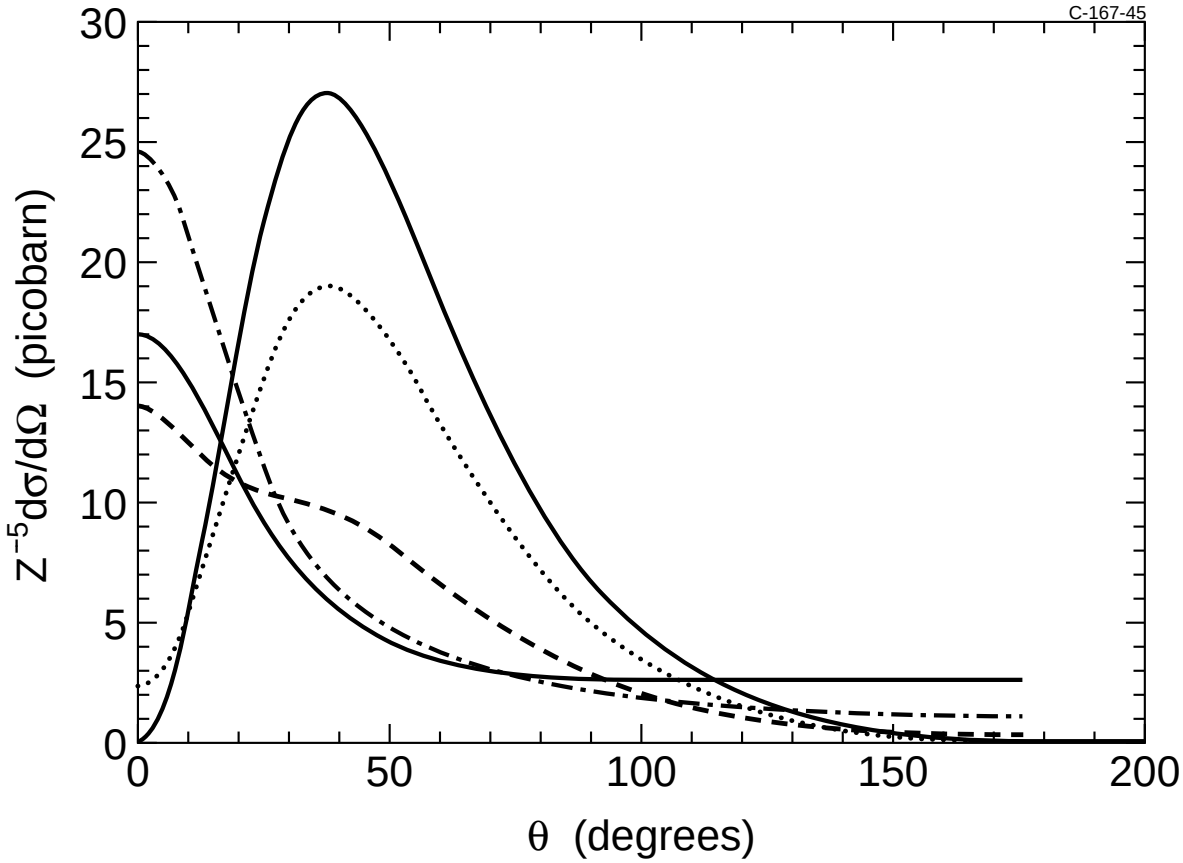

FIG. 8 Angular distribution of positrons at an energy of 1.5 mc^2 for pair production with K-shell capture (Agger and Sørensen, 1997). The charge numbers of the bare ion targets assume values of Z=1 (full curve), 8 (dotted), 26 (dashed), 55 (chained) and 92 (full, with a maximum in the forward direction). The exact differential cross sections are scaled by Z^5 and the ordinate is given in units of 10^{-33} cm^2 per steradian.

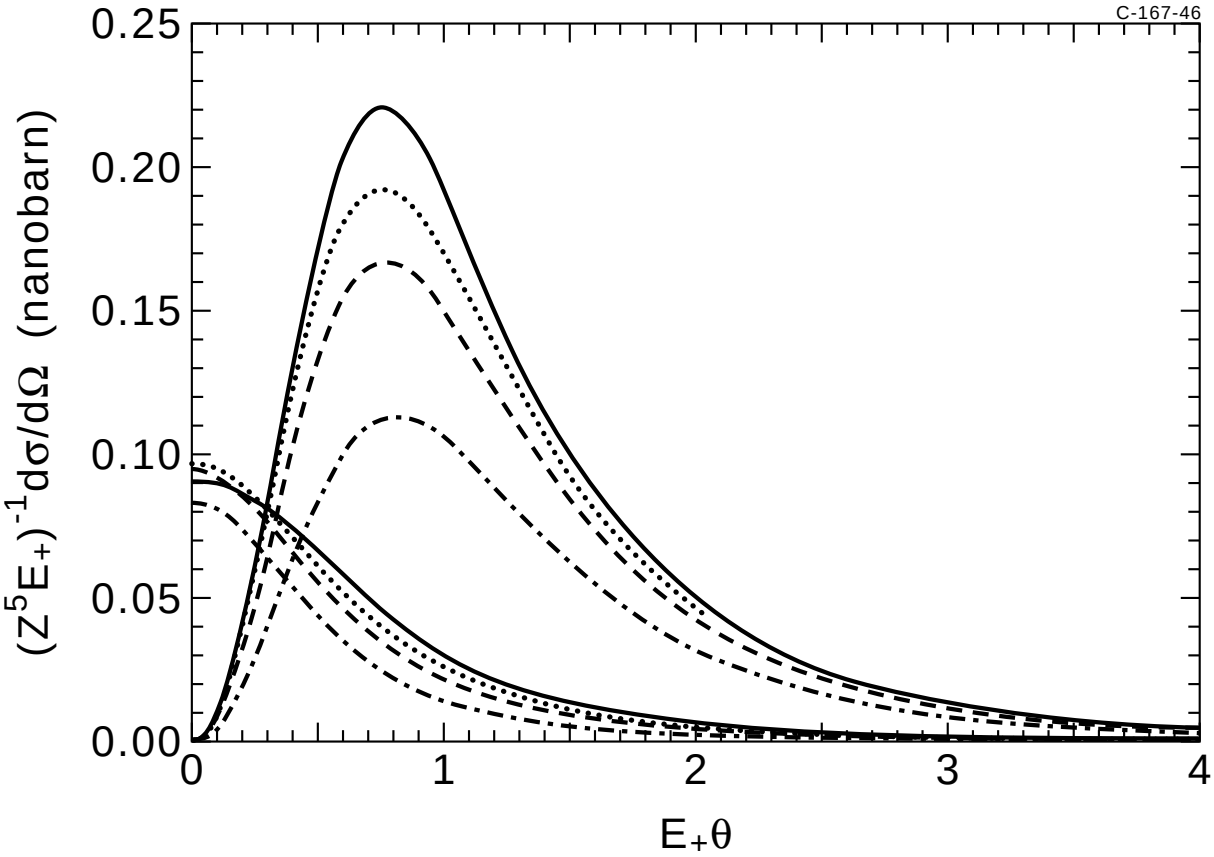

FIG. 9 Angular distribution of positrons at various energies for pair production with K-shell capture (Agger and Sørensen, 1997). Results are displayed for targets with Z=92 (curves peaking at zero angle) and Z=1 (curves peaking for $E_+\theta$ near 1). The abscissa is the product of positron emission energy E_+ and angle θ, the ordinate is the exact differential cross section divided by E_+Z^5; units are mc^2 for E_+, radians for θ, and 10^{-33} cm^2 per steradian for the scaled differential cross section. The positron energies are 25 mc^2 (full curve), 15 mc^2 (dotted), 10 mc^2 (dashed) and 5 mc^2 (chained).

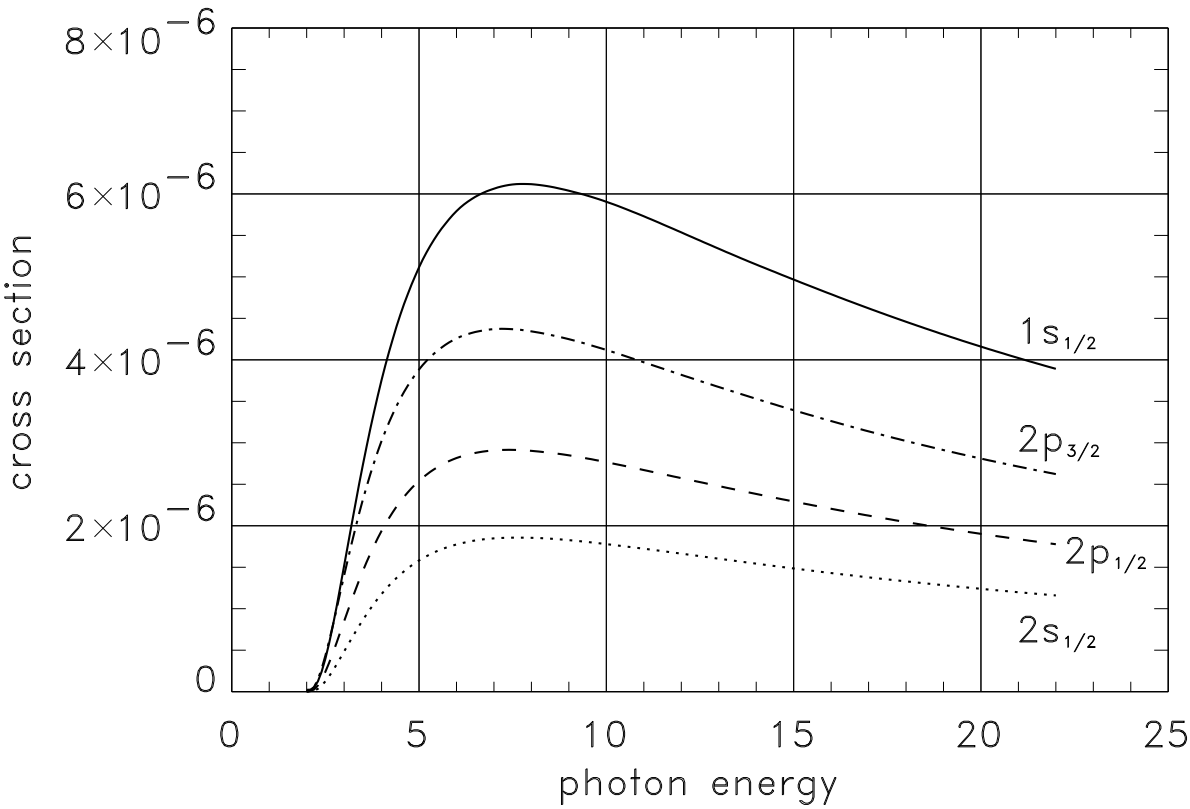

FIG. 10 Cross section for photon induced muon pair production with the negative muon bound in the K- or the L-shell of a bare uranium ion as a function of the photon impact energy (Belkacem and Sørensen, 1998). The nucleus is assumed to be a homogeneously charged sphere. The photon energy is given in units of the muon rest energy and the cross section is given in units of 3.488×10^{-26} cm^2, the square of the muon Compton wavelength.

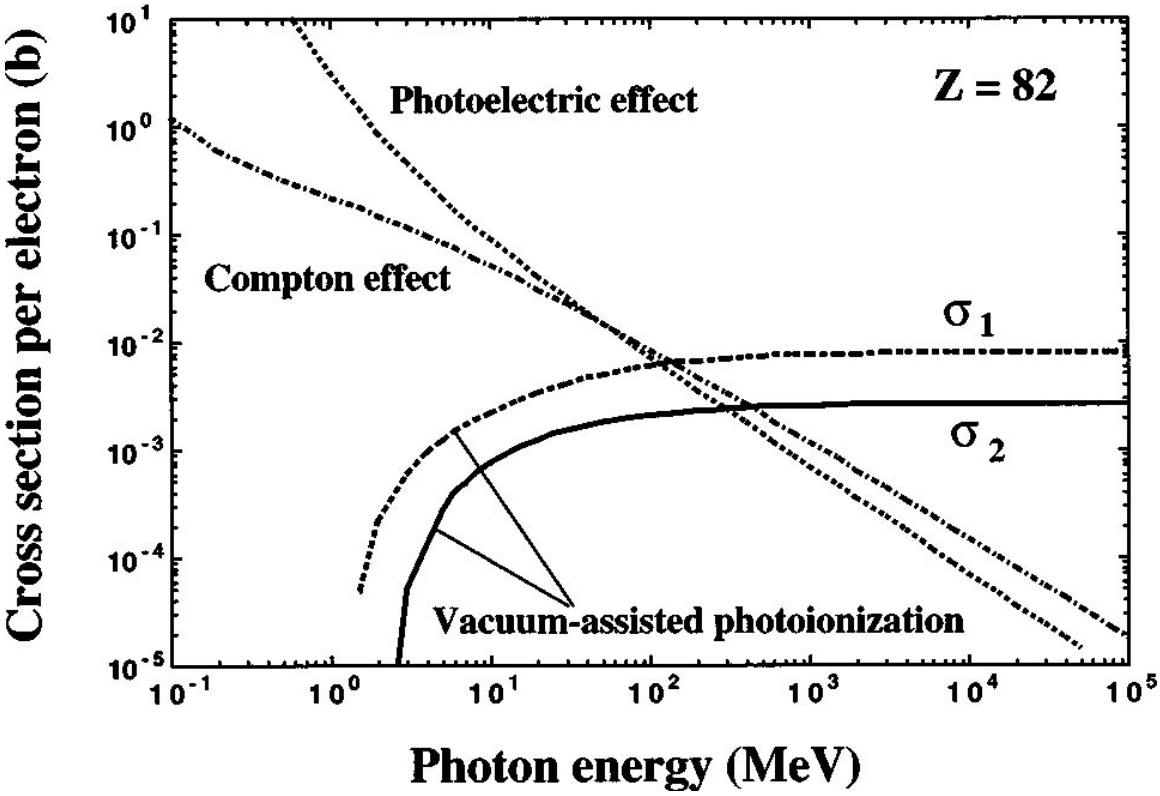

FIG. 11

FIG. 11 Cross section for creation of a K-shell vacancy for lead for different photoionization processes as a function of the photon energy (Ionescu *et al.*, 1999). The dashed-dotted line corresponds to the Compton effect and the dotted line to the photoelectric effect. Vacuum-assisted photoionization is represented by the dashed line (mechanism 1, i.e. pair production in the nuclear field with subsequent $e^{\pm} - e^{-}$ encounter) and by the solid line (mechanism 2, i.e. pair production in the electron field), respectively. The cross sections are per K-shell electron.

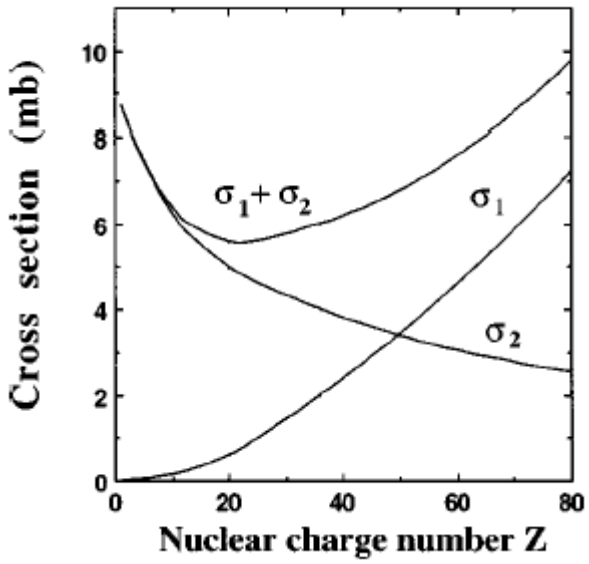

FIG. 12

FIG. 12 High-energy asymptote of vacuum-assisted photoionization. The cross sections σ_1 and σ_2 associated with pair creation in the nuclear and electron field, respectively, are shown as functions of the target atomic number Z (Ionescu *et al.*, 1999). The upper curve corresponds to the sum $\sigma_1 + \sigma_2$.

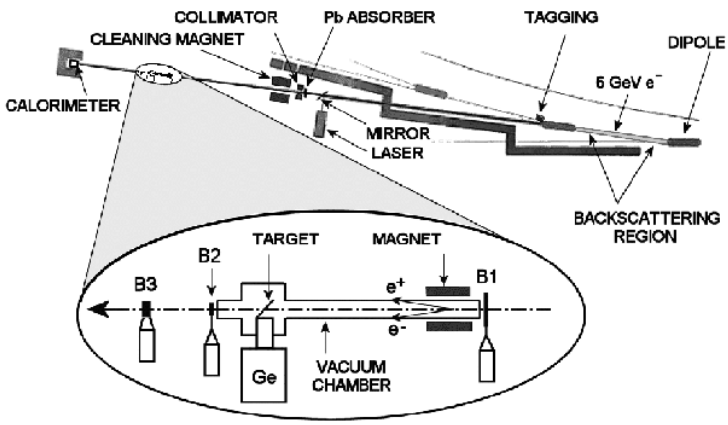

FIG. 13

FIG. 13 Experimental setup at the high-energy photon-GRAAL beam line of ESRF. The inset shows details of the target area (Dauvergne *et al.*, 2003).

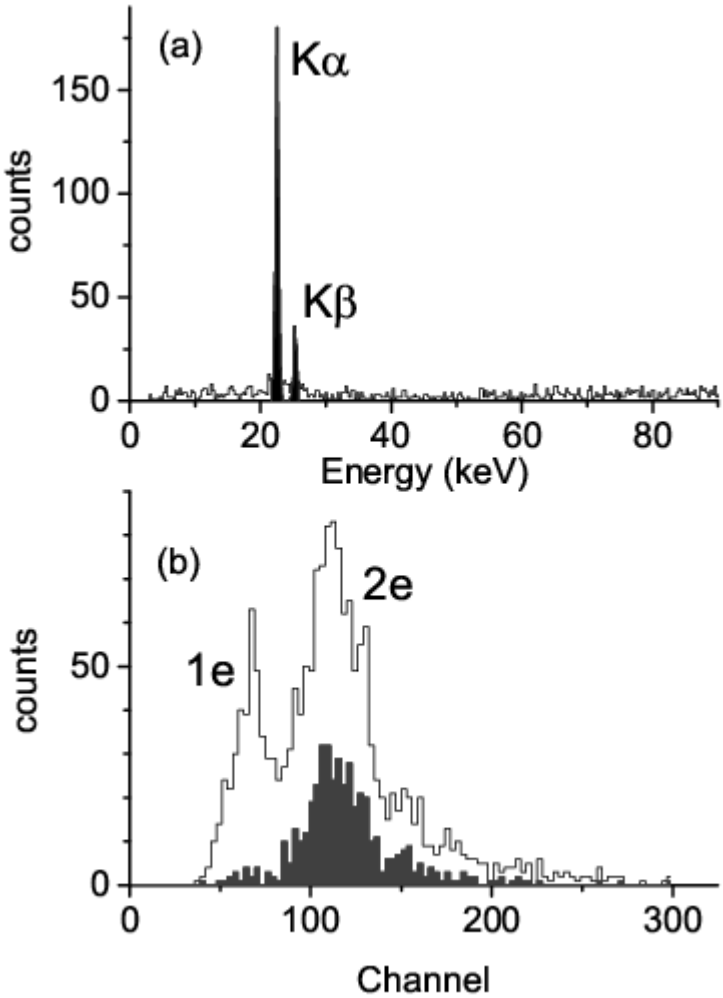

FIG. 14

FIG. 14 (a) Energy spectrum of x-rays detected in coincidence with a charged particle for a 15.3 mg/cm^2 thick Ag target. (b) corresponding amplitude spectrum in the thick scintillator B3. The gray zones of both spectra correspond to the selection of events containing only photons detected by the Ge detector (Dauvergne *et al.*, 2003).

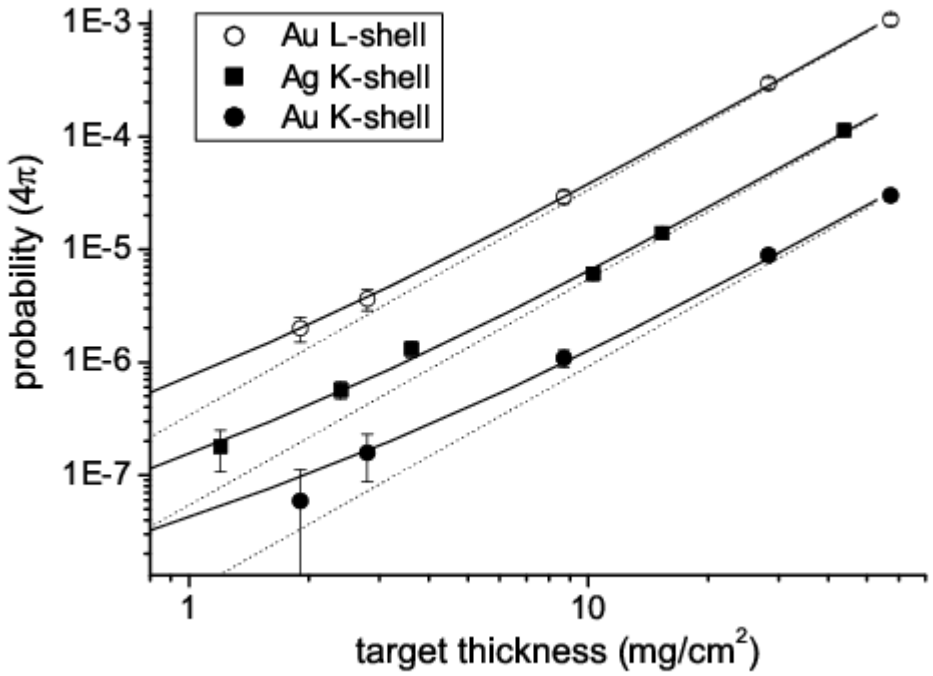

FIG. 15

FIG. 15 Probabilities for K- or L-shell vacancy production in coincidence with pair creation in gold and silver targets. Error bars correspond to statistical and absolute dose determination uncertainties. Solid lines are fits using the sum of a linear and a quadratic function. Dashed lines are the corresponding quadratic functions (Dauvergne *et al.*, 2003).

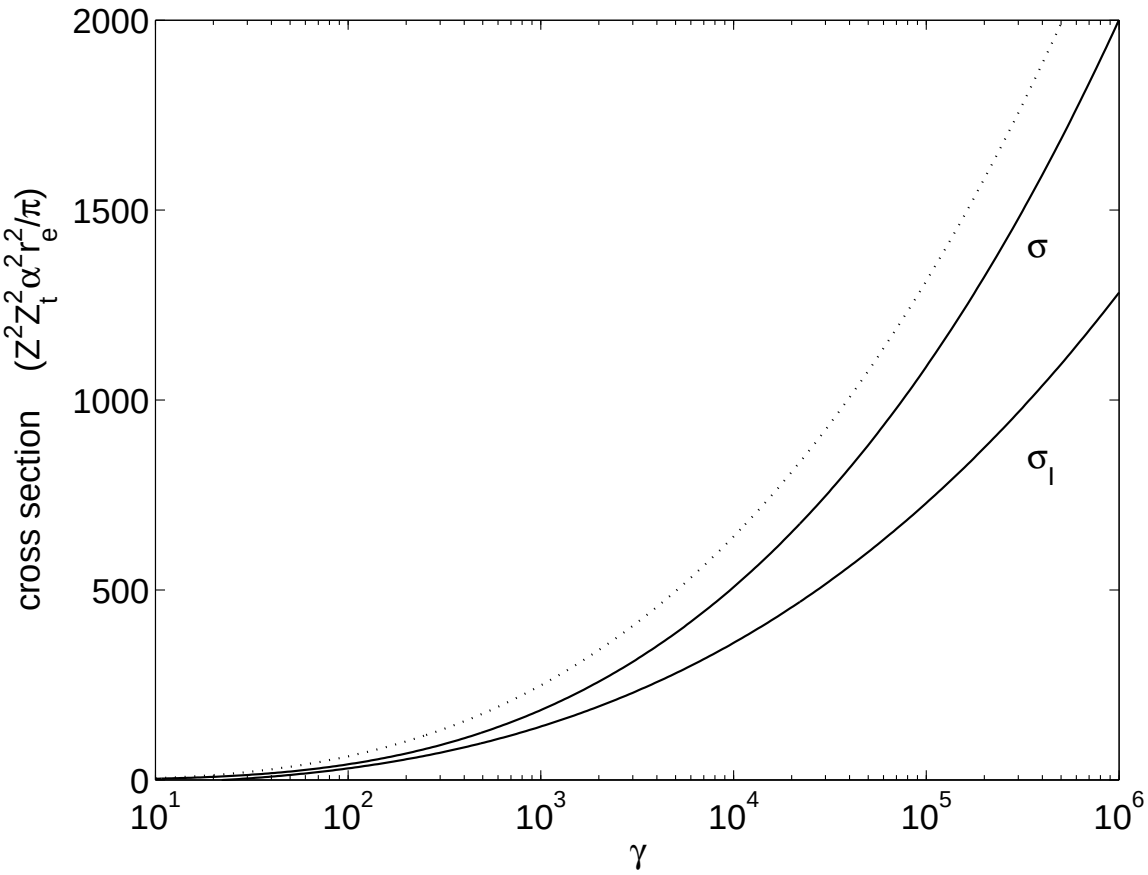

FIG. 16 Cross section for pair production in collisions between two bare heavy ions as a function of the γ-value of the projectile. The target ion is assumed at rest. The full-drawn curves display the cross sections (53–54) obtained by Racah (with $\overline{\epsilon}$ entering the expression for σ_I chosen as $\sqrt{\gamma}$). The dashed curve is the result quoted by Heitler (1954) with $\beta = 1/4$ (as recommended by Heitler).

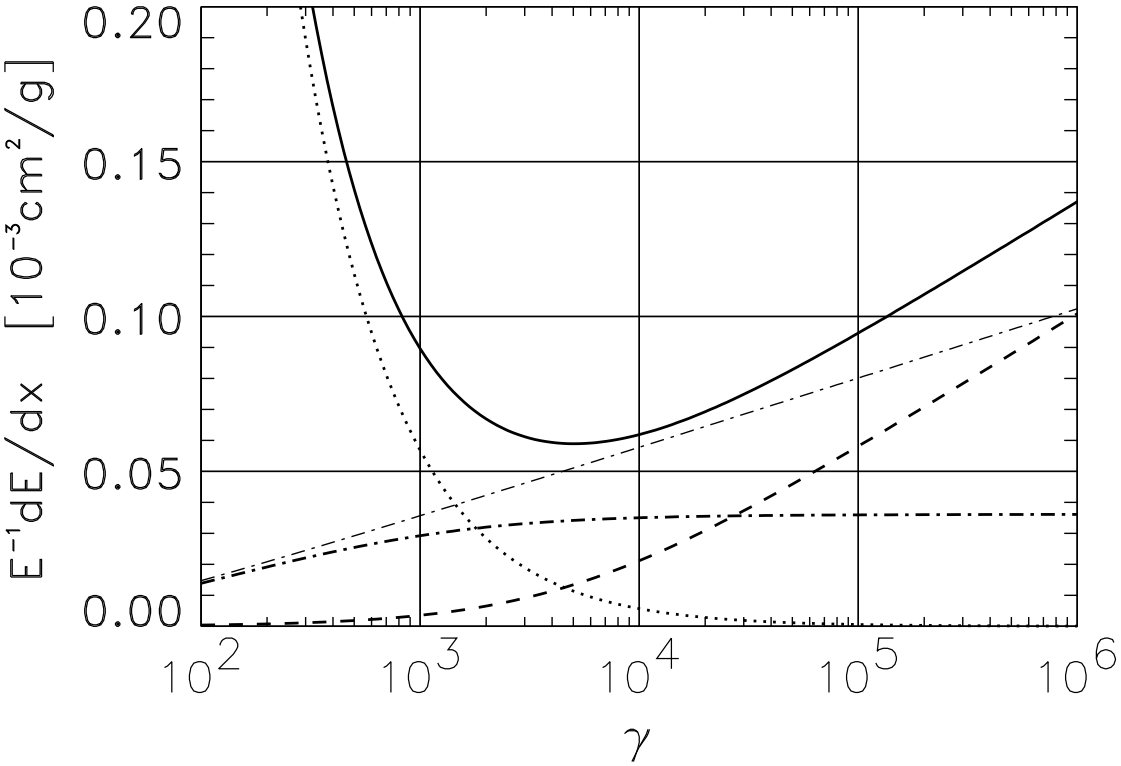

FIG. 17 Relative energy-loss rate as a function of $\gamma \equiv E/Mc^2$ for bare lead ions in a lead target (Sørensen, 2003). The dotted curve shows the ionization contribution, the chained curve displays the pair-production channel (thin curve obtains by neglect of screening), the dashed curve is an estimate of the bremsstrahlung loss, and the full-drawn curve shows the sum of all contributions.

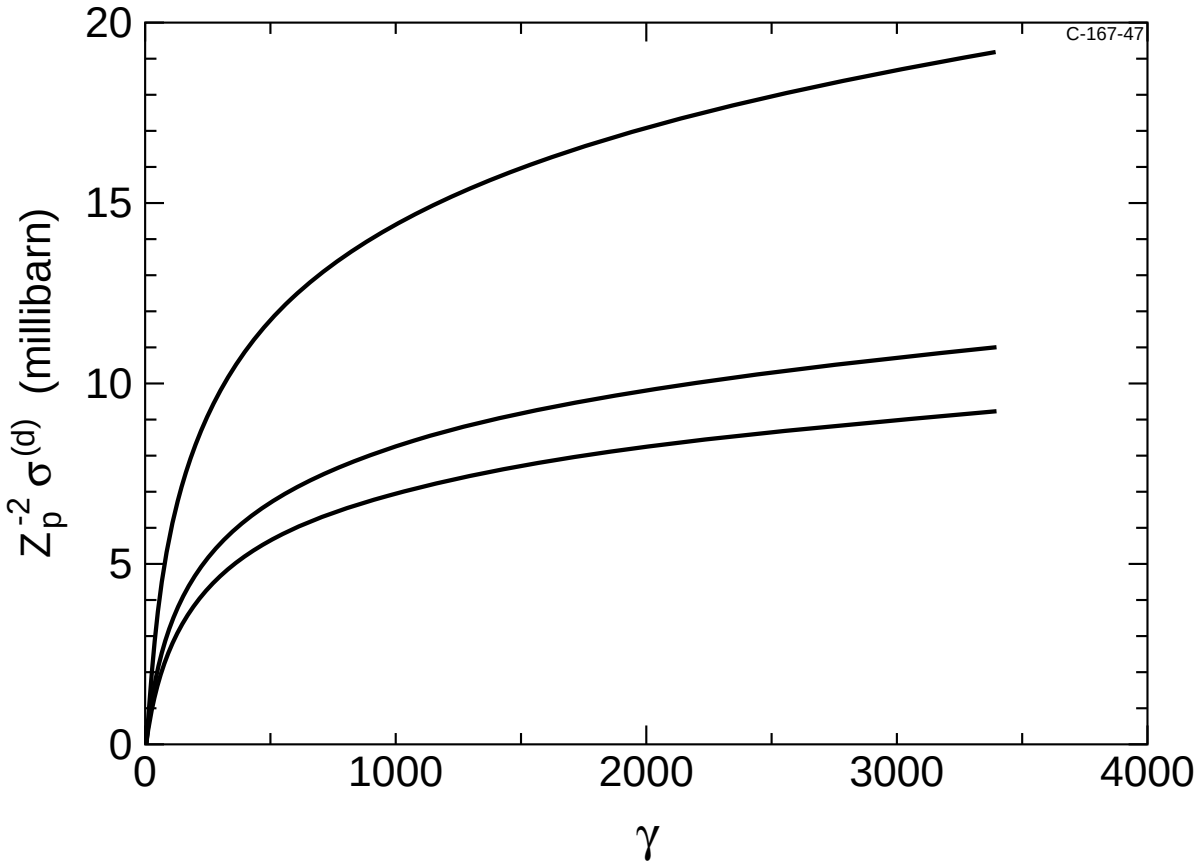

FIG. 18 Distant collision contribution to the cross section for electron-positron pair production with capture to the K-shell for ion impact with γ-values up to 3400 (Agger and Sørensen, 1997). The cross section, which is obtained by the perturbative virtual photon method, has been divided with the square of the projectile charge number, and the ordinate is given in units of 10^{-27} cm^2. The lower curve corresponds to a target charge number of 79, the central curve to 82 while the upper curve corresponds to Z=92.

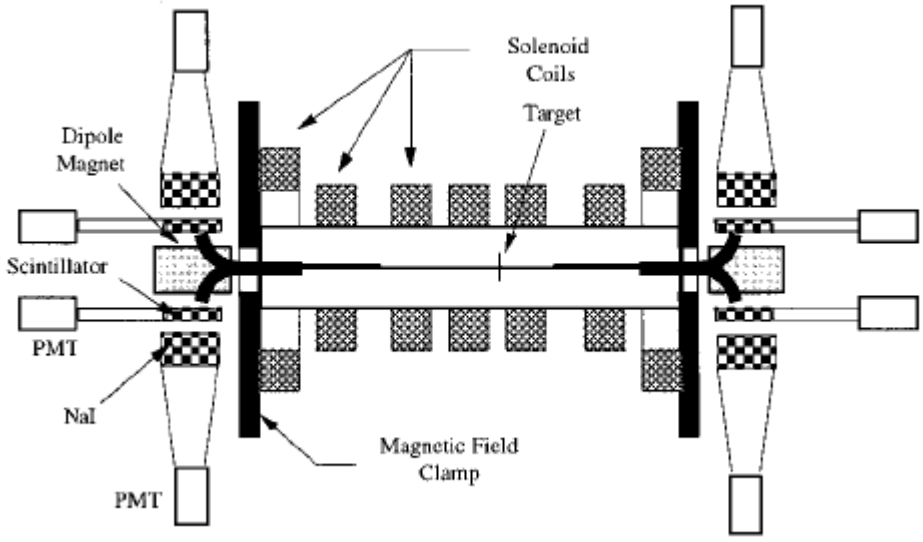

FIG. 19

FIG. 19 Schematic diagram of the advanced positron spectrometer (sectional view from the top). The solenoidal field decreases adiabatically from the target toward the ends, causing the divergence of the electrons and positrons to decrease, allowing them to be swept by the dipole magnets into the scintillator detectors (Belkacem *et al.*, 1997).

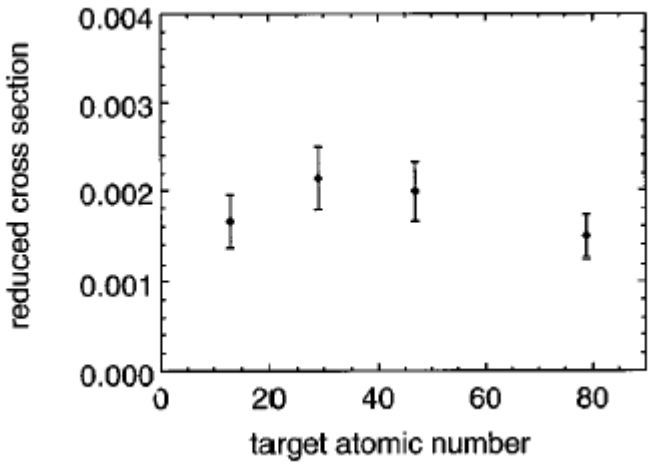

FIG. 20

FIG. 20 Measured bound-free pair production cross sections divided by Z_t^2 for targets of Al, Cu, Ag, and Au. The projectile is a 10.8 GeV/n bare Au^{79+} ion (Belkacem *et al.*, 1998).

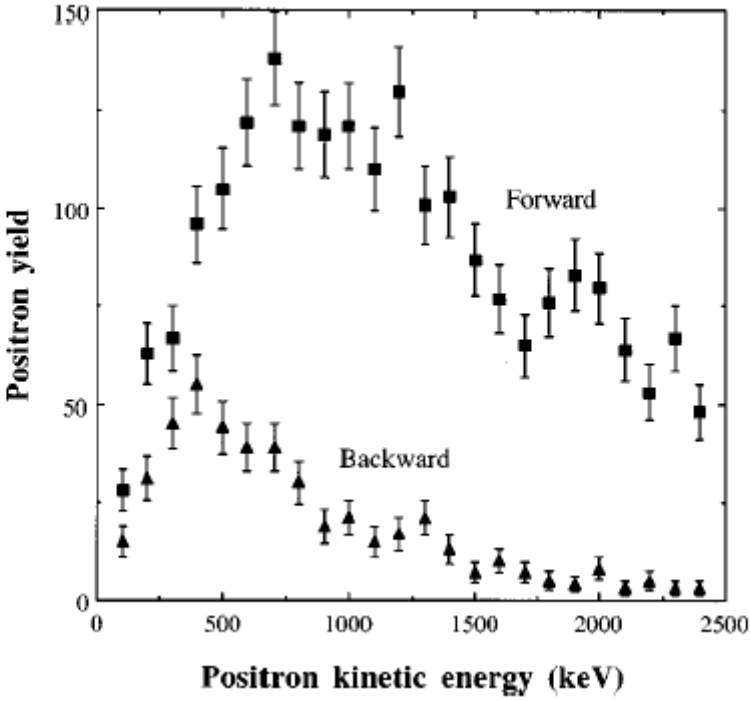

FIG. 21

FIG. 21 Positron energy spectrum for bound-free pair production measured for 0.96-GeV/nucleon U^{92+} on Au target. Each data point is the result of integration over all angles between 0° and 75° (forward and backward with respect to the beam direction) and over an energy interval of 100 keV (Belkacem *et al.*, 1997).

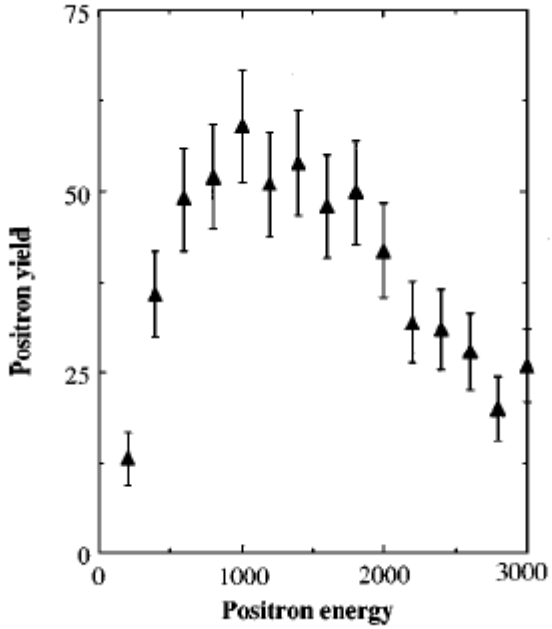

FIG. 22

FIG. 22 Positron energy spectrum for bound-free pair production measured for 1.3-GeV/nucleon La^{57+} on a Au target (Belkacem *et al.*, 1997).

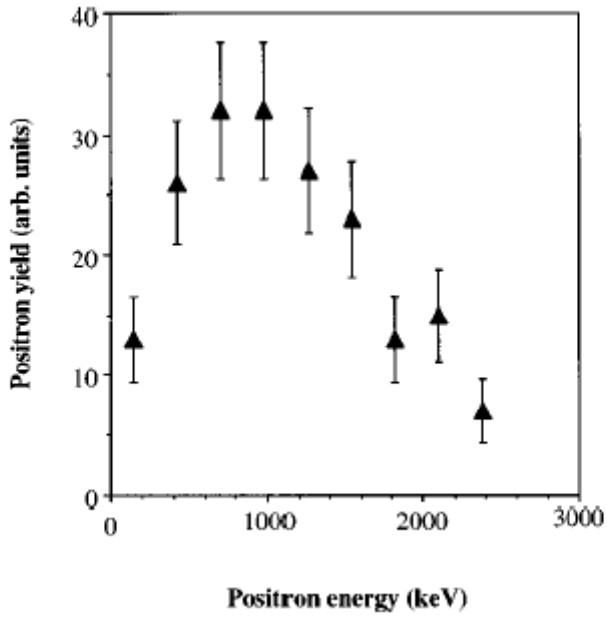

FIG. 23

FIG. 23 Positron energy spectrum for bound-free pair production measured for 0.96 GeV/nucleon U^{92+} on Cu (Belkacem *et al.*, 1997).

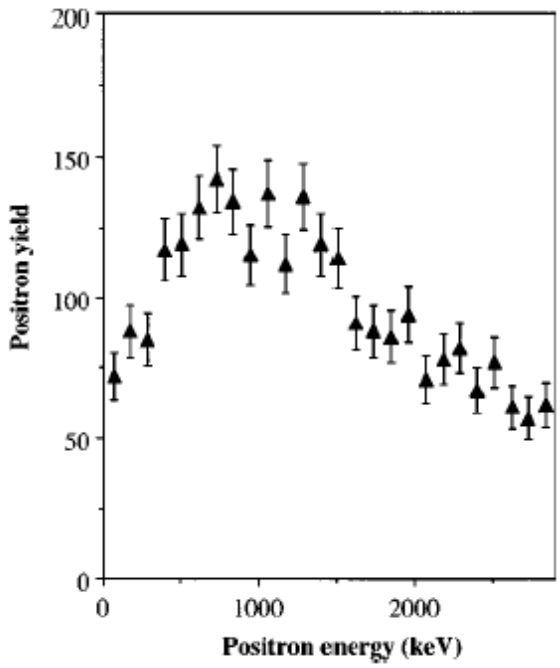

FIG. 24

FIG. 24 Positron energy spectrum for free-free pair production measured for 1.3 GeV/nucleon La^{57+} on Au (Belkacem *et al.*, 1997).

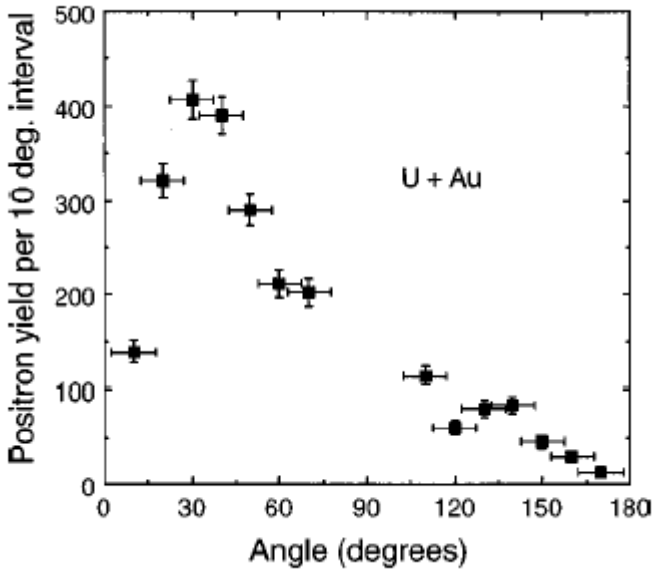

FIG. 25

FIG. 25 Total yield of positrons as a function of positron emission angle with respect to the beam direction. Each data point is a result of an integration over all positron kinetic energies between 0.1 and 2.5 MeV. The data are for 0.96-GeV/nucleon U^{92+} on Au (Belkacem *et al.*, 1997).

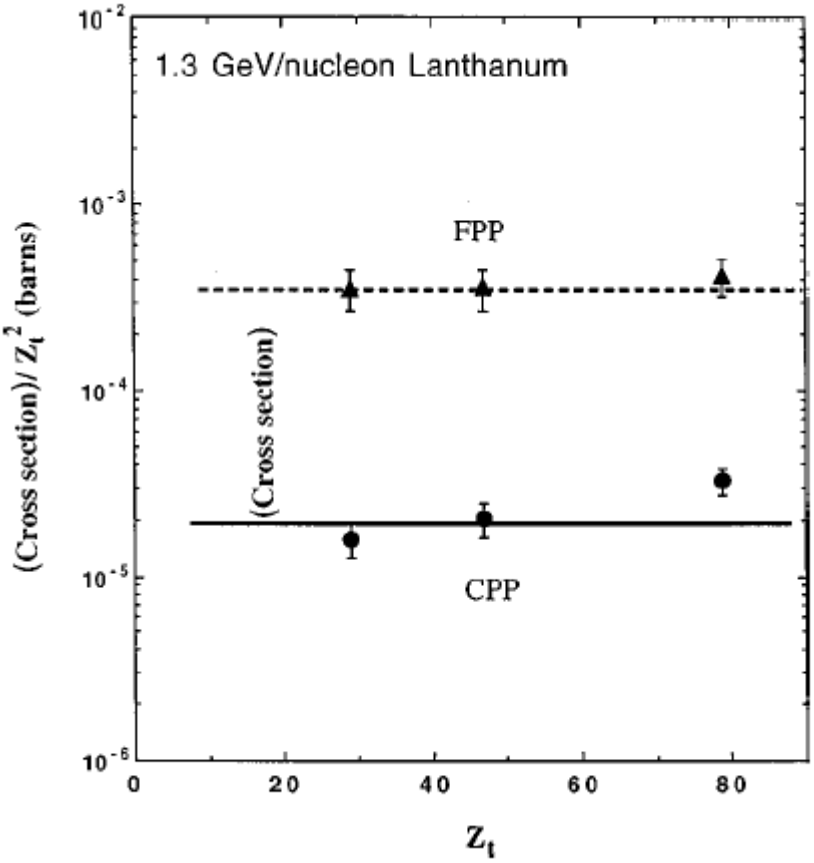

FIG. 26

FIG. 26 Free-free pair production (FPP) and bound-free pair production (CPP) cross sections, divided by Z_t^2, as a function of the target atomic number measured for 1.3-GeV/nucleon La^{57+} projectile. The horizontal line is a guide to the eye to highlight a Z_t^2 dependence (Belkacem *et al.*, 1997).

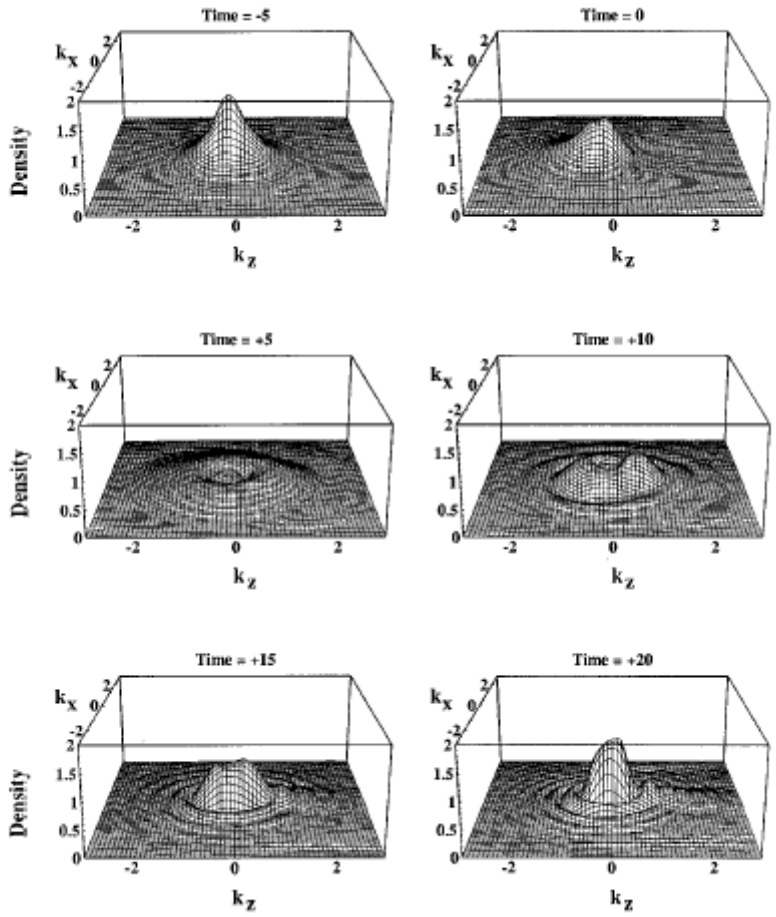

FIG. 27

FIG. 27 Time evolution of the momentum space density shown in the collision system Au + U at 0.93 GeV/nucleon and impact parameter zero (Momberger *et al.*, 1996).

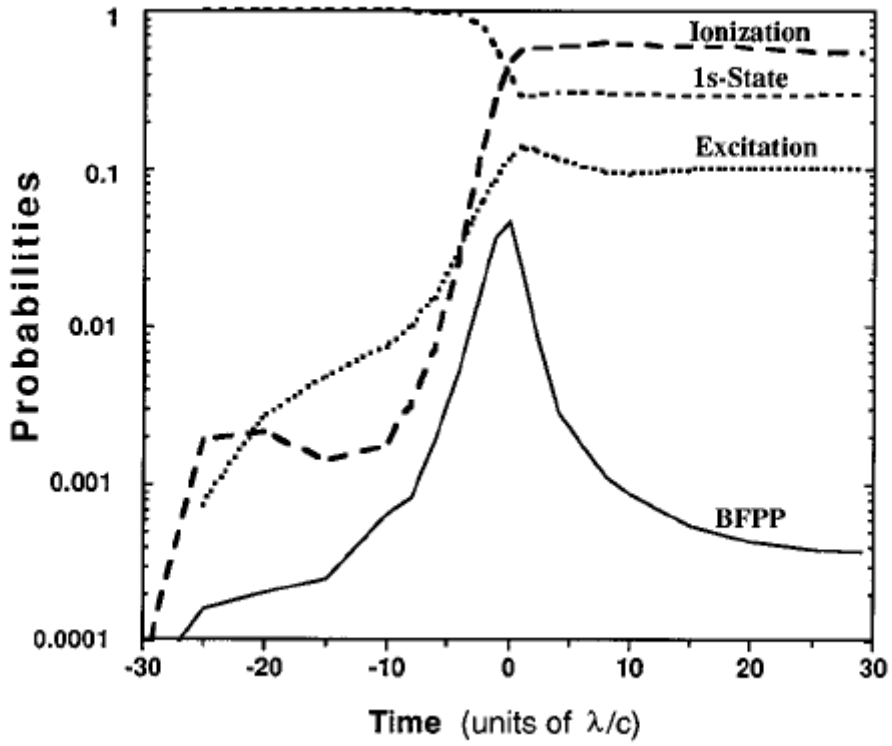

FIG. 28

FIG. 28 Time evolution of the occupation probabilities for collision system shown in Fig. 27 obtained by projection on the various sets of target states. The corrections with respect to the overlap of the projectile states with the target states have not been included here, since K-shell transfer amounts only to 2.5% (Momberger *et al.*, 1996).

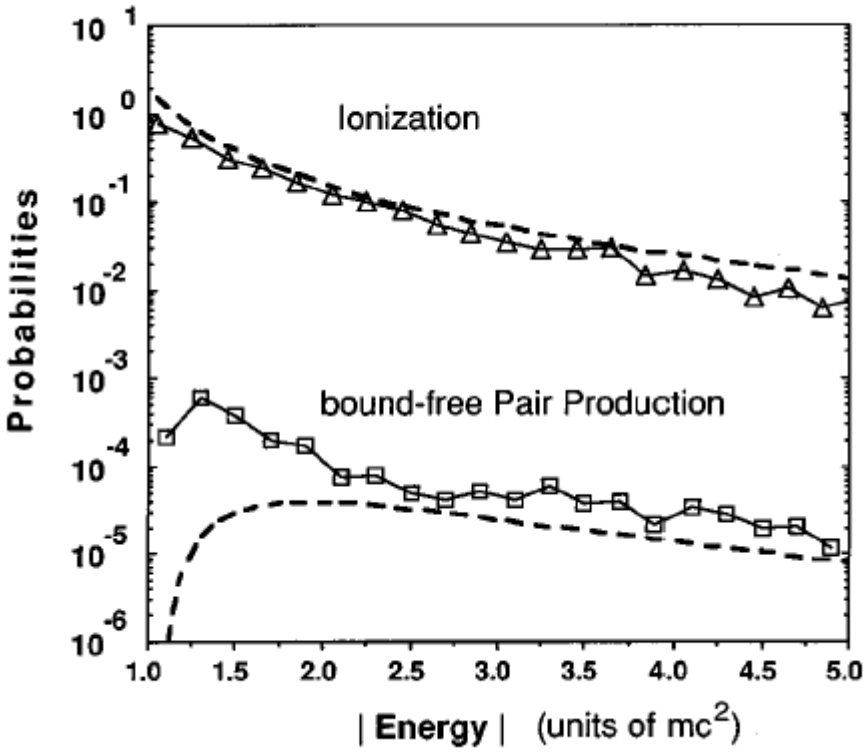

FIG. 29

FIG. 29 Results of the projections of the time evolved state taken at time $t = 20$ onto the positive and negative continuum as a function of the absolute value of the energy. The dashed lines show the corresponding perturbation theory results for ionization and bound-free pair production (Momberger *et al.*, 1996).

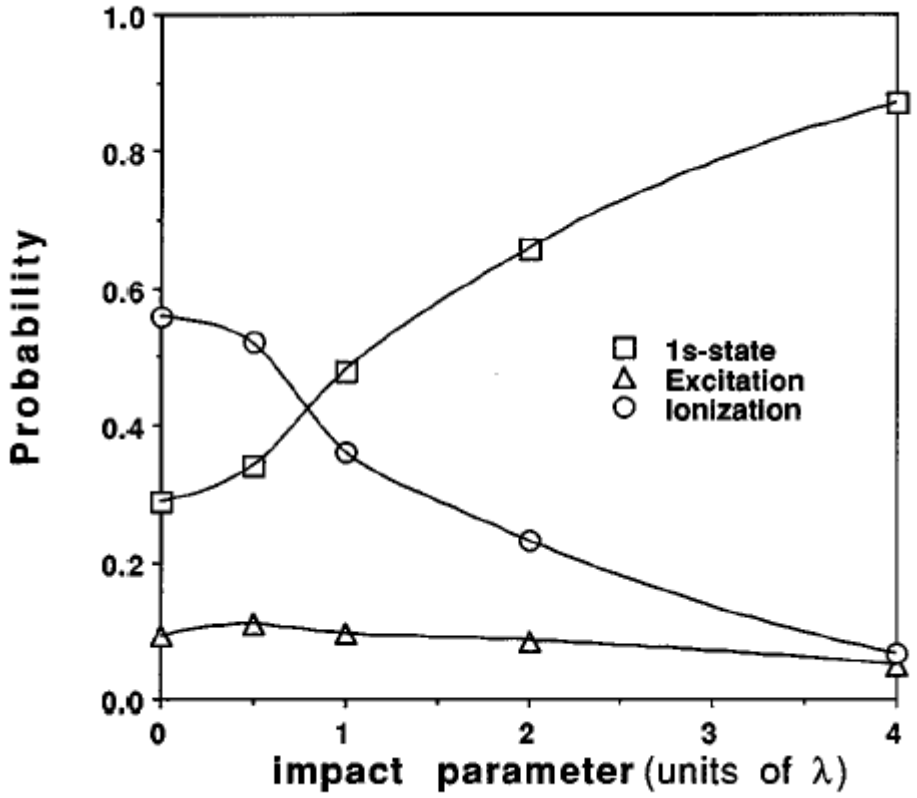

FIG. 30

FIG. 30 Impact parameter dependences for the 1s state, total excitation, and ionization for the collision system Au + U at 0.93 GeV/nucleon (Momberger *et al.*, 1996).

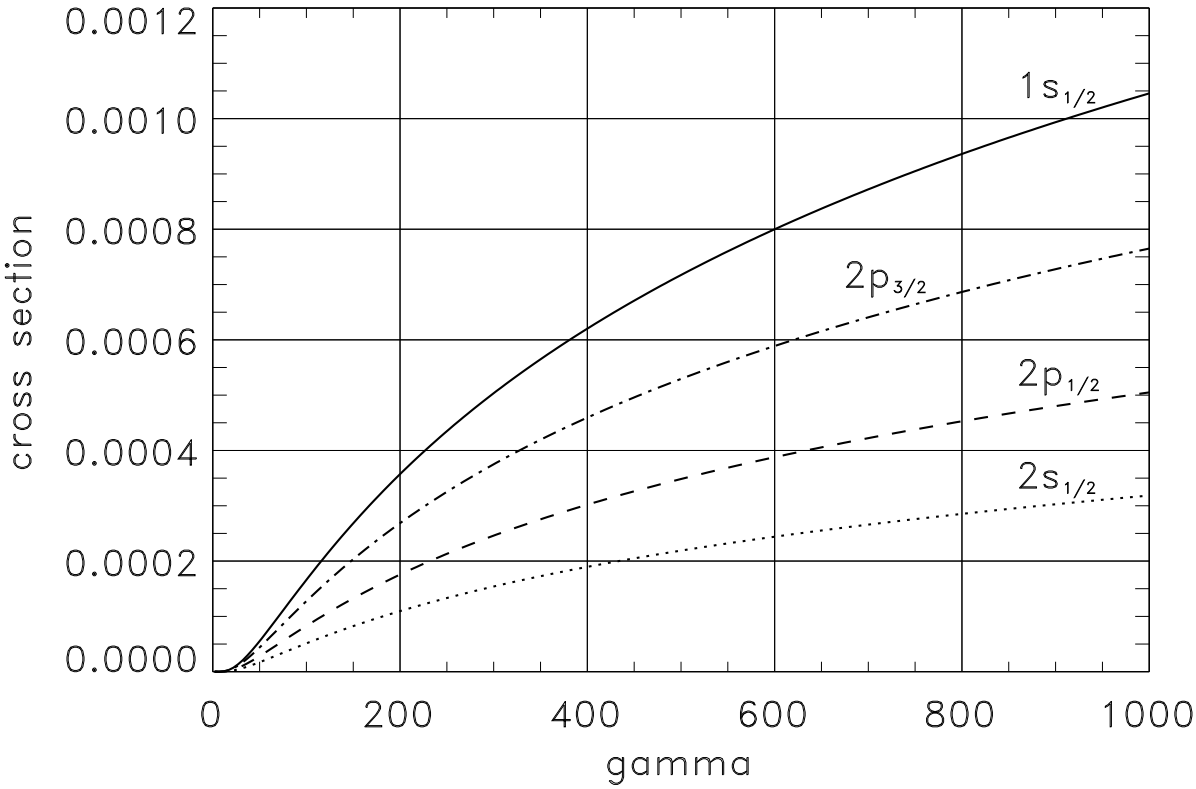

FIG. 31 Cross section for heavy-ion induced muon pair production with the negative muon bound in the K- or the L-shell of a bare uranium ion as a function of the Lorentz-γ of the projectile (Belkacem and Sørensen, 1998). The cross section is proportional to the square of the charge of the projectile ion and is shown here for impact of a bare uranium ion. It is given in units of 3.488×10^{-26} cm^2, the square of the muon Compton wavelength.

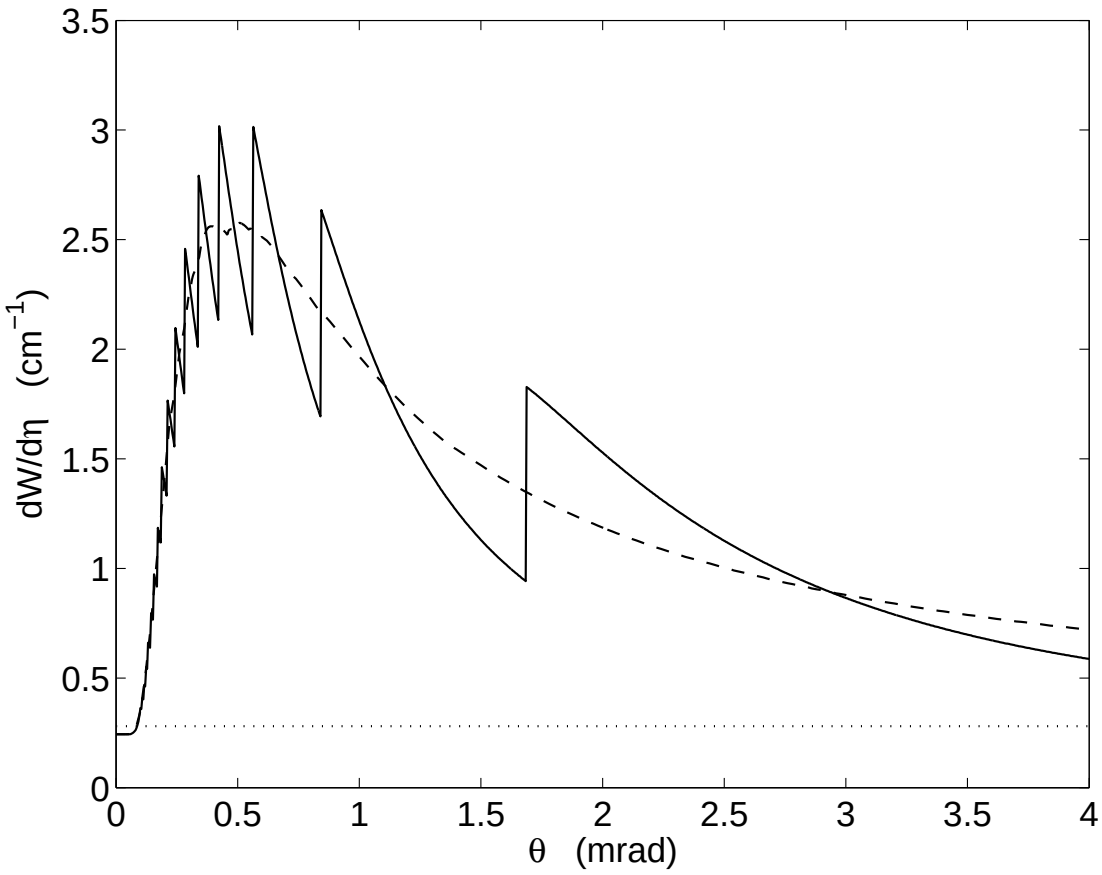

FIG. 32 Coherent electron-positron pair production. The figure shows the differential production rate obtained in the perturbation limit for symmetric pairs ($\eta \equiv E_+/\hbar\omega = 0.5$) for 100 GeV photons incident on a germanium crystal kept at 100 K as a function of the angle of incidence θ relative to the direction of the $\langle 110 \rangle$ axis. The full-drawn curve obtains for incidence parallel to the $\{100\}$ planes, the dashed curve displays the average over azimuthal angle for fixed polar angle θ, and the dotted curve shows the rate for the corresponding amorphous medium.

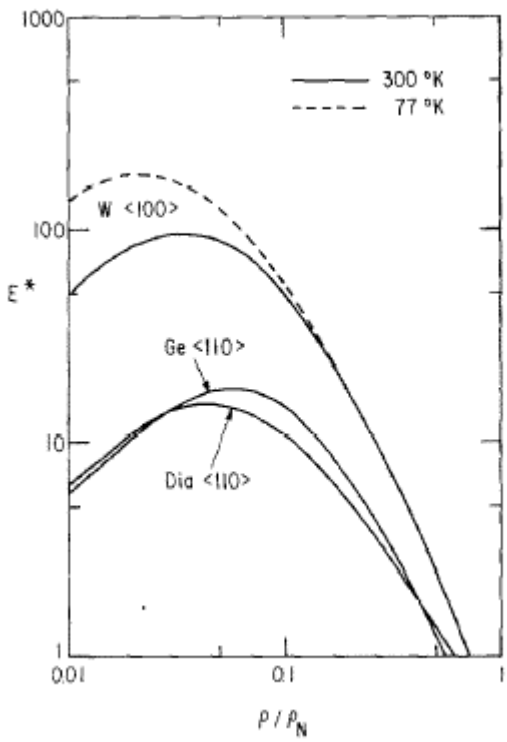

FIG. 33

FIG. 33 The electric field of the continuum potential for axial channeling in diamond, silicon and tungsten crystals. The electric field is in atomic units, and ρ_N is the effective radius of the string. Note the logarithmic scales (Kimball *et al.*, 1986).

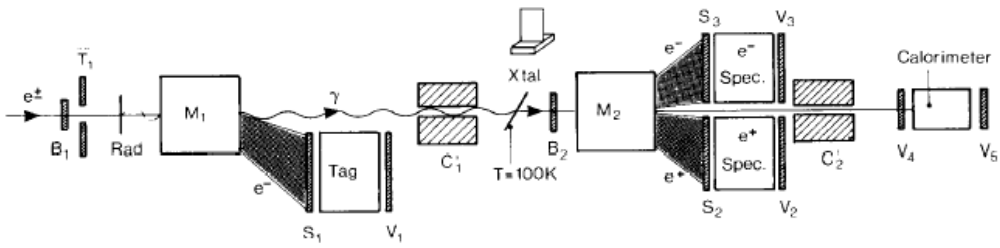

FIG. 34

FIG. 34 Setup of the CERN-NA33 experiment, see text for details (Belkacem *et al.*, 1986).

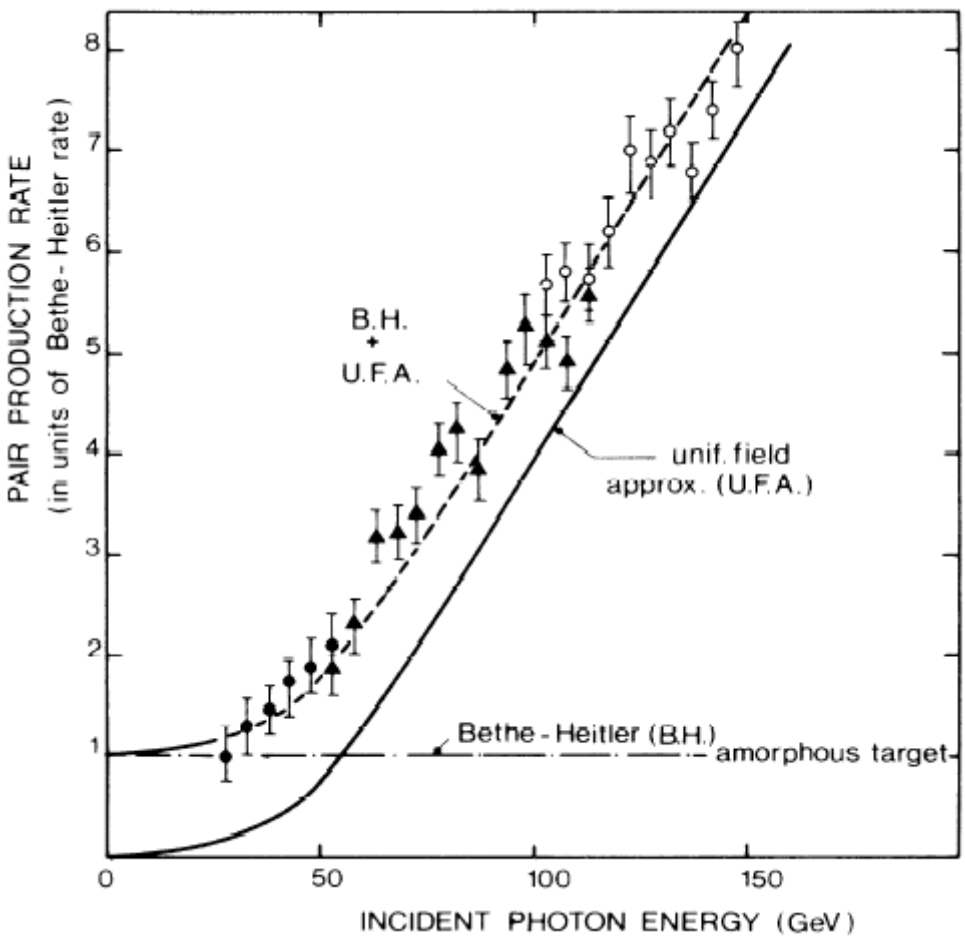

FIG. 35

FIG. 35 Energy dependence of the total pair-production rate when photons are incident along the ⟨110⟩ axial direction of a 1.4 mm-thick Ge crystal cooled to 100 K. The three different symbols correspond to three different energies of the primary electron beam (see text). The solid curve represents the theoretical predictions of the uniform-field approximation. The dot-dashed line corresponds to the rate in an amorphous target. The dashed curve gives the sum of the calculated rates of the coherent and incoherent processes (Belkacem *et al.*, 1987).

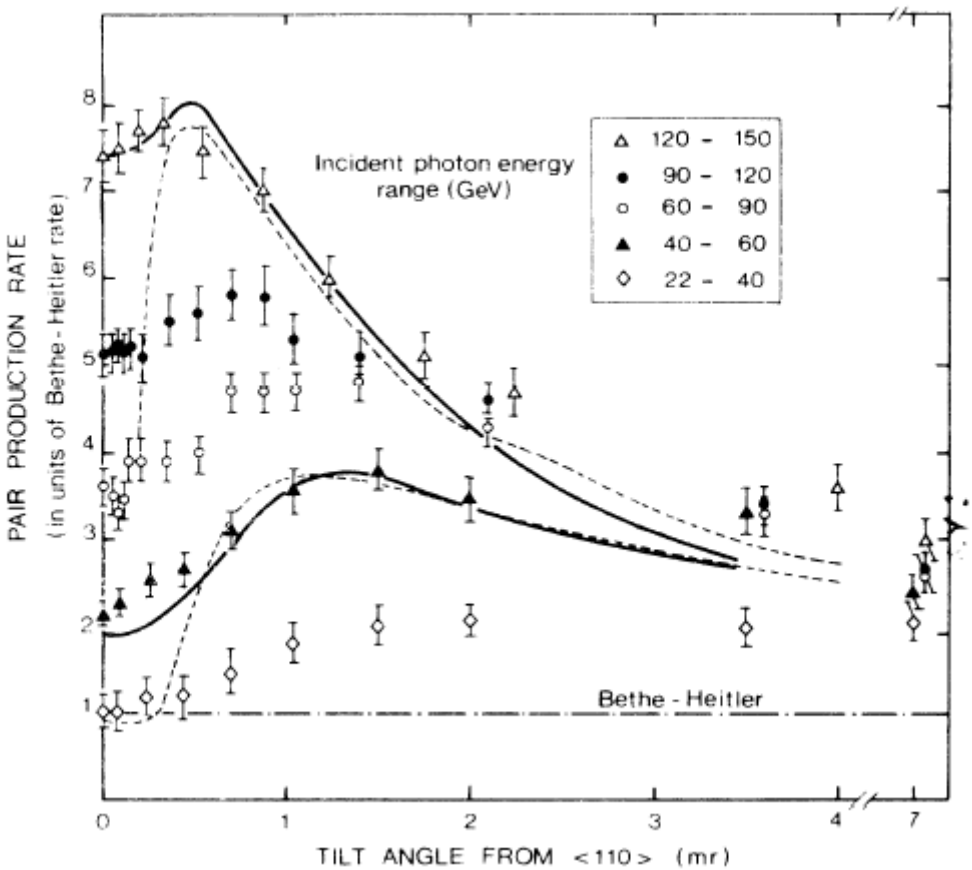

FIG. 36

FIG. 36 Angular scan of the total pair-production rate around the ⟨110⟩ direction of a 1.4 mm-thick Ge crystal cooled to 100 K. Each data point corresponds to an integration of the rate over the indicated photon energy range. The solid curves correspond to the theoretical predictions based on the time-dependent-field model (Kimball *et al.*, 1986). The dashed curves correspond to the Born approximation. The dot-dashed line corresponds to the Bethe-Heitler rate.

Tables

TABLE I High-energy limit of the cross section for photoinduced bound-free pair production with K-shell capture (Agger and Sørensen, 1997). The table shows the cross section relative to the Born value σ_0 for various targets. First column gives the atomic number of the capturing target ion, second column the results of Agger and Sørensen (1997), third column the results of Pratt (1960a), while the last two columns correspond to the expressions (27) (Aste *et al.*, 1994) and (28) (Pratt, 1960a). The numbers marked with an asterisk are extrapolated from the data given by Pratt *et al.* (1973).

Z	Agger-Sørensen	Pratt	Eq. (27)	Eq. (28)
92	0.196	0.203	0.182	0.175
82	0.216	0.223	0.197	0.201
79	0.222	0.228*	0.203	0.209
55	0.293	0.310*	0.271	0.305
26	0.518	0.532*	0.4875	0.529
8	0.798	0.793*	0.784	0.805
1	0.971	-	0.969	0.972

TABLE II Inner-shell ionization by 1 GeV photons (Dauvergne *et al.*, 2003). Theoretical values for the creation of free pairs (FPP; specific to the target but not the shell) as well as for Compton scattering and the photoelectric effect (CSandPE) are from Hubbell *et al.* (1980), while theoretical values for vacuum-assisted photoionization (VAP) are from Ionescu *et al.* (1999). Cross sections are given in barns per target atom for pair creation, respectively per target shell in millibarns for vacuum-assisted photoionization and for Compton scattering and the photoelectric effect.

	FPP experiment	FPP theory	VAP experiment	VAP theory	CSandPE
Au K-shell	35.1	36.6	8.3 $\pm$6.2	19.4	2.3
Au L-shell			116 $\pm$76	42.2	9.3
Ag K-shell	14.2	14.7	18 $\pm$6	13.2	2.3

TABLE III Cross section in barn for pair production for bare sulphur ions incident on a gold target at an energy of 200 GeV per nucleon. See text for explanation of entries in the table; H stands for Heitler (1954), Ion-Eich for Ionescu and Eichler (1993), and the column marked $\mathrm{WW}_{1/2}$ gives the result of the numerical WW-approach with $b_{min} = 1/2$ while the column marked $\mathrm{WW}_{1/2}^{bare}$ gives the corresponding result for incidence on a bare ion rather than an atomic target.

	H (20)	$\mathrm{WW}_{1/2}$	MCQED	Ion-Eich	experiment	H (19)	$\mathrm{WW}_{1/2}^{bare}$	Racah
total	141	138	140	130		141	156	158
< 17 MeV		97	98	75	85 ($\pm$22)			

TABLE IV Pair-production contribution to the energy loss of lead ions at $\gamma = 168$ compared to the deviations from ionization theory measured at CERN. The table lists corrections to the stopping number L. The numbers in the second column correspond to Eqs. (55–57) except for including the additional factor $(1 + 1/Z_t)$. The numbers in the third column are obtained similarly but with Λ_0 replaced by Λ_0^{screen}. The experimental values were recorded by Datz *et al.* (1996).

Z_t	PP theory	with screening	experiment
6	0.066	0.064	0.30
14	0.141	0.135	0.30
29	0.282	0.267	0.48
50	0.479	0.449	0.48
82	0.780	0.722	0.73

TABLE V Distant collision contribution to the cross section for pair production for bare gold ions incident on a bare uranium nucleus (Agger and Sørensen, 1997). The produced electron ends up in the K-shell of the hydrogen-like uranium system. The first column identifies the impact kinetic energy given in GeV/amu, the next two give the WW results for b_{min}=2 and b_{min}=1, the fourth column compares to the results of Aste *et al.* (1994), and the last two compare to the Born approximation results of Becker *et al.* (1987) and Baltz *et al.* (1994). The Born results for the total cross section are taken from Becker *et al.* (1987) for the two lower energies and estimated for the higher by scaling the result $\sigma_{pert}^{total} \simeq 14.3 \ln \gamma - 31$ given by Baltz *et al.* (1994) for impact of lead on lead with $Z_p^2 Z^5 f(Z)$ where $f(Z)$ is defined by Eq. (26) and listed in Table I. The Born results for $b \leq 2$ are estimated on the basis of the publications by Becker *et al.* (1987) and Baltz *et al.* (1994) by numerical integration of data presented in a figure respectively by scaling a fitting formula with $Z_p^2 Z^5 f(Z)$. Cross sections are given in barn.

Energy	Agger-S; b_{min}=2	Agger-S; b_{min}=1	Aste *et al.*; b_{min}=1	$\sigma_{pert}^{b\leq 2}$	σ_{pert}^{total}
10	5.58	13.1	-	8	15
100	39.8	54.8	54.4	13	50
20.000	165	182	185	22	167

TABLE VI Cross sections (in barns) for bound-free pair production for 10.8 GeV/nucleon Au^{79+} (Belkacem *et al.*, 1998).

Z_t	experiment	perturbative result
79	8.8 ±1.5	10.1
47	4.4 ±0.73	3.60
29	1.77 ±0.31	1.36
13	0.28 ±0.052	0.27